VOLUME 48 NUMBER 4
APRIL 1982

[illegible] of the [illegible]

[illegible]

[illegible]

[illegible]

[illegible]

[illegible]

Journal of the
ENGINEERING MECHANICS DIVISION
Proceedings of the American Society of Civil Engineers

CONTENTS

April, 1957

Papers

Journal of the
ENGINEERING MECHANICS DIVISION
Proceedings of the American Society of Civil Engineers

BENDING OF A RECTANGULAR PLATE WITH ONE FREE EDGE

W. Nachbar[1]
(Proc. Paper 1196)

ABSTRACT

A rectangular plate, simply supported along three edges and free on the fourth, is subjected on one face to a lateral pressure which is uniform parallel to the free edge but can vary linearly in a direction perpendicular to the free edge. Infinite series for deflections, moments, shear and reaction force distribution were derived and programmed for computation on a high-speed digital computer. Numerical values are presented in graphs and tables for the two special cases of completely uniform and triangular loading; the more general loading is given by superposition. The discussion of results includes (a) comparison of results for plates with different values for Poisson's ratio, (b) computational difficulties and methods used to overcome them, and (c) approximate formulas in closed form.

INTRODUCTION

This note considers bending, according to the classical thin plate theory of Poisson-Kirchoff, as presented in Timoshenko's standard text on plates, [1] * of a homogeneous isotropic, rectangular plate which is free on one edge and simply supported on the remaining three edges. The contour of the lateral pressure loading on the plate is trapezoidal parallel to the simply supported edges and uniform parallel to the other pair (See Figure 1). Formulas in the form of infinite series are derived for deflections, bending and twisting moment distribution, shear distribution, support reaction distribution and corner reactions. These series are presented in a form which was found to be particularly convenient for numerical computation using a high-speed digital computer.

The bending of an isotropic rectangular plate which has three simply supported edges and one free edge is treated briefly in Timoshenko [1] pages 218-219, and a table of values is given there for deflection and maximum

Note: Discussion open until September 1. 1957. Paper 1196 is part of the copyrighted Journal of the Engineering Mechanics Division of the American Society of Civil Engineers, Vol. 83, No. EM 2, April, 1957.

1. Research Branch, Missile Systems Div., Lockheed Aircraft Corp., Palo Alto, Calif.

* Numbers in square brackets refer to corresponding items in the list of references below.

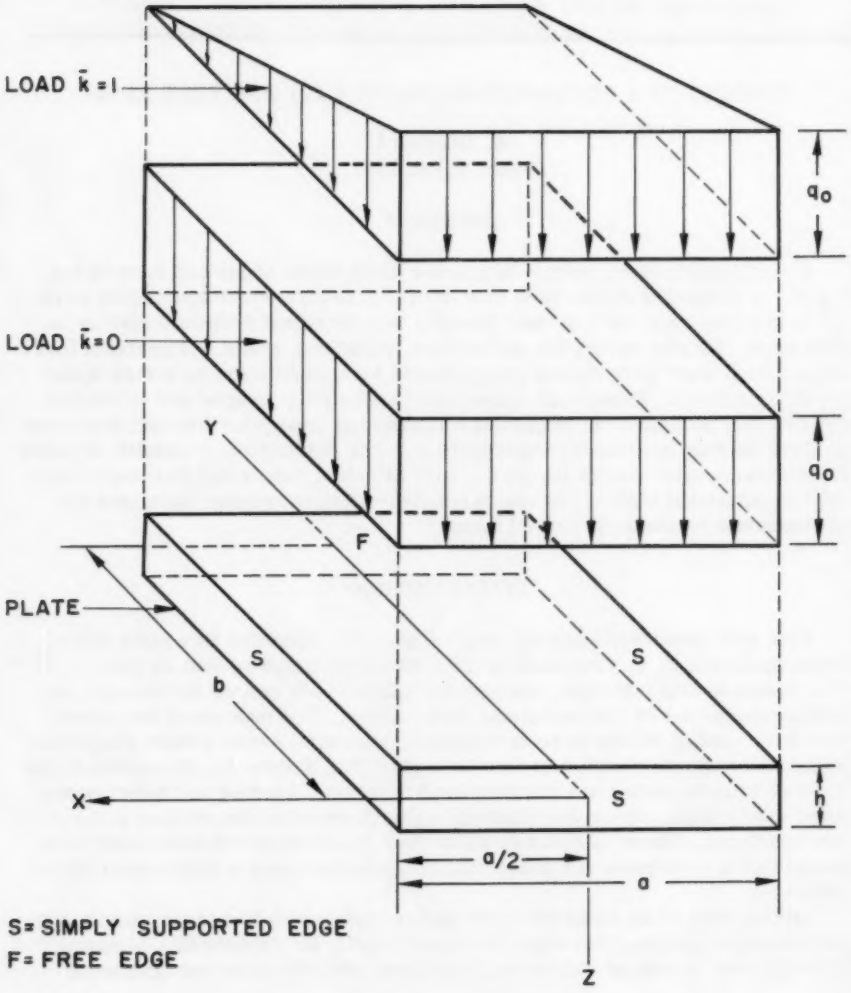

Figure 1. Geometry Loading and Edge Conditions for Plate.

bending moment under a uniform load. More recently, Goriupp[2] derived the Green's Function for this plate and integrated this to obtain the solutions in series form for the plate under uniformly and under triangularly distributed lateral pressure. A numerical table of moment, shear and reaction values was presented in this paper only for a ratio of plate length to breadth, b/a, equal to 0.75. The main emphasis of this paper, however, was on the development of simple finite approximating formulas rather than on presentation of numerical results.

The infinite series found by Goriupp were not used for present purposes for two principal reasons. First, they were derived by setting Poisson's ratio μ equal to zero in the free edge boundary conditions; hence, the series were exact only for the case $\mu = 0$. The finite formulas which were developed involved the same assumption. Secondly, the series coefficient were defined using the hyperbolic functions. While such definition makes for compact notation, it leads to difficulty when computing such slowly converging series as for the edge reactions. The coefficients of high order in this case are discovered to be computed as the very small differences between very large numbers, with a consequent loss of numerical accuracy. This difficulty, and the step taken to avoid this for the present work, are further discussed in the following section.

The analysis derives a single series solution for the general trapezoidal loading, the contour of which is governed by a parameter $\bar{k}$ (Equation 1). Using the solutions for the two special cases of uniform load, $\bar{k} = 0$, and triangular,load, $\bar{k} = 1$, the solution for any general trapezoidal loading may be found by linear superposition. For the value $\mu = 0.3$, the derived series were computed for both loading cases and over a wide range of values for b/a; the results are presented graphically on a non-dimensional scale in Figures 8 through 22 below. In addition, for the single value b/a = 0.75, the series were computed for several values of μ including 0 and 1/2. The results are presented graphically in Figures 3 through 7, and in Table 5, and are used to observe the effect of Poisson's ratio upon deflection and stress distribution.

Formal Solution

Let (x, y) be a cartesian coordinate system in the middle plane of the plate, and let w(x,y) be the lateral deflection* of the middle surface (Fig. 1). The lateral loading q(x,y) on the rectangular plate of side lengths a, b is assumed to be in the form

$$q(x, y) = q_o \left(1 - \bar{k} \frac{y}{b}\right) \tag{1}$$

The differential equation for w(x,y) is then

$$\nabla^4 w \equiv \frac{\partial^4 w}{\partial x^4} + 2\frac{\partial^4 w}{\partial x^2 \partial y^2} + \frac{\partial^4 w}{\partial y^4} = \frac{q_o}{D}\left(1 - \bar{k}\, y/b\right) \tag{2}$$

For simple support along edges $x = \pm a/2$ we seek to represent w(x,y) by

* The coordinate system is assumed to be right-handed with w and q positive in the + z direction.

a Fourier series as follows:

$$w(x, y) = \sum_{n=1,2,\ldots}^{\infty} \bar{w}_n (y) \cos \frac{n\pi x}{a} \quad . \tag{3}$$

The Fourier expansion

$$1 = \frac{4}{\pi} \sum_{n=1,3,\ldots}^{\infty} \frac{1}{n} (-1)^{\frac{n-1}{2}} \cos \frac{n \pi x}{a} \tag{4}$$

convergent for $-\frac{a}{2} < x < \frac{a}{2}$, is used to represent the right hand side of Equation (2). When Equations (3) and (4) are substituted into Equation (2) and the Fourier coefficients on each side are equated, the following set of differential equations are found for $w_n(y)$ for the odd values of n only:*

$$w_n'' - 2\left(\frac{n\pi}{a}\right)^2 w_n'' + \left(\frac{n\pi}{a}\right)^4 w_n = (-1)^{\frac{n-1}{2}} \frac{4 q_0}{n \pi D} \left(1 - \bar{k} \frac{y}{b}\right) \tag{5}$$

$$n = 1, 3, 5, \ldots$$

For n even, the $w_n(y)$ are identically zero because of the symmetry of the loading and the boundary conditions. For n odd, the dimensionless variables μ and β are defined for convenience as follows:

$$\mu \equiv \frac{\pi b}{a} \; ; \quad \beta = \frac{n \pi y}{b} \equiv n \mu y / b$$

and we let (6)

$$w_n (y) \equiv \bar{w}_n (\beta)$$

Then Equation (5) can be written

$$\bar{w}_n'' - 2 \bar{w}_n'' + \bar{w}_n = (-1)^{\frac{n-1}{2}} \frac{\bar{q}}{n^5} \left(1 - \frac{\bar{k} \beta}{n \mu}\right) \tag{7}$$

$$n = 1, 3, 5, \ldots$$

where $\bar{q} \equiv \frac{4 q_0}{\pi D} \left(\frac{a}{\pi}\right)^4$.

* Primes indicate differentiation.

Now substituting the Fourier series of Equation (3) into the well-known formulas [1] for the stress resultants, i.e., for moment, shear and edge reaction distributions (see Figure 2), leads to Equations (9) through (18) below.

$$M_x(x,y) = -D\left(\frac{\partial^2 w}{\partial x^2} + \mu\frac{\partial^2 w}{\partial y^2}\right) = D\sum_{n=1,3,\ldots}^{\infty}\left(\frac{n\pi}{a}\right)^2\left[\bar{w}_n(\beta) - \mu\,\bar{w}_n''(\beta)\right]\cos\frac{n\pi x}{a} \tag{9}$$

$$M_y(x,y) = -D\left(\frac{\partial^2 w}{\partial y^2} + \mu\frac{\partial^2 w}{\partial x^2}\right) = -D\sum_{n=1,3,\ldots}^{\infty}\left(\frac{n\pi}{a}\right)^2\left[\bar{w}_n''(\beta) - \mu\,\bar{w}_n(\beta)\right]\cos\frac{n\pi x}{a} \tag{10}$$

$$M(x,y) = \frac{M_x + M_y}{1+\mu} = -D\left[\frac{\partial^2 w}{\partial x^2} + \frac{\partial^2 w}{\partial y^2}\right] = D\sum_{n=1,3,\ldots}^{\infty}\left(\frac{n\pi}{a}\right)^2\left[\bar{w}_n(\beta) - \bar{w}_n''(\beta)\right]\cos\frac{n\pi x}{a} \tag{11}$$

$$Q_x(x,y) = \frac{\partial M}{\partial x} = -D\sum_{n=1,3,\ldots}^{\infty}\left(\frac{n\pi}{a}\right)^3\left[\bar{w}_n(\beta) - \bar{w}_n''(\beta)\right]\sin\frac{n\pi x}{a} \tag{12}$$

$$Q_y(x,y) = \frac{\partial M}{\partial y} = D\sum_{n=1,3,\ldots}^{\infty}\left(\frac{n\pi}{a}\right)^3\left[\bar{w}_n'(\beta) - \bar{w}_n'''(\beta)\right]\cos\frac{n\pi x}{a} \tag{13}$$

$$M_{xy}(x,y) = -M_{yx}(x,y) = D(1-\mu)\frac{\partial^2 w}{\partial x\,\partial y} = -D(1-\mu)\sum_{n=1,3,\ldots}^{\infty}\left(\frac{n\pi}{a}\right)^2 w_n'(\beta)\sin\frac{n\pi x}{a} \tag{14}$$

$$V_x = -D\left[\frac{\partial^3 w}{\partial x^3} + (2-\mu)\frac{\partial^3 w}{\partial x\,\partial y^2}\right] = -D\sum_{n=1,3,\ldots}^{\infty}\left(\frac{n\pi}{a}\right)^3\left[\bar{w}_n(\beta) - (2-\mu)\,\bar{w}_n''(\beta)\right]\sin\frac{n\pi x}{a} \tag{15}$$

$$V_y = -D\left[\frac{\partial^3 w}{\partial y^3} + (2-\mu)\frac{\partial^2 w}{\partial y\,\partial x^2}\right] = -D\sum_{n=1,3,\ldots}^{\infty}\left(\frac{n\pi}{a}\right)^3\left[\bar{w}_n'''(\beta) - (2-\mu)\,\bar{w}_n'(\beta)\right]\cos\frac{n\pi x}{a} \tag{16}$$

The concentrated corner reaction forces are found from Equation (14) above through the relations (cf. [1] page 92):

$$R(a/2,\,0) = -2\,M_{xy}(a/2,\,0) \tag{17}$$

$$R(a/2,\,b) = 2\,M_{xy}(a/2,\,b) \tag{18}$$

The edge y = 0 is assumed simply supported while the edge y = b is assumed free. The boundary conditions are then (using Equations (10) and (16)):

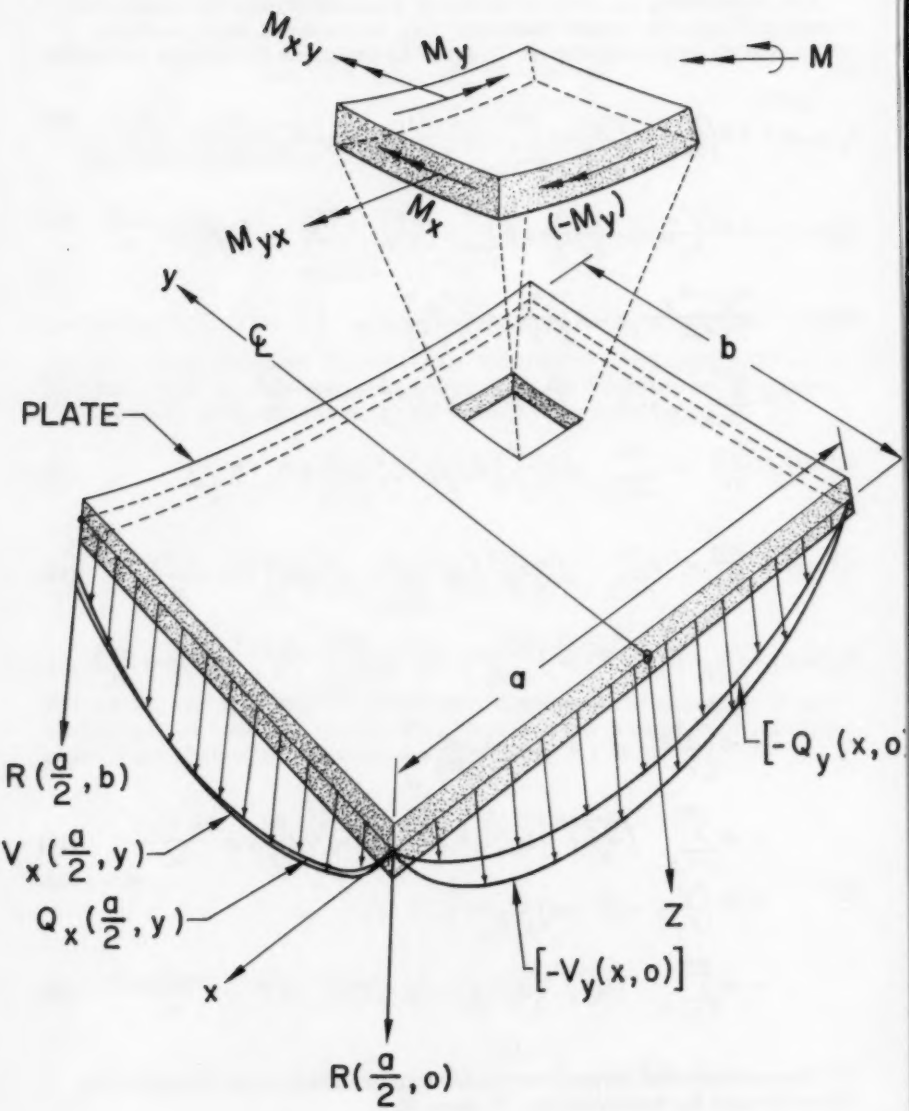

Figure 2. Sign Convention for Plate Stress Resultants.

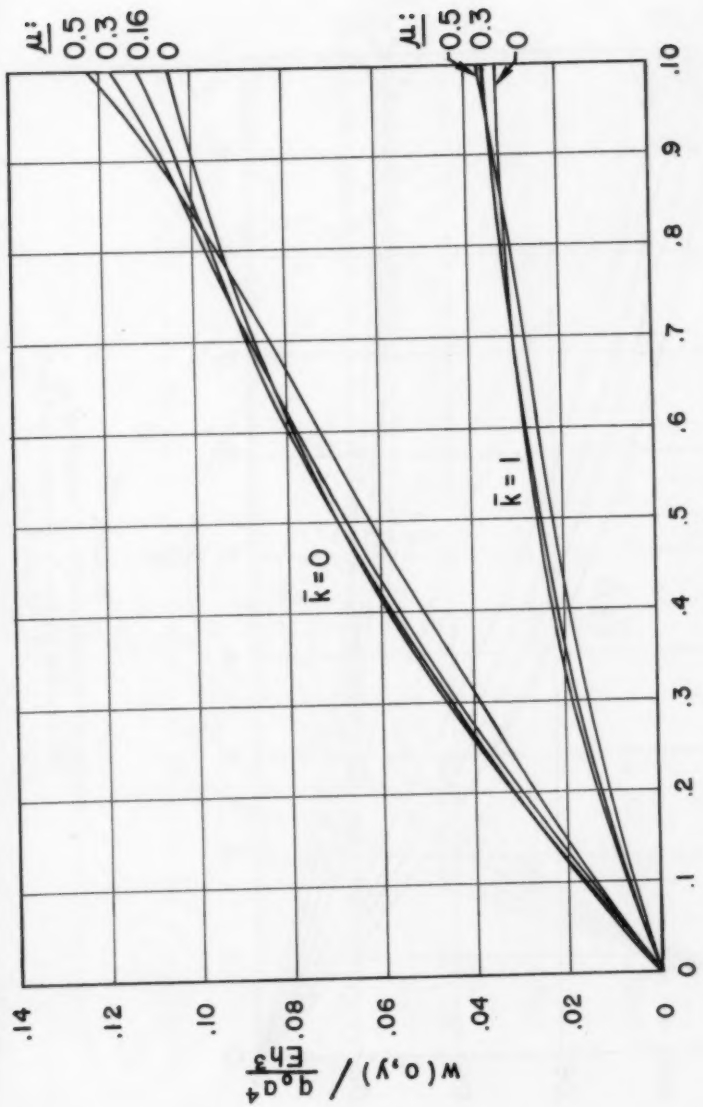

Figure 3
CENTERLINE DEFLECTION w(0, y)
For Various Poisson's Ratios; b/a = 0.75,
k̄ = 0 and k̄ = 1

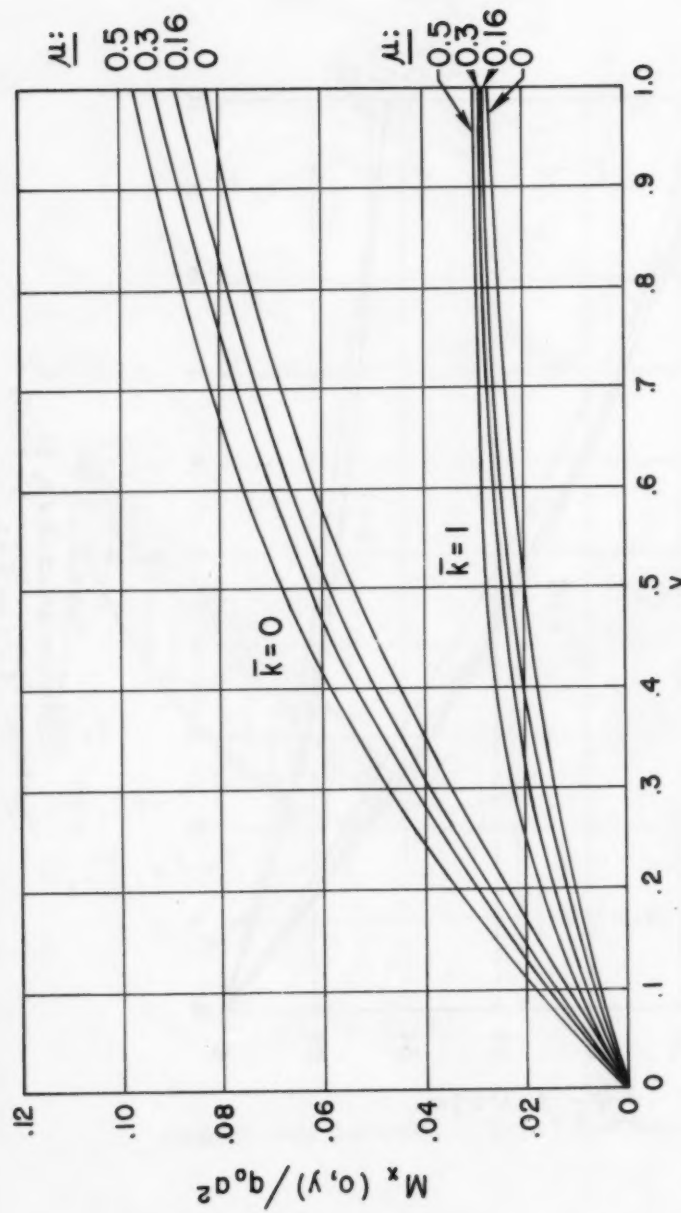

Figure 4
CENTERLINE BENDING MOMENT DISTRIBUTION M_x (0, y)
For Various Poisson's Ratios; b/a = 0.75,
$\bar{k}$ = 0 and $\bar{k}$ = 1

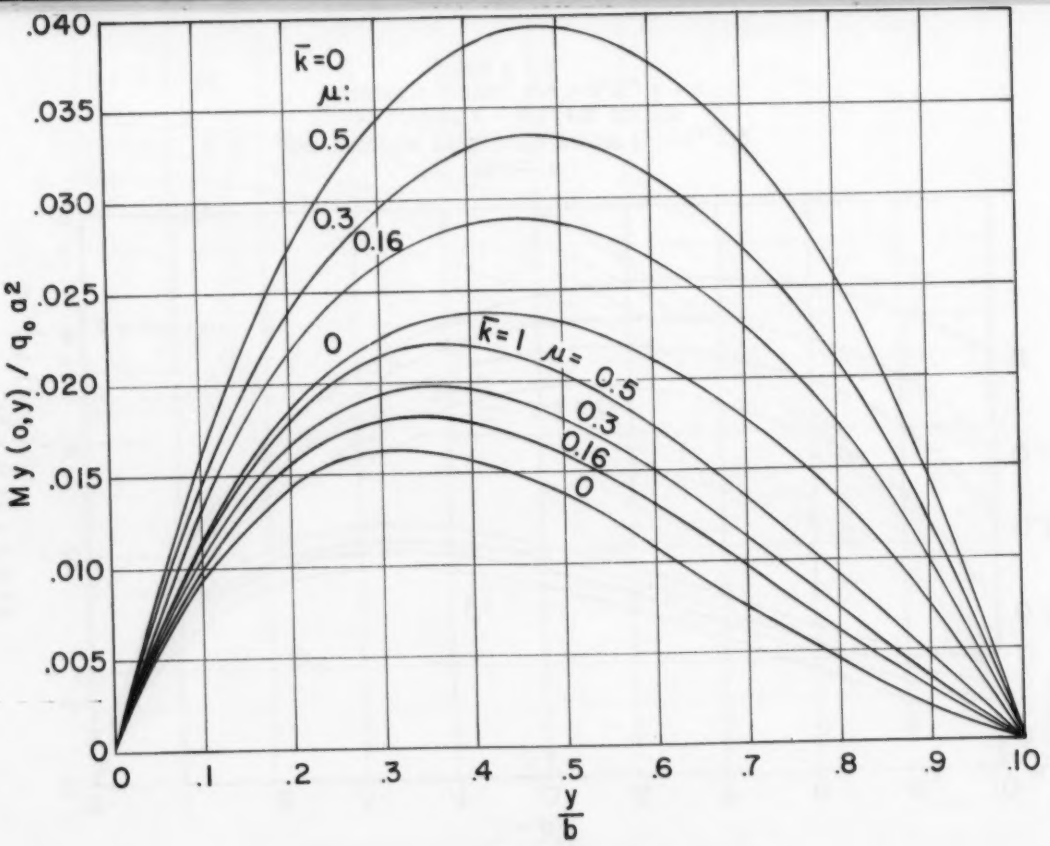

Figure 5

CENTERLINE BENDING MOMENT DISTRIBUTION M_y (0, y)
For Various Poisson's Ratios; b/a = 0.75,
$\bar{k}$ = 0 and $\bar{k}$ = 1

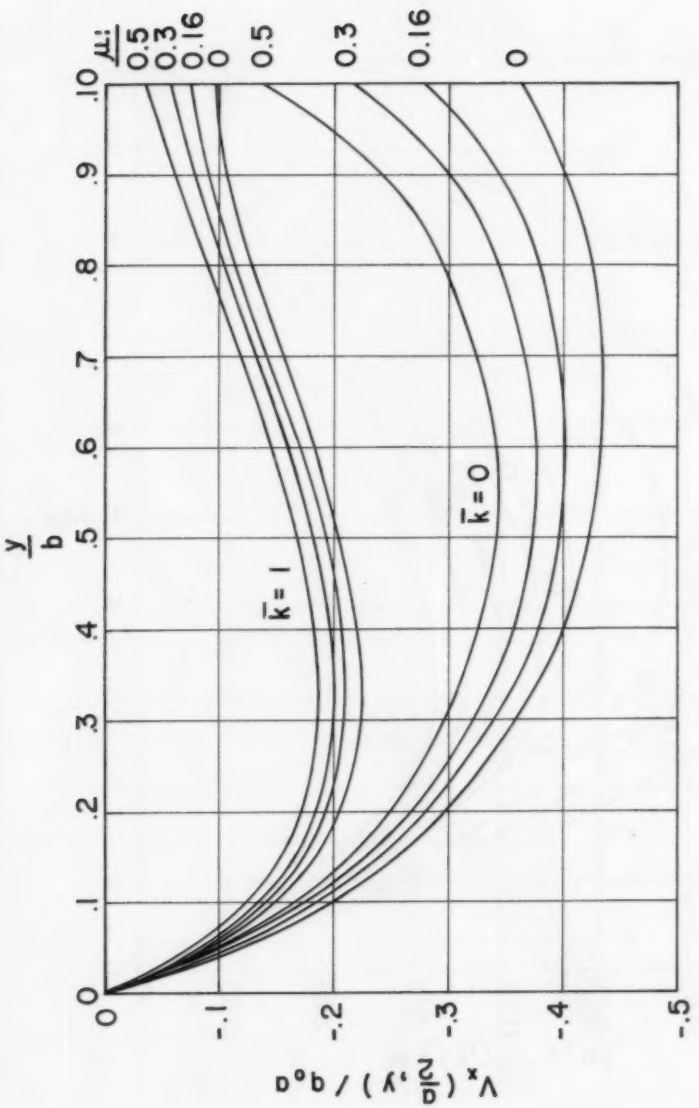

Figure 6
EDGE REACTION FORCE DISTRIBUTION $V_x(a/2, y)$,
AT SUPPORT x = a/2, FOR VARIOUS
POISSON'S RATIOS; b/a = 0.75, $\bar{k}$ = 0
AND $\bar{k}$ = 1

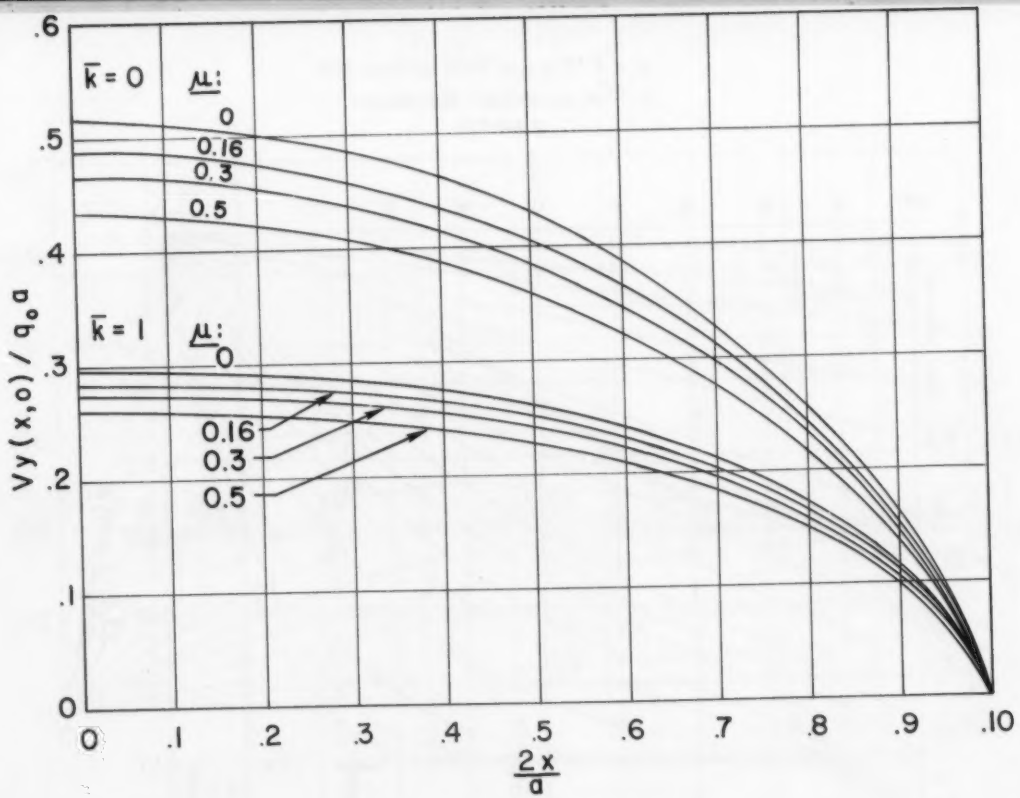

Figure 7
EDGE REACTION FORCE DISTRIBUTION V_y (0, x),
AT SUPPORT y = 0, FOR VARIOUS POISSON'S RATIOS;
b/a = 0.75, $\bar{k}$ = 0 AND $\bar{k}$ = 1

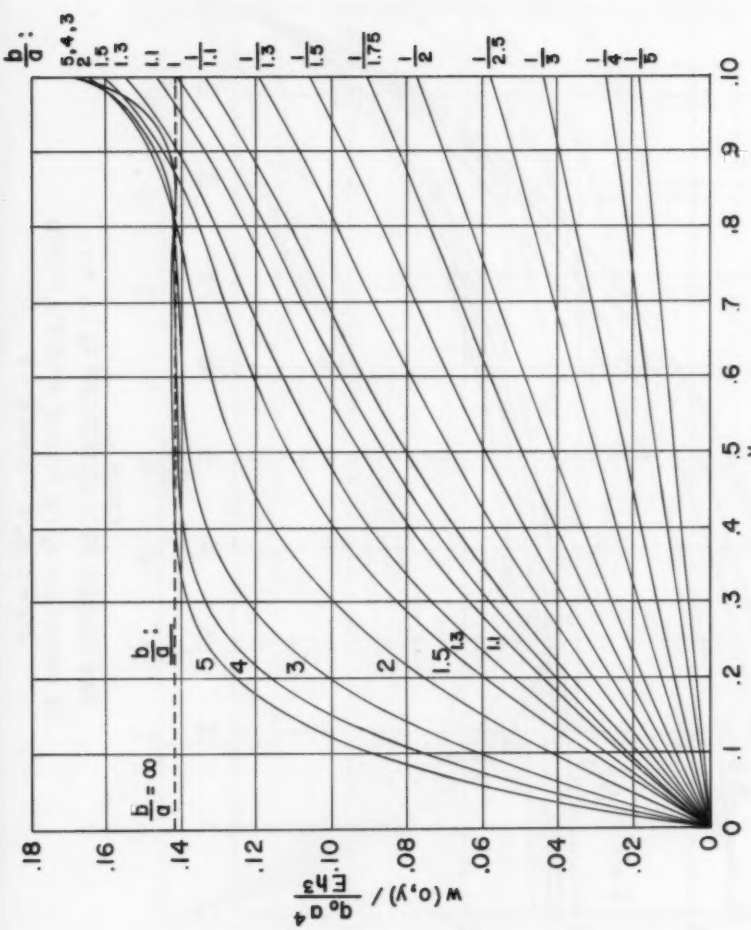

Figure 8

CENTERLINE DEFLECTION w(0, y)

FOR VARIOUS b/a; μ = 0.3, $\tilde{k}$ = 0

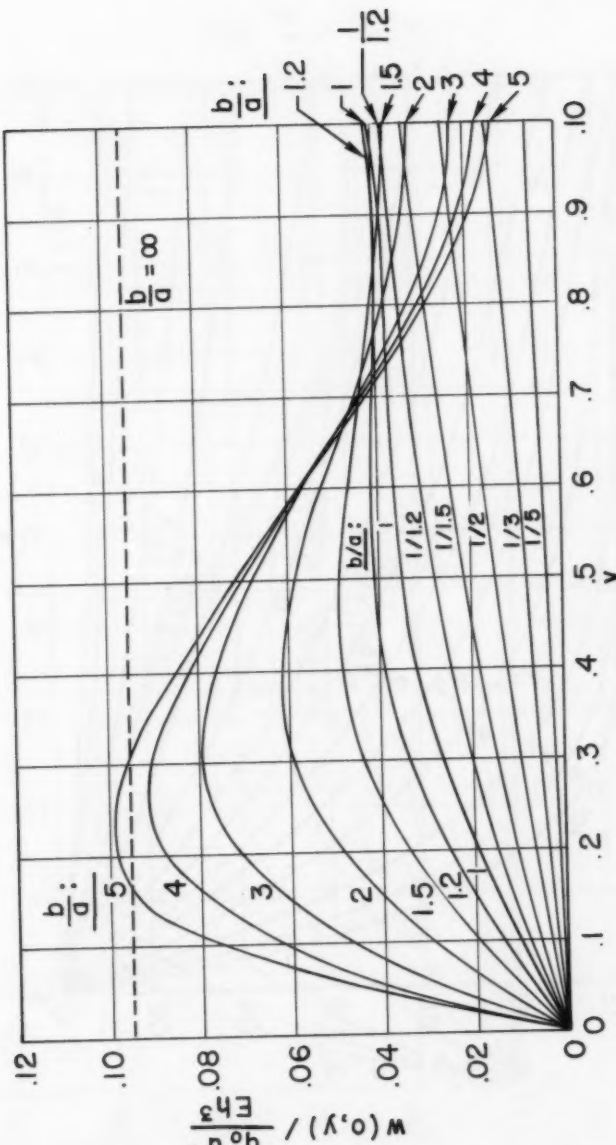

Figure 9
CENTERLINE DEFLECTION w(0,y)
FOR VARIOUS b/a; μ = 0.3, k = 1

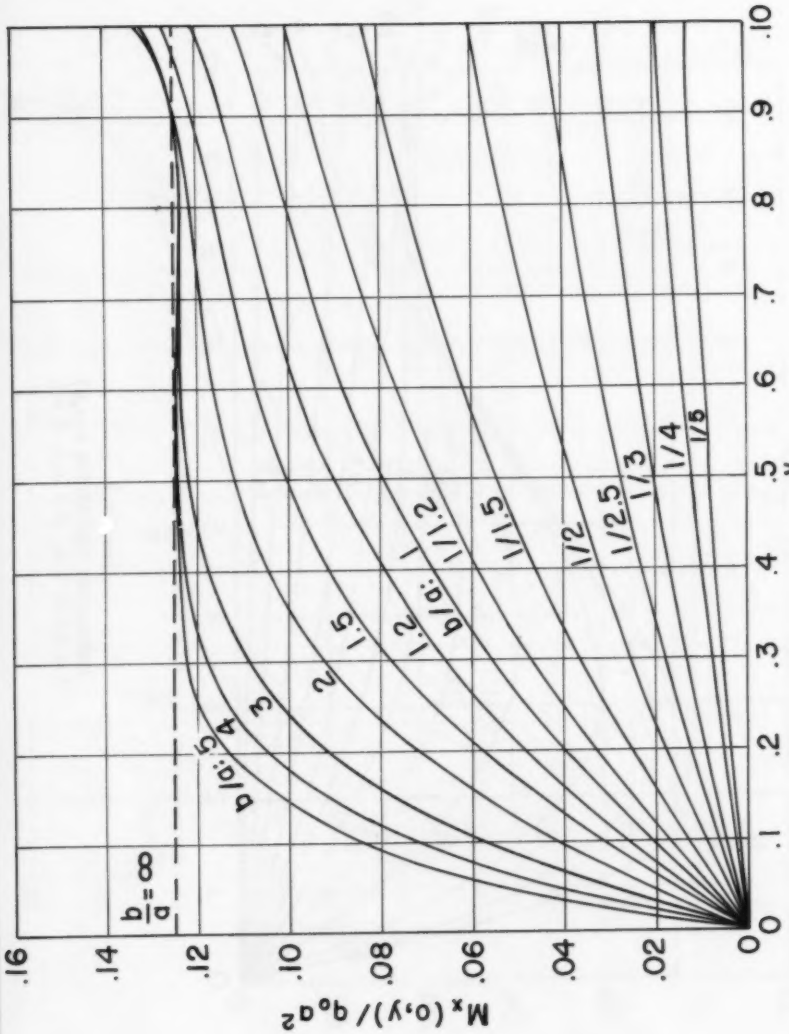

Figure 10

CENTERLINE BENDING MOMENT DISTRIBUTION M_x (0,y)

FOR VARIOUS b/a; $\mu = 0.3$, E=0

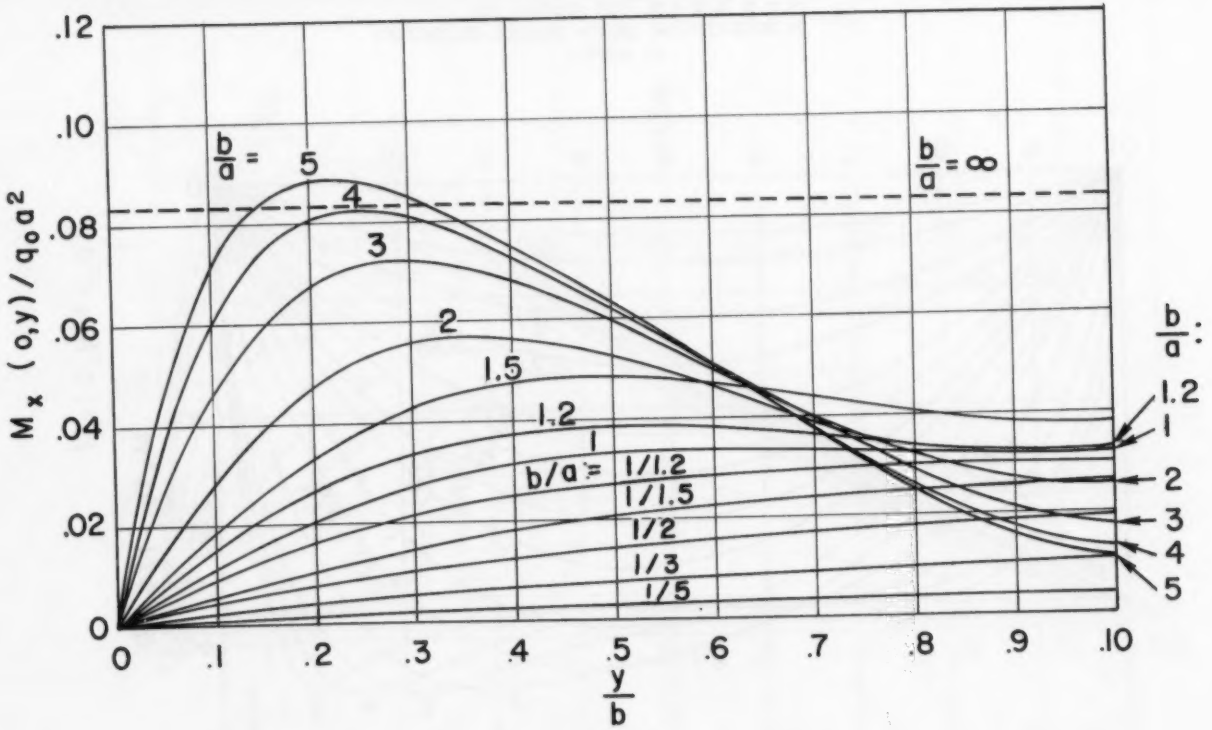

Figure 11
CENTERLINE BENDING MOMENT DISTRIBUTION M_x 0,y)
FOR VARIOUS b/a; $\mu = 0.3$, $\bar{k} = 1$

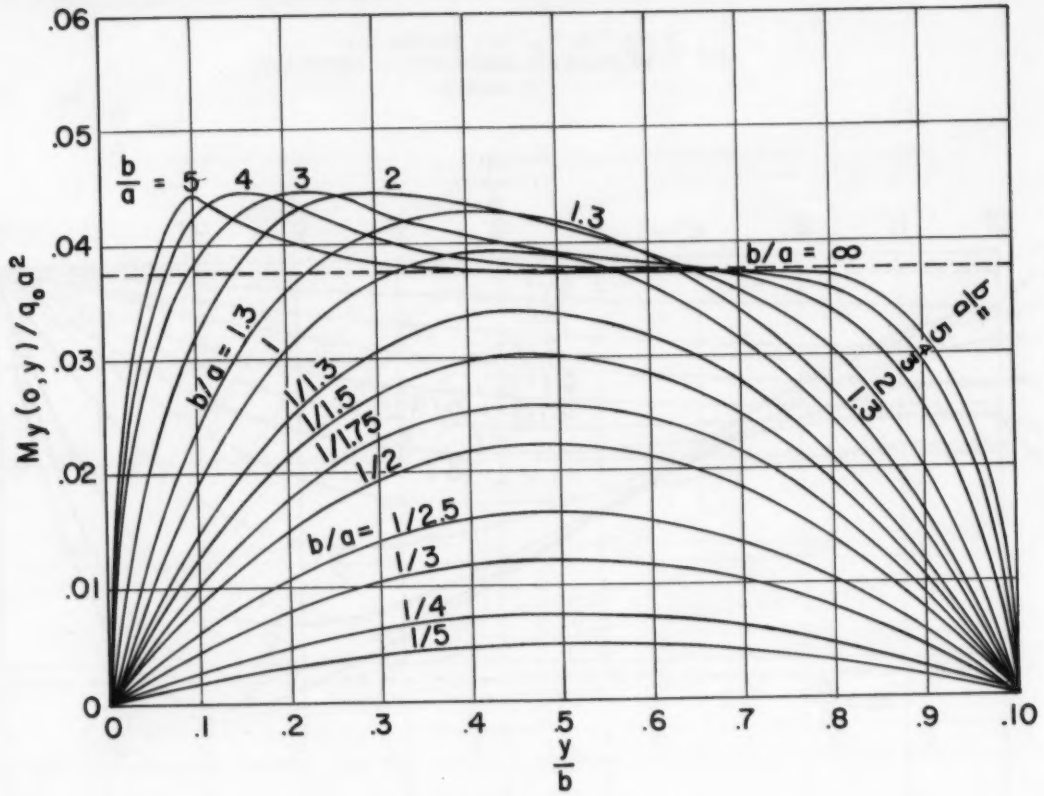

Figure 12
CENTERLINE BENDING MOMENT DISTRIBUTION M_y 0,y)
FOR VARIOUS b/a; $\mu = 0.3$, $\bar{k} = 0$

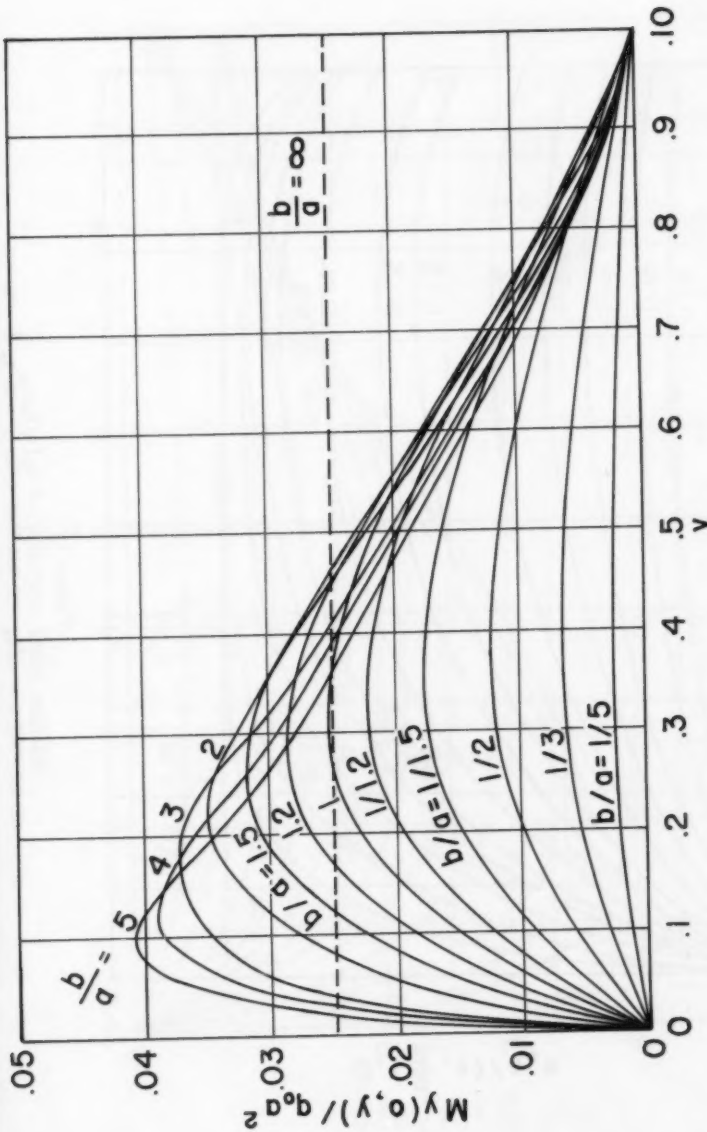

Figure 13
CENTERLINE BENDING MOMENT DISTRIBUTION $M_y(0,y)$
FOR VARIOUS b/a; $\mu = 0.3$, $K = 1$

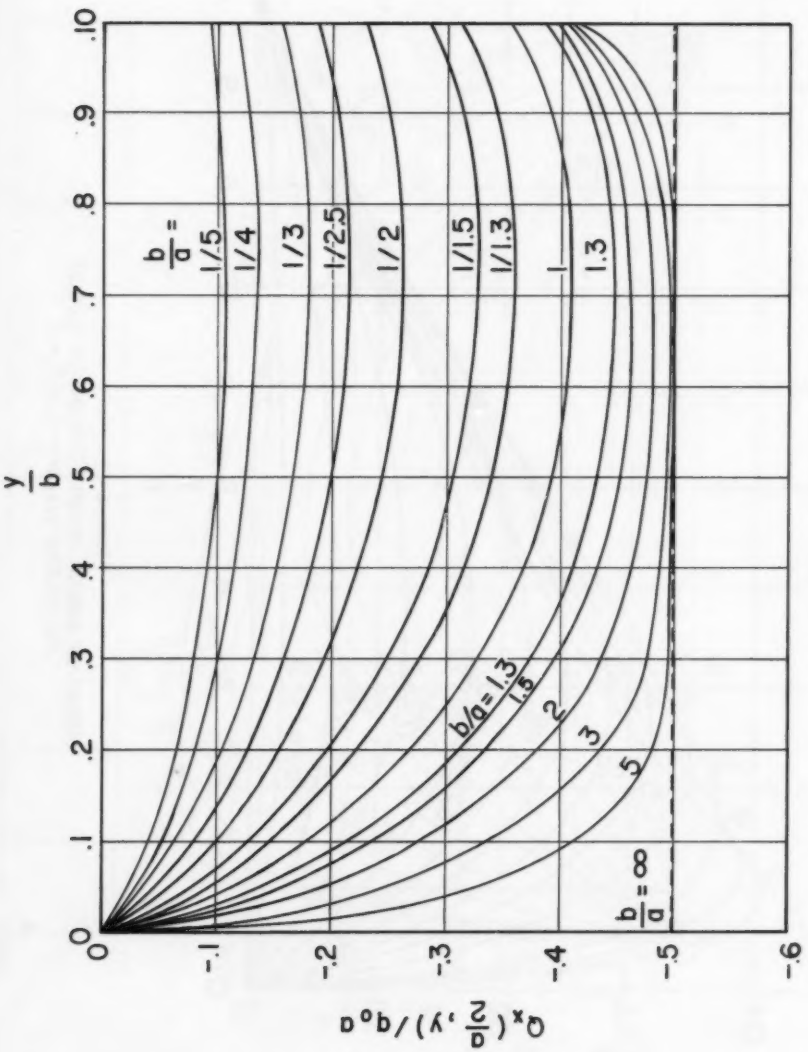

Figure 14
SHEARING FORCE DISTRIBUTION $Q_x(a/2,y)$, AT SUPPORT x = a/2, FOR VARIOUS b/a; μ = 0.3, k = 0

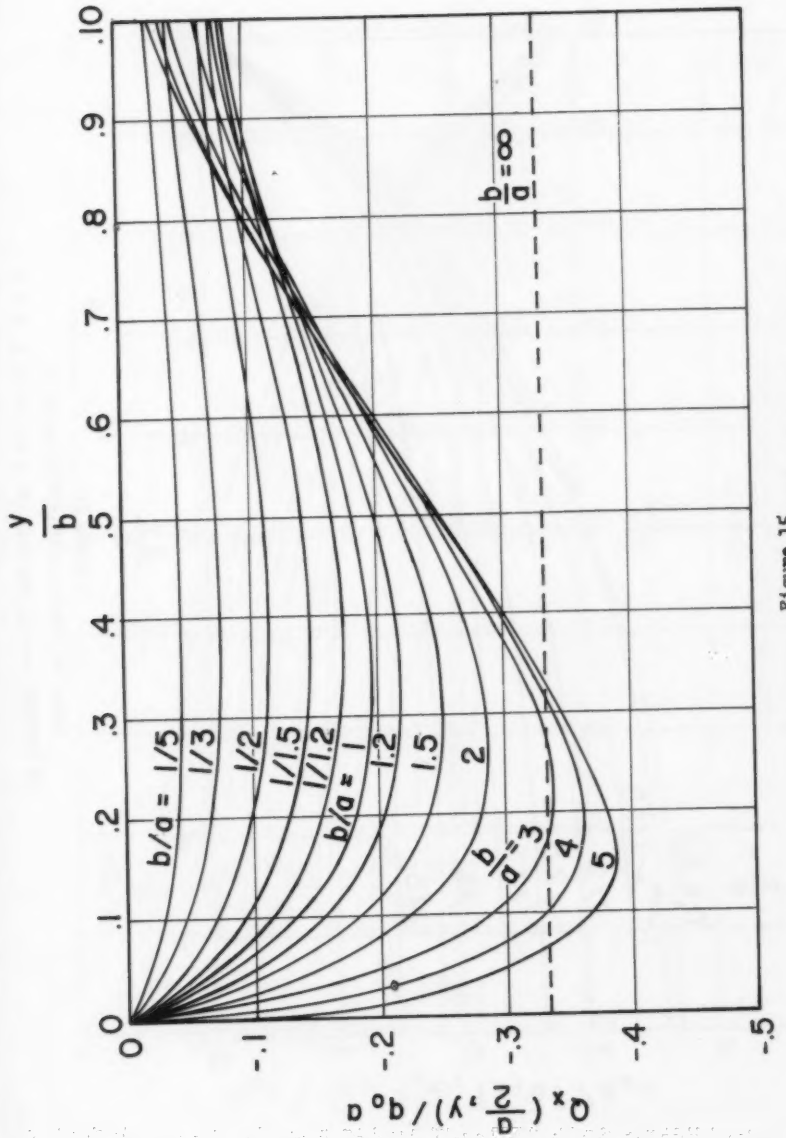

Figure 15
SHEARING FORCE DISTRIBUTION $Q_x(a/2,y)$,
AT SUPPORT x = a/2, FOR VARIOUS b/a; μ=0.3, k = 1

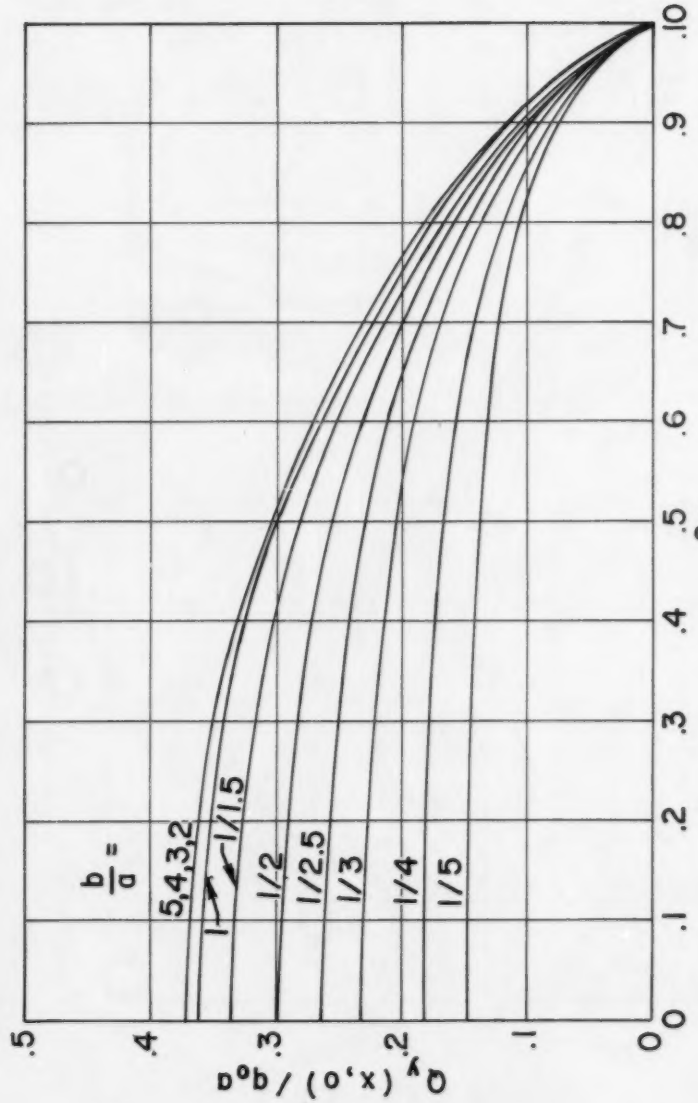

Figure 16
SHEARING FORCE DISTRIBUTION $Q_y(x,0)$,
AT SUPPORT $y = 0$, FOR VARIOUS b/a; $\mu = 0.3$, $\bar{k} = 0$

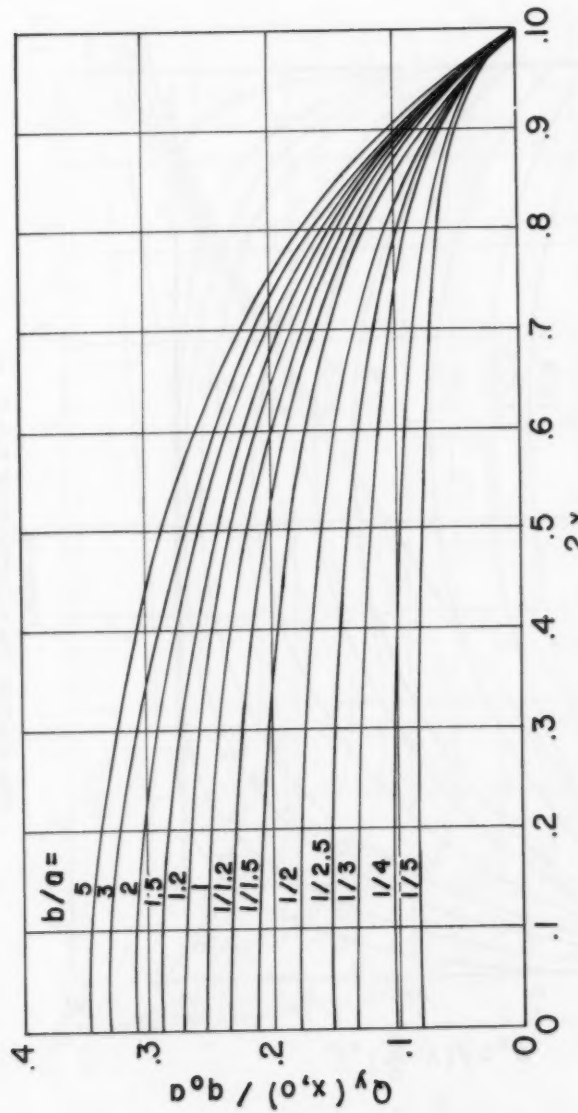

Figure 17
SHEARING FORCE DISTRIBUTION $Q_y(x,0)$,
AT SUPPORT $y = 0$, FOR VARIOUS b/a; $\mu = 0.3$, $k = 1$

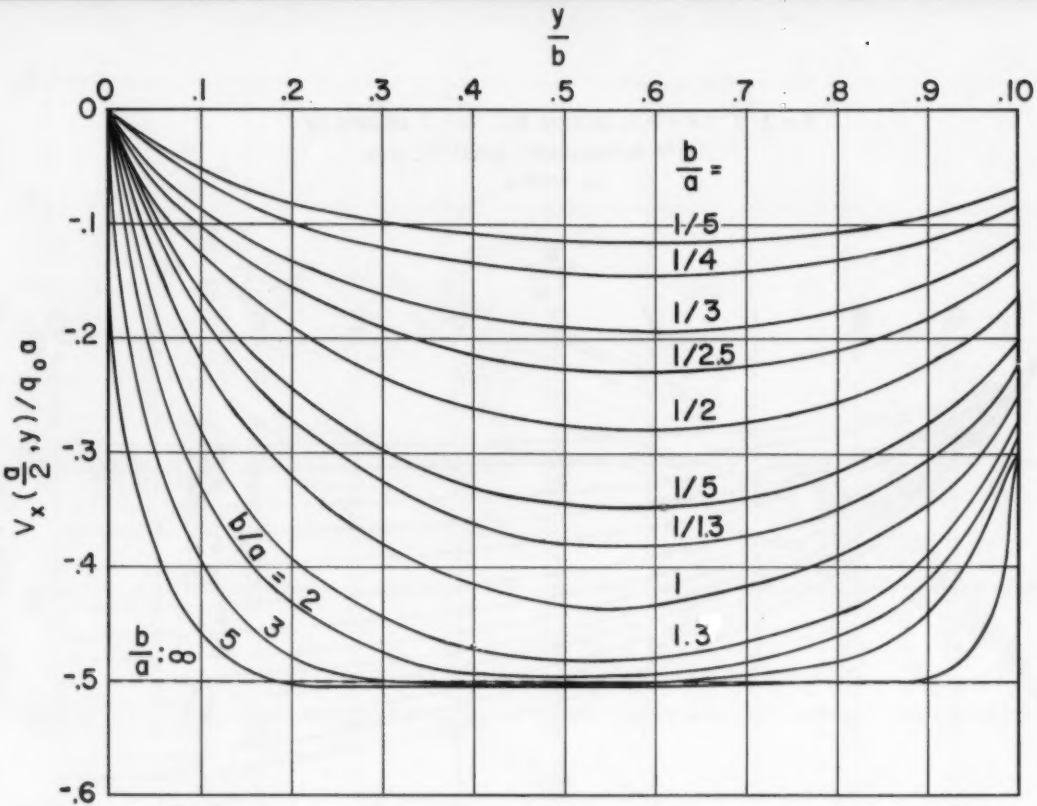

Figure 18

EDGE REACTION FORCE DISTRIBUTION $V_x(a/2, y)$,

AT SUPPORT x = a/2, FOR VARIOUS b/a; $\mu = 0.3$, $\bar{k} = 0$

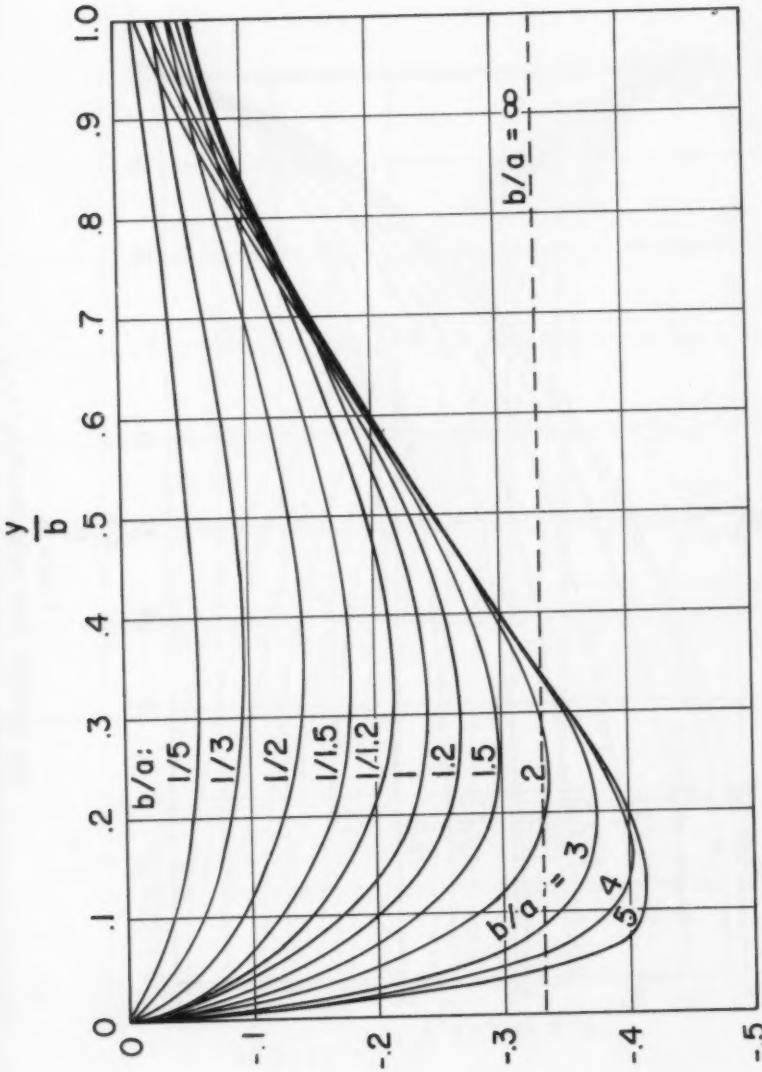

Figure 19

EDGE REACTION FORCE DISTRIBUTION $V_x(a/2, y)$, AT SUPPORT $x = a/2$, FOR VARIOUS b/a; $\mu = 0.3$, $k = 1$

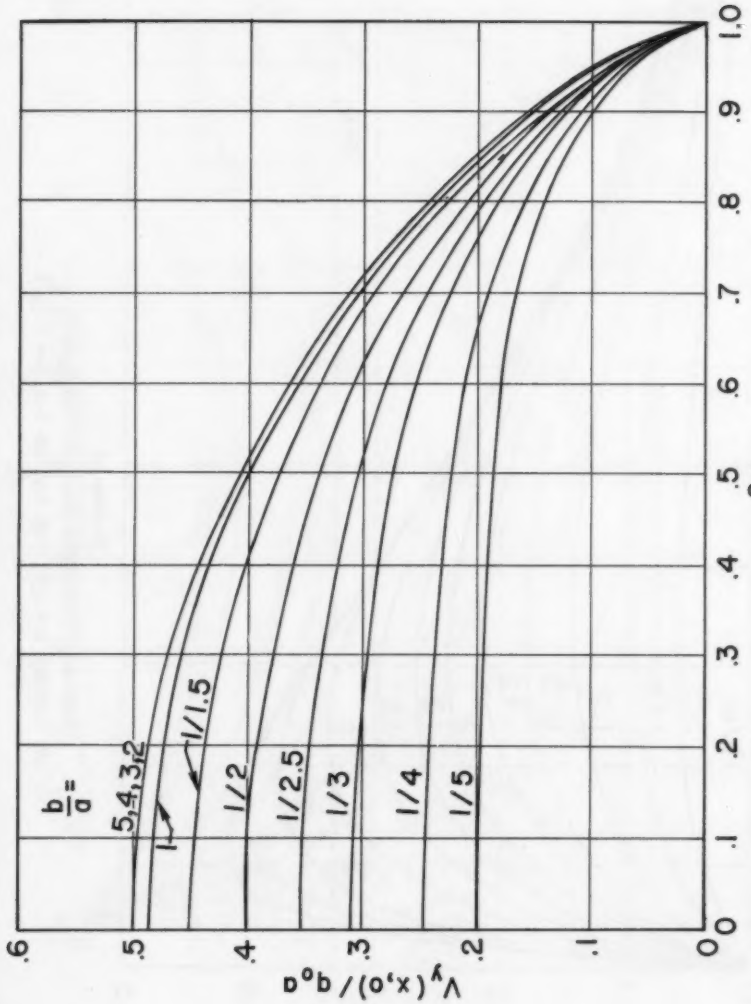

Figure 20

EDGE REACTION FORCE DISTRIBUTION $V_y(0,x)$, AT SUPPORT $y = 0$, FOR VARIOUS b/a; $\mu = 0.3$, $k = 0$

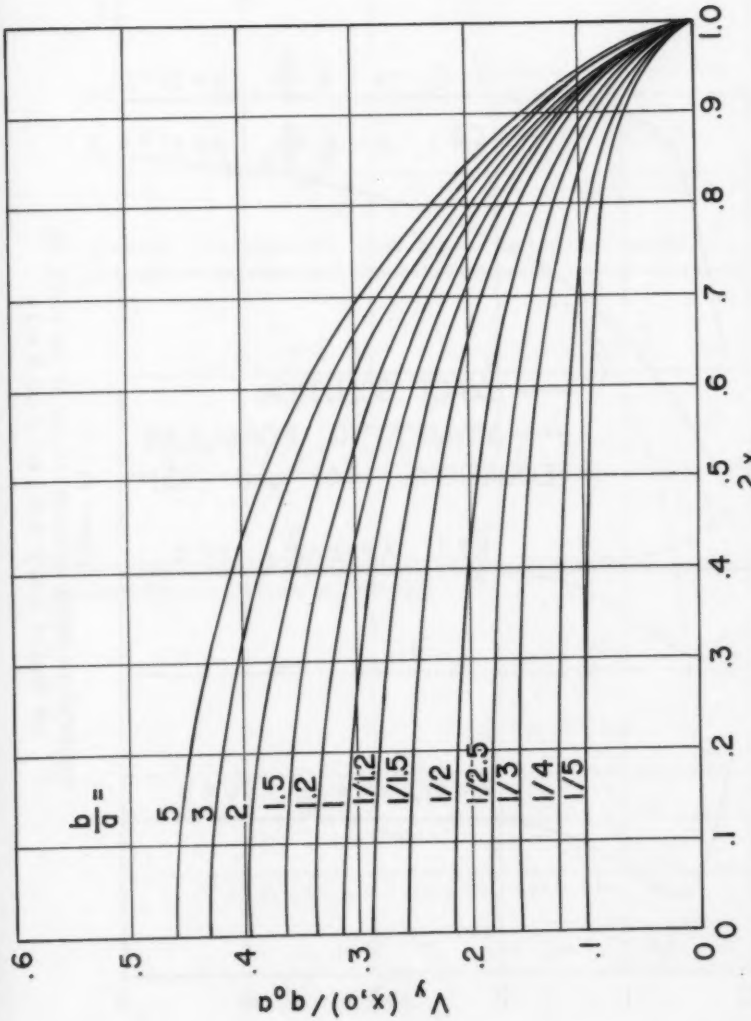

Figure 21
EDGE REACTION FORCE DISTRIBUTION $V_y(O, x)$,
AT SUPPORT $y = O$, FOR VARIOUS b/ε_1, $\mu = 0.3$, $K = 1$

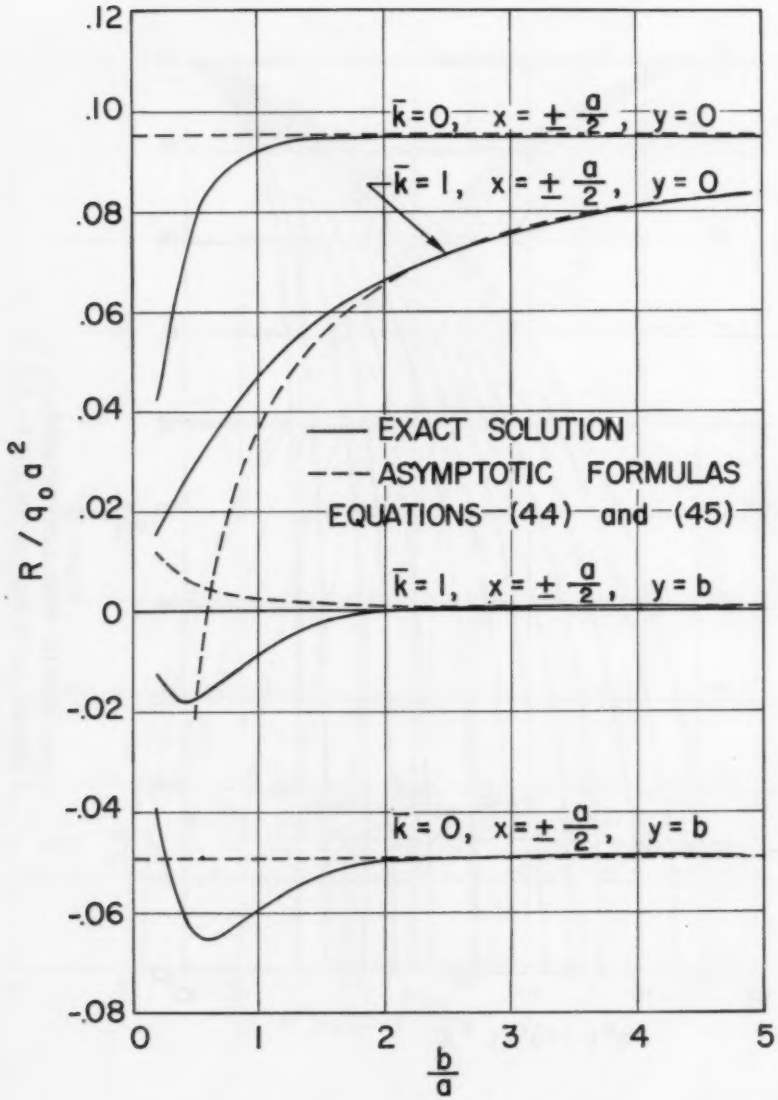

Figure 22
CONCENTRATED CORNER REACTIONS R(a/2, 0) and R(a/2, b)
FOR VARIOUS b/a; μ = 0.3 k = 0 and k̄ = 1

$y = 0$

$$\left.\begin{aligned} w(x,0) &= 0 \\ M_y &= 0 \end{aligned}\right\} \Longrightarrow \quad \begin{aligned} \bar{w}_n(0) &= 0 \\ \bar{w}_n''(0) &= 0 \end{aligned} \qquad (19\ a,b)$$

$y = b$

$$\left.\begin{aligned} M_y &= 0 \\ V_y &= 0 \end{aligned}\right\} \Longrightarrow \quad \begin{aligned} \bar{w}_n''(n\pi) - \mu\,\bar{w}(n\pi) &= 0 \\ \bar{w}'''(n\pi) - (2-\mu)\,\bar{w}_n'(n\pi) &= 0 \end{aligned} \qquad (20\ a,b)$$

The solution of Equation (7), which also satisfies the boundary conditions (19 a,b), can be expressed in the following form:

$$\bar{w}_n(\beta) = \frac{1}{2}(-1)^{\frac{n-1}{2}} \frac{\bar{q}}{n^5} \left\{ 2\left[1 - \frac{\bar{k}\beta}{n\pi}\right] + \left[A_n + D_n\beta\right]e^{\beta} - \left[2 + A_n + \beta(1 - D_n)\right] e^{-\beta} \right\} \qquad (21)$$

$$n = 1, 3, \ldots$$

By substituting Equation (21) into Equations (20 a,b) there results two linear equations for coefficients A_n and D_n:

$$a_{1n} A_n + d_{1n} D_n = g_{1n} \qquad (22)$$

$$a_{2n} A_n + d_{2n} D_n = g_{2n} \qquad (23)$$

where

$$a_{1n} = (1-\mu)\sinh n\pi$$

$$d_{1n} = 2\sinh n\pi + (1-\mu)\, n\pi \cosh n\pi$$

$$g_{1n} = \left[\frac{1-\mu}{2} n\pi - \mu\right] e^{-n\pi} + \mu(1-\bar{k})$$

$$a_{2n} = (1-\mu)\cosh n\pi$$

$$d_{2n} = (1-\mu)\, n\pi \sinh n\pi - (1+\mu)\cosh n\pi$$

$$g_{2n} = -\frac{1}{2}\left[3 - \mu + (1-\mu) n\pi\right] e^{-n\pi} + \left(\frac{2-\mu}{n\pi}\right)\bar{k}$$

A_n and D_n can be found explicitly by Cramer's Rule, but a better method for purposes of computation is to express them as a series in ascending powers of e^{-nu}. The leading terms in these series have the form

$$A_n = 2\,\frac{\mu[1+\mu-(1-\mu)n\alpha](1-\bar{k})+[2+(1-\mu)n\alpha]\left(\frac{2-\mu}{n\alpha}\right)\bar{k}}{(3+\mu)(1-\mu)}\,e^{-n\alpha} + O\left((n\alpha)^2 e^{-2n\alpha}\right) \tag{24}$$

$$D_n = 2\,\frac{\mu(1-\bar{k})-\left(\frac{2-\mu}{n\alpha}\right)\bar{k}}{3+\mu}\,e^{-n\alpha} + O\left(n\alpha e^{-2n\alpha}\right) \tag{25}$$

The form of Equation (21) is superior to the conventional expression* employing hyperbolic sines and cosines. The latter is unsatisfactory particularly for computing numerical value from the series for distributed edge reactions, where more than just the first few terms are included in the sum. For $w_n(y)$ and its derivatives, in the interval $0 \leqq y/b \leqq 1$, the expression within the curley brackets on the right hand side of Equation (21) remains bounded as n increases. Each of the separately computed terms, which must be summed to form this expression, are also bounded. These observations can be easily verified by using Equations (24) and (25). Hence, because of the form we have used, it follows that for any value of n there will be no loss of significant figures in the sum through subtraction of large magnitudes. However, if the hyperbolic sines and cosines are used, these quantities become exponentially large with increasing n and cause the number of significant figures obtained in the sum to decrease (even to zero!) as n increases. This behavior would seriously affect the automatic computation program described in the following section.

Computation of Series

a) Using Equation (21) with Equation (9) through (18), the deflections and stress resultants throughout the plate can be calculated. In the following formulas, use is made of sums in closed form for certain simple trigonometric series; these are given in Appendix A below. The series for plate deflections is

$$w(x,y)\Big/\frac{q_0 a^4}{E h^3} = (1-\bar{k}\,y/b)\,\frac{1-\mu^2}{32}\left[5-6\left(\frac{2x}{a}\right)^2+\left(\frac{2x}{a}\right)^4\right] + \frac{24(1-\mu^2)}{\pi^5}\sum_{n=1,3,\ldots}^{\infty}\frac{(-1)^{\frac{n-1}{2}}}{n^5}\left\{\left[A_n + D_n\,n\alpha\,y/b\right]e^{n\alpha y/b} - \left[A_n + 2 + (1-D_n)n\alpha\,y/b\right]e^{-n\alpha y/b}\right\}\cos\frac{n\pi x}{a} \tag{26}$$

* See, for example, [1] Section 42, Equation (f).

The stress resultants of greatest numerical interest for engineering purposes were taken as listed in Table I below, and explicit series for these quantities follow in Equations (27) through (36). The uniform convergence of these series can be demonstrated with the use of Equations (24) and (25).

Range		Quantity
$x = 0;$	$0 \leq y \leq b$	w, M_x, M_y
$x = a/2;$	$0 \leq y \leq b$	V_x, M_{xy}, Q_x
$y = 0;$	$0 \leq x \leq a/2$	V_y, Q_y
$y = b;$	$0 \leq x \leq a/2$	M_x
$x = a/2;$	$y = 0, y = b$	R

TABLE I

The physical quantity is obtained by multiplying the computed number on the right by a dimensional factor; the dimensionless ratios were chosen to agree with Timoshenko ([1], Section 42, particularly Table 28).

$$w(0,y)/\frac{q_0 a^4}{Eh^3} = \frac{5(1-\mu^2)}{32}(1-\bar{k}y/b) + \frac{24(1-\mu^2)}{\pi^5}\sum_{n=1,3..}^{\infty} \frac{(-1)^{\frac{n-1}{2}}}{n^5}\left\{[A_n + D_n n\alpha y/b]e^{n\alpha y/b} - [A_n + 2 + (1-D_n)n\alpha y/b]e^{-n\alpha y/b}\right\} \quad (27)$$

$$M_x(0,y)/q_0 a^2 = \frac{1}{8}(1-\bar{k}y/b) + \frac{2}{\pi^3}\sum_{n=1,3,}^{\infty} \frac{(-1)^{\frac{n-1}{2}}}{n^3}\left\{[(1-\mu)A_n - D_n[2\mu - (1-\mu)n\alpha y/b]]e^{n\alpha y/b} - [(1-\mu)(A_n+2) + (1-D_n)[2\mu + (1-\mu)n\alpha y/b]]e^{-n\alpha y/b}\right\} \quad (28)$$

$$M_y(0,y)/q_0a^2 = \frac{\mu}{8}\left(1-\bar{k}\,y/b\right) - \frac{2}{\pi^3}\sum_{n=1,3,\ldots}^{\infty}\frac{(-1)^{\frac{n-1}{2}}}{n^3}\Big\{$$

$$\left[(1-\mu)A_n + D_n\left[2+(1-\mu)n\pi y/b\right]\right]e^{n\pi y/b} -$$

$$\left[(1-\mu)(A_n+2) - (1-D_n)\left[2-(1-\mu)n\pi y/b\right]\right]e^{-n\pi y/b}\Big\} \tag{29}$$

$$Q_x(a/2,y)/q_0a = -\frac{1}{2}\left(1-\bar{k}\,y/b\right) + \frac{4}{\pi^2}\sum_{n=1,3,\ldots}^{\infty}\frac{1}{n^2}\Big\{$$

$$D_n e^{n\pi y/b} + (1-D_n)e^{-n\pi y/b}\Big\} \tag{30}$$

$$V_x(a/2,y)/q_0a = -\frac{1}{2}\left(1-\bar{k}\,y/b\right) + \frac{2}{\pi^2}\sum_{n=1,3,}^{\infty}\frac{1}{n^2}\Big\{$$

$$\left[(1-\mu)A_n + D_n\left[2(2-\mu)+(1-\mu)n\pi y/b\right]\right]e^{n\pi y/b}$$

$$-\left[(1-\mu)(A_n+2) - (1-D_n)\left[2(2-\mu)\right.\right.$$

$$\left.\left.-(1-\mu)n\pi y/b\right]\right]e^{-n\pi y/b}\Big\} \tag{31}$$

$$M_{xy}(a/2,y)/q_0a^2 = \bar{k}\,\frac{\pi(1-\mu)}{24\pi} - \frac{2(1-\mu)}{\pi^3}\sum_{n=1,3,\ldots}^{\infty}\frac{1}{n^3}\Big\{$$

$$\left[A_n + D_n\left(1+n\pi y/b\right)\right]e^{n\pi y/b}$$

$$+\left[A_n + 2 - (1-D_n)\left(1-n\pi y/b\right)\right]e^{-n\pi y/b}\Big\} \tag{32}$$

$$R(a/2, b)/q_0 a^2 = \frac{\pi(1-\mu)}{12u}\bar{k} - \frac{4(1-\mu)}{\pi^3}\sum_{n=1,3,}^{\infty}\frac{1}{n^3}\Big\{$$

$$[A_n + D_n(1+nu)]e^{nu} + [A_n + 2 - (1-D_n)(1-nu)]e^{-nu}\Big\} \tag{33a}$$

$$R(a/2, 0)/q_0 a^2 = -\frac{\pi(1-\mu)}{12u}\bar{k} + \frac{8(1-\mu)}{\pi^3}\sum_{n=1,3,}^{\infty}\frac{A_n + D_n + 1/2}{n^3} \tag{33b}$$

$$V_y(x, 0)/q_0 a = -\frac{(2-\mu)\pi\bar{k}}{8u}\left[1-\left(\frac{2x}{a}\right)^2\right] + \frac{4}{\pi^2}\sum_{n=1,3,\cdots}^{\infty}\frac{(-1)^{\frac{n-1}{2}}}{n^2}\Big\{$$

$$(1-\mu)A_n - (1+\mu)D_n\Big\}\cos\frac{n\pi x}{a} + \frac{2}{\pi^2}(3-\mu)f_2(x) \tag{34}$$

$$M_x(x, b)/q_0 a^2 = \frac{1}{8}(1-\bar{k})\left[1-\left(\frac{2x}{a}\right)^2\right] + \frac{2}{\pi^3}\sum_{n=1,3,\cdots}^{\infty}\frac{(-1)^{\frac{n-1}{2}}}{n^3}\Big\{$$

$$\Big[(1-\mu)A_n - D_n[2\mu - (1-\mu)nu]\Big]e^{nu} -$$

$$\Big[(1-\mu)(A_n+2) + (1-D_n)[2\mu + (1-\mu)nu]\Big]e^{-nu}\Big\}\cos\frac{n\pi x}{a} \tag{35}$$

$$Q_y(x, 0)/q_0 a = -\frac{\pi\bar{k}}{8u}\left[1-\left(\frac{2x}{a}\right)^2\right] - \frac{8}{\pi^2}\sum\frac{(-1)^{\frac{n-1}{2}}}{n^2}D_n\cos\frac{n\pi x}{a}$$

$$+ \frac{4}{\pi^2}f_2(x) \tag{36}$$

In Equations (34) and (36) above, $f_2(x)$ stands for the rapidly convergent series derived in Appendix A below.

b) The first nine* quantities listed in Table I were computed by an IBM Electronic Data Processing Machine, Model 701, which was programeed according to the Speedcode I manual. This program is capable of computing

* Concentrated corner reactions R were not computed individually as such, but were obtained from the computed twisting moments by use of Equations (33) and (34).

numerical values of the functions represented by the right hand sides of Equations (27) to (32) and (34) to (36) for arbitrary values of u, μ and $\bar{k}$. For predetermined values of these three parameters, a single run of the program computed simultaneously the nine functions at station values $\frac{2x}{a}$ or $\frac{y}{b}$ at intervals of 0.1 in the range 0 to 1.0.

In order to obtain uniform accuracy in all nine functions, the program made the following convergence test for the infinite series portion of each function:

$$\left| \frac{a_n}{S_n} \right| < \text{Convergence Factor} \qquad (37)$$

where a_n is the nth term of the series, S_n is the partial sum,

$$S_n = \sum_{j=1}^{n} a_j \qquad (38)$$

and the Convergence Factor, (abbreviated as C. F.) is a preassigned positive number. If the C. F. is sufficiently small, and if inequality (37) is satisfied for some value of n and for no smaller value, then the summation error at this n is found to be close to (although not necessarily bounded by) the C. F. The program computed successive partial sums for each series up to this value of n, which is generally different for different series and at different stations. In this way, the summation error was kept approximately uniform for all functions and over the entire plate.

A study was made to determine the optimum value for the convergence factor. Considerations of actual machine computing time, of machine round-off error and of limits on certain machine subprograms (e.g. calculation of exponentials), as well as consideration of the desired number of significant figures* were factors limiting the lowest value which could be taken for the convergence factor.

A series of runs for several values of u, k and μ and convergence factors of $2x10^{-3}$, $2x10^{-4}$, $2x10^{-5}$, $2x10^{-6}$, $2x10^{-7}$, were made. An examination of these results showed that the important function values were computed to five significant figures at interior points, and to at least four significant figures at corner points, if the convergence factor was $2x10^{-5}$. Decreasing the convergence factor to $2x10^{-6}$ was seen in some cases to cause a subprogram error to enter; choosing a larger convergence factor reduced the accuracy of edge and corner reaction calculations with little reduction in computing time. A convergence factor of $2x10^{-5}$ was chosen therefore as optimum. The computing time per "run" with this convergence factor was eight minutes on the average.

c) As an internal check on the accuracy of computation it appeared convenient to test the condition of equilibrium of the forces acting on the plate in the z direction. This condition states that the sum of all distributed edge

* The program used was of the floating decimal type, in which all numbers are stored in the form of eight digits and an appropriate power of 10.

reactions, concentrated corner reactions and the lateral load on the plate, all taken with proper algebraic sign, shall vanish; its mathematical statement is:

$$\int\int q \, dx \, dy + \oint V_n \, ds + \sum R = 0 \tag{39}$$

Over half of the plate, this equation can be written in a form suitable for computation as

$$\frac{u}{2\pi}\left[1 - \frac{1}{2}\bar{k}\right] - \frac{1}{2}\int_0^1 \left[\frac{V_y\left(\frac{2x}{a}, 0\right)}{q_o \, a}\right] d\left(\frac{2x}{a}\right)$$

$$+ \frac{u}{\pi}\int_0^1 \left[\frac{V_x\,(a/2,\, y/b)}{q_o \, a}\right] d\,(y/b)$$

$$-2\left[\frac{M_{xy}\,(a/2,\, 0)}{q_o \, a^2} - \frac{M_{xy}\,(a/2,\, b)}{q_o \, a^2}\right] = 0 \tag{40}$$

A numerical evaluation of the left hand side of Equation (40), using computed function values will, of course, not produce an identical zero. The actual computed value of the left hand side is called the equilibrium condition residual. The ratio of this residual to the lateral load on the plate, which is the first term on the left hand side of Equation (40), is called the relative equilibrium condition residual.

The integrals in Equation (40) must be evaluated numerically. Since the function values at the corners are generally computed less accurately than the values in the interior, the integrals from 0 to 1 are expressed by means of a nine point, "open end," integration formula using the function values at 0.1, 0.2, . . . , 0.8, 0.9.

$$\int_{x_o}^{x_{10}} y \, dx = \frac{10\,h}{9072}\left[4045\, y_1 - 11690\, y_2 + 33340\, y_3 - 55070\, y_4\right.$$

$$\left. + 67822\, y_5 - 55070\, y_6 + 33340\, y_7 - 11690\, y_8 + 4045\, y_9\right] \tag{41}$$

The equilibrium condition residual and the relative equilibrium condition residual are tabulated at the end of each run and graphs of these quantities over a range of plate sizes $1/5 \leq b/a \leq 5$ are shown in Figure 23. Although the residuals are small, it is surprising to note the rapid increase of the residual with increasing u. This result seemingly contradicts the analytical result that convergence of the series should improve with increasing u. The explanation is seen, however, from the shape of the curves for $V_x\,(a/2, y)/q_o a$ for large u (cf. Figures 18 and 19). The slope of these curves at y = 0 approaches closer and closer to the vertical, and the curvature likewise increases, as u or b/a increases. It is to be expected and can be shown

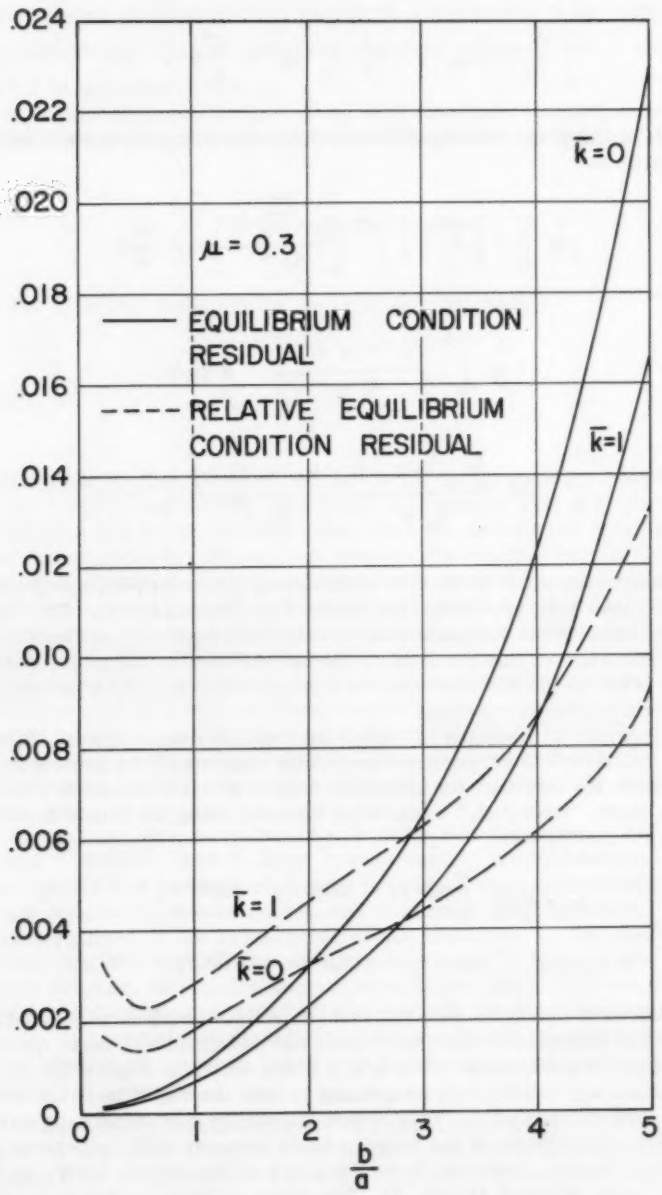

Figure 23
EQUILIBRIUM CONDITION RESIDUAL
FOR VARIOUS b/a; μ = 0.3, $\bar{k}$ = 0 and $\bar{k}$ = 1

(cf. Section IV-d below), that the integration error in Formula (41), when applied to the second integral of Equation (40), will increase markedly with increasing u.

Despite this difficulty, the equilibrium condition test does provide an internal check on random error in addition to other external checks on accuracy discussed elsewhere. In the experience with this program, no random error has ever been detected in the results of a completed run.

Discussion of Results and Comparison with References

a) Numerical Calculations for $\mu = 0.3$

The program was run with $\mu = 0.3$ and with both $\bar{k} = 0$ and $\bar{k} = 1$ for some twenty one values of b/a in the range $1/5 \leqq b/a \leqq 5$. As an aid in the design of structures incorporating plates, these results are presented in graphical form in Figures (8) through (22). The sign convention for the various quantities described is the conventional one [1] and should be apparent from Figure 2. Also, the method of obtaining the results for an arbitrary trapezoidal loading by a linear combination of the results for $\bar{k} = 0$ and $\bar{k} = 1$ should again be evident.

On many of the graphs are shown for comparison dotted lines or curves labelled $b/a = \infty$. For $\bar{k} = 0$, these curves correspond to values for the infinite strip plate. For $\bar{k} = 1$, these curves represent the values of $y = b/3$ (the resultant load point) for very large b/a.

There are a number of instances where it would be desirable to know function values to more significant figures than the graphs could present. These might be to check approximate formulas which are accurate for u large or to check finite difference methods of solution to this or similar problems. A table of values for small u is therefore appended to the end of this paper.

b) Poisson's Ratio Effects

To demonstrate the effect of Poisson's ratio μ, the plate with length to breadth ratio b/a = 3/4 was chosen, both because it is a median size and because it was chosen for previous computations [2] (see Section (c) below). Some typical values of Poisson's ratio for different materials are:

$\mu = 0.16$ fiberglass
$\mu = 0.20$ concrete
$\mu = 0.25$ reinforced concrete
$\mu = 0.30$ - 0.33 steel and aluminum alloys
$\mu = 0.49$ rubber

A nearly uniform increment in the computed functions was found by selecting the values $\mu = 0, 0.16, 0.3, 0.5$. The results of the computations for both $\bar{k} = 0$ and $\bar{k} = 1$ are seen in the five sets of curves of Figures (3-7) and in Table (5). The variation in maximum deflections, stresses* and shears over the range of μ from .16 to .5 appears to be less than 5% of the 0.3 values.

The deviation from the $\mu = 0$ values is in some cases considerably greater, however. The treatment in [2] uses the values for $\mu = 0$ as approximation for the values at near-zero μ. There is some gain in mathematical simplicity in doing this, but as our data shows, the gain seems insufficient to warrant the errors incurred.

The greatest effect of variation of Poisson's ratio is apparent in the distributed edge reactions and the concentrated corner reactions. The general result of increasing Poisson's ratio is to induce a more uniform distribution of reaction pressures along the supported edge. Increasing u results in decreasing the maximum magnitudes of both the distributed edge reactions (cf Figures 6,7) and the largest concentrated corner reaction. In Table 5, looking at R(a/2, 0), which is positive in sign because it is directed to prevent that corner from rising, and at R(a/2, b), which is negative in sign because it is directed to support the load, it is seen for $\mu = 0$, the reaction R(a/2, 0) at the interior is much larger numerically than the reaction R(a/2, b) at the free edge. With increasing μ, the tendency of the interior corner to rise from its supports is reduced and so R(a/2, 0) decreases numerically. The concentrated reaction at the free edge at the same time assumes more of the load, and so R(a/2, b) increases numerically (or becomes larger negatively).

c) Comparison of Results with References

The numerical values given by Goriupp [2] were limited to the case b/a = 0.75 and $\mu = 0$; case (b) of [2] corresponds to $\bar{k} = 0$, while $\bar{k} = 1$ is a linear combination of cases (b) and (c). A comparison with the values given by the IBM program for these same parameter settings revealed several discrepancies, which were in all cases traced back to errors in computation in [2]; when these errors were corrected (Goriupp's formulas computed correctly) agreement with the computer results was obtained to at least the first two significant digits. The incorrect values are found on page 95 and in Table 6, page 97, of [2]; these and the corrected values are as follows:

Goriupp Notation	Listed Value	Corrected Value
M_{xy} (1/2, λ)	.01690	.01239
$\bar{q}_y$ (0, 0)	.19663	.07454
$\bar{q}_y$ (1/6, 0)	.17597	.06736
$\bar{q}_y$ (1/3, 0)	.11215	.03787
p (1/2, λ)	.03380	.02478

TABLE 2

In [1], page 219, Table 28, and in [3], cases (7) and (8), data is presented on maximum deflection and maximum moment as taken from the work of B. G. Galerkin. Agreement with these results are obtained here to two significant digits.

d) Formulas for Large u

The exponential series representations of A_n and D_n, Equations (24) and

(25), can be used to obtain approximate, closed form representations for the Fourier expansions. In these "asymptotic" representations, the neglected terms vanish exponentially as u tends towards infinity. To provide an external check on the computation, asymptotic formulas were obtained for the concentrated corner reactions R(a/2, 0) and R(a/2, b) and for the distributed edge reaction V_x (a/2, b).

1. The asymptotic forms of Equations (33a), (33b) are

$$R(a/2,b)/q_o\, a^2 = \frac{\bar{k}\pi}{12u}\left[1 - \mu - \frac{(2-\mu)(1+\mu)}{3+\mu}\right] - \frac{16.8288\mu}{\pi^3(3+\mu)}(1-\bar{k}) + O(ue^{-u}) \qquad (42)$$

$$R(a/2,0)/q_o\, a^2 = -\frac{\pi(1-\mu)}{12u}\bar{k} + \frac{4.2072\,(1-\mu)}{\pi^3} + O(ue^{-u}) \qquad (43)$$

Writing this as

$$R(a/2,b)/q_o\, a^2 = r_1\, a\, \bar{k}/b - r_2\,(1-\bar{k}) \qquad (44)$$

$$R(a/2,0)/q_o\, a^2 = -r_3\, a\, \bar{k}/b + r_4 \qquad (45)$$

the values of r_1, r_2, r_3, r_4 as functions of μ are given in Table 3.

μ	r_1	r_2	r_3	r_4
0	.027712	0	.083333	.135689
.1	.018773	.017508	.075000	.122120
.2	.010392	.033922	.066667	.108550
.3	.002519	.049341	.058333	.094982
.5	-.011877	.077536	.041667	.067844

TABLE 3

The influence of Poisson's ratio upon the magnitude of the concentrated corner reactions is considerable, as the Table shows. Values of the concentrated corner reactions at the free edge for uniform loading ($\bar{k} = 0$) agree with those given by Holl [4], pp. 22-23, particularly the curves for "corner loads" in Figure (5) for large b/a ratio. Similar agreement is found at the other corners with the values in Timoshenko ([1], Table 5, page 133 and Table 13, Page 142). In fact, values for n_2 in the latter table agree with those found by Equation (57), for $\bar{k} = 1$ and $\mu = 0.3$, to two significant figures for all plate ratios b/a greater than 1.2, that is $u > 3.8$.

2. The asymptotic form of Equation (31) for the interval $0 \leq y/b \leq 1$ is

$$V_x(a/2,y)/q_o a = -\frac{1}{2}(1-\bar{k}\,y/b) + \frac{2}{\pi^2}\sum_{n=1,3,5,..}^{\infty}\frac{1}{n^2}\left\{\frac{2\mu}{3+\mu}\left[5-\mu-(1-\mu)(1-y/b)nu\right](1-\bar{k})e^{-nu(1-y/b)} - \frac{2(1-\mu)(2-\mu)}{(3+\mu)\,nu}\left[2-nu(1-y/b)\right]\bar{k}\,e^{-nu(1-y/b)} + \left[2-(1-\mu)nuy/b\right]e^{-nuy/b} + O(nue^{-nu})\right\} \quad (46)$$

At the corner y = b, the infinite series in Equation (58) can be summed, using a formula in Appendix A, to give

$$V_x(a/2,b)/q_o a = -\frac{1}{2}(1-\bar{k})\left[1-\frac{5-\mu}{3+\mu}\right] - \frac{8.4144}{\pi^3}\,\frac{(2-\mu)\,(1-\mu)}{3+\mu}\,\frac{a\,\bar{k}}{b} + O(e^{-u}) \quad (47)$$

and this can be written as

$$V_x(a/2,b)/q_o a = -v_1\,(1-\bar{k}) - v_2\left(\frac{a\,\bar{k}}{b}\right) \quad (48)$$

Some values for v_1 and v_2 as functions of μ are given in Table 4.

μ	v_1	v_2
0	0.500000	0.180918
.1	0.420468	0.149695
.2	0.350000	0.122119
.3	0.286364	0.097860
.5	0.178572	0.058152

TABLE 4

To check the integration error mentioned in Section III-c above, Equation (46) is integrated over the interval $0 \leq y/b \leq 1$ to obtain the following asymptotic form:

$$\frac{1}{q_o ab}\int_o^b V_x(a/2,y)dy = -\frac{1}{2}(1-\bar{k}/2)+\frac{2}{\pi^2 u}\left\{1.05180(1+\mu)+\frac{8.4144}{(3+\mu)}(1-\bar{k})\right.$$
$$-2.029356\,\frac{(1-\mu)(2-\mu)}{(3+\mu)u}\,\bar{k}+e^{-u}\left[\left[(1-\mu)u-4\right]\frac{2\mu}{3+\mu}(1-\bar{k})-\frac{2(1-\mu)(2-\mu)}{3+\mu}\,\frac{u-1}{u}\,\bar{k}\right.$$
$$\left.\left.+(1-\mu)u-(1+\mu)\right]+O(u^2e^{-2u})\right\} \qquad (49)$$

u	$\bar{k}$	μ	$\frac{R(\frac{a}{2},b)}{q_o a^2}$	$\frac{R(\frac{a}{2},o)}{q_o a^2}$	$Q_y(o,o)$
$\frac{3}{4}\pi$	0	0	-0.03706	0.12156	0.35309
$\frac{3}{4}\pi$	0	.16	-0.05220	0.10330	0.34902
$\frac{3}{4}\pi$	0	.3	-0.06435	0.08806	0.34575
$\frac{3}{4}\pi$	0	.5	-0.08018	0.06737	0.34150
$\frac{3}{4}\pi$	1	0	-0.004034	0.05580	0.22830
$\frac{3}{4}\pi$	1	.16	-0.009356	0.04704	0.22681
$\frac{3}{4}\pi$	1	.3	-0.013629	0.03964	0.22562
$\frac{3}{4}\pi$	1	.5	-0.019195	0.02947	0.22406

TABLE 5

CORNER REACTIONS AND CENTRAL SHEAR
FOR VARIOUS POISSON'S RATIOS; b/a = 0.75 $\bar{k}$ = 0 and $\bar{k}$ = 1

APPENDIX A

SUMMATION OF ELEMENTAL SERIES

Upon repeated integration of Equation (3), the following Fourier series are obtained which are uniformly convergent in the interval $-\frac{a}{2} \leq x \leq \frac{a}{2}$ and represent there polynomials in $\left(\frac{2x}{a}\right)$:

$$\sum_{n=1,3,\ldots}^{\infty} \frac{(-1)^{\frac{n-1}{2}}}{n^2} \sin \frac{n\pi x}{a} = \frac{\pi^2}{8} \cdot \left(\frac{2x}{a}\right) \tag{1A}$$

$$\sum_{n=1,3,\ldots}^{\infty} \frac{(-1)^{\frac{n-1}{2}}}{n^3} \cos \frac{n\pi x}{a} = \frac{\pi^3}{32} \left[1 - \left(\frac{2x}{a}\right)^2\right] \tag{2A}$$

$$\sum_{n=1,3,\ldots}^{\infty} \frac{(-1)^{\frac{n-1}{2}}}{n^4} \sin \frac{n\pi x}{a} = \frac{\pi^4}{64} \left(\frac{2x}{a}\right)\left[1 - \frac{1}{3}\left(\frac{2x}{a}\right)^2\right] \tag{3A}$$

$$\sum_{n=1,3,\ldots}^{\infty} \frac{(-1)^{\frac{n-1}{2}}}{n^5} \cos \frac{n\pi x}{a} = \frac{\pi^5}{1536} \left[5 - 6\left(\frac{2x}{a}\right)^2 + \left(\frac{2x}{a}\right)^4\right] \tag{4A}$$

These same series, with the sine replaced by the cosine, or vice versa, are no longer Fourier expansions of polynomials. Such a series is $f_2(x)$, defined as:

$$f_2(x) = \sum_{n=1,3,5,\ldots}^{\infty} \frac{(-1)^{\frac{n-1}{2}}}{n^2} \cos \frac{n\pi x}{a} \qquad -1 \leq \frac{2x}{a} \leq 1 \tag{5A}$$

This Fourier series converges too slowly for practical computational purposes. A rapidly converging series representation for $f_2(x)$ is found as follows. Let $z = \frac{1}{2}\left[1 - \frac{2x}{a}\right]$. Then $F_2(z) = f_2(x)$ and

$$F_2(z) = \sum_{n=1,3,\ldots}^{\infty} \frac{1}{n^2} \sin n\pi z \qquad 0 \leq z \leq 1 \tag{6A}$$

Now, by [5] page 350,

$$\frac{1}{\pi} \frac{dF_2}{dz} = \sum_{n=1,3,\ldots}^{\infty} \frac{1}{n} \cos n\pi z = -\frac{1}{2} \log \tan \frac{\pi z}{2}$$

$$= -\frac{1}{2}\left[\log\left(\frac{\pi z}{2}\right) + \frac{1}{3}\left(\frac{\pi z}{2}\right)^2 + \frac{7}{90}\left(\frac{\pi z}{2}\right)^4 + \cdots\right. \tag{7A}*$$

$$\left. + (-1)^{n-1} \frac{(2^{2n-1}-1)2^{2n}B_n}{n(2n)!}\left(\frac{\pi z}{2}\right)^{2n} + \cdots\right] \qquad 0 < z < 1$$

* cf [6], Formula #784. The Bernoulli Numbers B_n here are defined in [7]: $B_2 = 1/6$, $B_4 = -1/30$, $B_6 = 1/42$, . . .

Then integrating Equation (7A)

$$F_2(z) = -\frac{\pi}{2}\int_0^z \log \tan\frac{\pi\xi}{2}\, d\xi$$

there results the following rapidly converging expansion for $f_2(x)$ which is used in the computation of Equations (34) and (36):

$$f_2(x) = \frac{\pi}{4}\left(1-\frac{2x}{a}\right)\left[1 - \log\frac{\pi}{4}\left(1-\frac{2x}{a}\right)\right] - \sum_{n=1,3,\ldots}^{\infty}(-1)^{n-1}\frac{(2^{2n-1}-1)\pi^{2n+1}}{2^{2n+2}\,n(2n+1)!}B_{2n}\left(1-\frac{2x}{a}\right)^{2n+1} \qquad (8A)$$

$$-1 < \frac{2x}{a} < 1$$

Harmonic series which have simple sums are evaluated by means of the following formulas from [7] pp. 236 to 240:

$$\sum_{n=1,3,\ldots}^{\infty}\frac{1}{n^{2p}} = (-1)^{p-1}\frac{2^{2p-1}}{2(2p)!}B_{2p}\pi^{2p} \qquad (9A)$$

$$\sum_{n=1,3,\ldots}^{\infty}\frac{(-1)^{\frac{n-1}{2}}}{n^{2p+1}} = (-1)^{p}\frac{1}{2^{2p+2}(2p)!}E_{2p}\pi^{2p+1} \qquad (10A)^*$$

The following harmonic series, however, can be summed by use of an identity for the Riemann Zeta Function $\zeta(z)$ (cf. [8] p. 269)

$$\sum_{n=1,3,\ldots}^{\infty}\frac{1}{n^{z}} = (1-2^{-z})\zeta(z) \qquad (11A)$$

For z an even integer, this formula is identical with Equation (9A); for z an odd integer, the following six-place numerical values for the zeta function are useful:

$$\zeta(3) = 1.202057, \qquad \zeta(5) = 1.036928$$

$$\zeta(7) = 1.008349.$$

* E_n are the Euler numbers: $E_2 = -1$, $E_4 = -5$, $E_6 = -61$, . . .

APPENDIX B TABLES OF NUMERICAL VALUES FOR SMALL b/a

2x/a | y/b	b/a	k	$\frac{w(0,y)}{q_o a^4/Eh^3}$	$\frac{M_x(0,y)}{q_o a^2}$	$\frac{M_y(0,y)}{q_o a^2}$	$\frac{M_{xy}(\frac{a}{2},y)}{q_o a^2}$	$\frac{Q_x(\frac{a}{2},y)}{q_o a}$	$\frac{V_x(\frac{a}{2},y)}{q_o a}$	$\frac{V_y(x,0)}{q_o a}$	$\frac{Q_y(x,0)}{q_o a}$
0.0	1/5	0	.000000	.000000	.0000000	-.021071	-.00000	-.00000	.19827	.14863
0.2			.003676	.003529	.0031616	-.020696	-.06495	-.07913	.19723	.14782
0.4			.007313	.006577	.0047359	-.020083	-.09372	-.10894	.19285	.14445
0.6			.010900	.009145	.0047322	-.019565	-.10734	-.11699	.17993	.13460
0.8			.014451	.011235	.0031545	-.019400	-.10894	-.10616	.14244	.10632
1.0			.018008	.012851	.0000000	-.019943	-.09610	-.06769	.00000	.00000
0.0	1/5	1	.0000000	.0000000	.0000000	-.007284	-.000000	-.000000	.099440	.082860
0.2			.001269	.001333	.0019054	-.007086	-.040771	-.052303	.099090	.082564
0.4			.002672	.002822	.0025356	-.006638	-.047336	-.058348	.097603	.081305
0.6			.003654	.003223	.0022144	-.006281	-.042983	-.049319	.093111	.077566
0.8			.004191	.003805	.0012629	-.006159	-.034061	-.033589	.079196	.065943
1.0			.005981	.004284	.0000000	-.006327	-.026073	-.018251	.000000	.000000
0.0	1/3	0	.000000	.000000	.000000	-.030784	-.00000	-.00000	.30991	.23181
0.2			.009220	.009174	.008072	-.029748	-.10790	-.13144	.30515	.22820
0.4			.018173	.017003	.011967	-.028056	-.15561	-.18078	.28891	.21592
0.6			.026775	.023503	.011888	-.026629	-.17814	-.19405	.25425	.18981
0.8			.035135	.028723	.007918	-.026181	-.18076	-.17609	.18391	.13706
1.0			.043548	.032758	.000000	-.027682	-.15929	-.11190	.00000	.00000
0.0	1/3	1	.000000	.000000	.0000000	-.011383	-.000000	-.000000	.15880	.13223
0.2			.003230	.003791	.0049907	-.010497	-.067826	-.087015	.15713	.13081
0.4			.006269	.006500	.0065418	-.009195	-.078692	-.096960	.15138	.12584
0.6			.009073	.008392	.0056254	-.008210	-.071381	-.081866	.13859	.11470
0.8			.011717	.009754	.0031593	-.007875	-.056504	-.055692	.10962	.08943
1.0			.014352	.010892	.0000000	-.008341	-.043236	-.030265	.00000	.00000
0.0	1/2	0	.000000	.000000	.000000	-.038544	-.00000	-.00000	.40132	.29933
0.2			.017504	.017666	.015026	-.036281	-.15848	-.19248	.39289	.29270
0.4			.033915	.032290	.021708	-.032649	-.22724	-.26297	.36416	.27147
0.6			.048945	.043983	.021253	-.029637	-.25927	-.28141	.30986	.23081
0.8			.063067	.053087	.011432	-.028738	-.26276	-.25551	.21360	.15892
1.0			.077468	.060159	.000000	-.032025	-.23142	-.16237	.00000	.00000

2x/a | y/b	b/a	$\bar{k}$	$\frac{w(0,y)}{q_o a^4/Eh^3}$	$\frac{M_x(0,y)}{q_o a^2}$	$\frac{M_y(0,y)}{q_o a^2}$	$\frac{M_{xy}(\frac{a}{2},y)}{q_o a^2}$	$\frac{Q_x(\frac{a}{2},y)}{q_o a}$	$\frac{V_x(\frac{a}{2},y)}{q_o a}$	$\frac{V_y(x,0)}{q_o a}$	$\frac{Q_y(x,0)}{q_o a}$
0.0	1/2	1	.000000	.000000	.000000	-.015324	-.00000	-.00000	.21608	.17944
0.2			.006514	.007624	.009757	-.013361	-.10049	-.12869	.21281	.17657
0.4			.012196	.012736	.012311	-.010514	-.11579	-.14223	.20204	.16709
0.6			.016899	.015937	.010182	-.008392	-.10421	-.11908	.18006	.14779
0.8			.020977	.017976	.005492	-.007697	-.08180	-.08033	.13563	.10949
1.0			.025050	.019710	.000000	-.008723	-.06233	-.04363	.00000	.00000
0.0	1/1.5	0	.00000	.000000	.000000	-.042770	-.00000	-.00000	.45039	.33524
0.2			.02584	.026062	.021326	-.038973	-.20241	-.24450	.43924	.32691
0.4			.04900	.046709	.029738	-.033089	-.28669	-.32933	.40410	.30067
0.6			.06894	.062352	.028585	-.028377	-.32470	-.35006	.33905	.25213
0.8			.08690	.074021	.019017	-.027112	-.32812	-.31810	.22902	.17017
1.0			.10570	.000000	.000000	-.032607	-.28869	-.20244	.00000	.00000
0.0	1/1.5	1	.000000	.000000	.000000	-.018456	-.00000	-.00000	.25753	.21273
0.2			.010353	.011915	.014567	-.015086	-.13055	-.16643	.25303	.20873
0.4			.018543	.019200	.017480	-.010329	-.14815	-.18074	.23839	.19501
0.6			.024330	.022977	.013746	-.006906	-.13105	-.14853	.20931	.17042
0.8			.028697	.024818	.007016	-.005885	-.10089	-.09828	.15337	.12282
1.0			.033160	.026513	.000000	-.007620	-.07610	-.05327	.00000	.00000
0.0	1	0	.00000	.00000	.000000	-.046029	-.00000	-.00000	.48726	.36192
0.2			.04088	.04068	.030660	-.038708	-.26988	-.32134	.47432	.35229
0.4			.07362	.06940	.039296	-.028516	-.36852	-.41508	.43400	.32228
0.6			.09781	.08825	.036439	-.021180	-.40815	-.43265	.36082	.26786
0.8			.11749	.10083	.024622	-.019812	-.40865	-.39397	.24049	.17845
1.0			.14035	.11170	.000000	-.030002	-.35790	-.25085	.00000	.00000
0.0	1	1	.000000	.000000	.000000	-.023425	-.00000	-.00000	.31312	.25467
0.2			.019126	.021041	.022722	-.016610	-.18179	-.22829	.30681	.24918
0.4			.031070	.031189	.024361	-.007804	-.19724	-.23533	.28655	.23165
0.6			.036057	.033564	.017222	-.002153	-.16559	-.18305	.24738	.19830
0.8			.037660	.032520	.007732	-.000989	-.11974	-.11391	.17585	.13894
1.0			.040177	.032511	.000000	-.001307	-.08688	-.06081	.00000	.00000

ACKNOWLEDGMENTS

The results presented in this paper were obtained while the author was with the Mathematical Services Unit of the Boeing Airplane Company, Seattle, Washington; they first appeared as Boeing Mathematical Notes Nos. 65 and 86. Considerable credit for the numerical data is due Mrs. Gladys Williams who devised the digital computer program used here.

NOTATION

x, y, z	Rectangular Coordinates
h	Thickness of Plate
q, q_o	Intensity of Continuously Distributed Lateral Load
$\bar{k}$	Loading Contour Factor: $q = q_o (1 - \bar{k}\, y/b)$
E	Modulus of Elasticity in Tension and Compression
μ	Poisson's Ratio
D	Flexural Rigidity of Plate = $\frac{Eh^3}{12(1-\mu^2)}$
w	Plate deflection
M_x, M_y	Bending moments per unit length of sections of a plate perpendicular to x- and y-axes respectively
M_{xy}	Twisting moment per unit length of a section of plate perpendicular to x-axis
Q_x, Q_y	Shearing Forces parallel to z-axis per unit length of sections of a plate perpendicular to x- and y- axes respectively
V_x, V_y	Edge Reaction Forces parallel to z-axis per unit length of sections of a plate perpendicular to x- and y-axes respectively
R	Concentrated Reaction Forces parallel to z-axis
a, b	Side dimensions of rectangular plate
u	$= \frac{\pi b}{a}$
$\bar{q}$	$= \frac{4\, q_o}{\pi\, D} \left(\frac{a}{\pi}\right)^4$
β	$= nuy/b = n\pi\, y/a$
n	A positive integer used for summation index
A_n, D_n	Series coefficients
$w_n(y) = \bar{w}_n(\beta)$	Fourier coefficient in expansion of w(x,y)

REFERENCES

1. Timoshenko, S., "Theory of Plates and Shells," First Edition, McGraw-Hill, New York, 1940.

2. Goriupp, K., "Die Dreiseitig Gelagerte Rechteckplatte," Arch 16; Part I, 77-98 (1947); Part II, 153-163 (1948).

3. Wojtaszak, I. A., "Stress and Deflection of Rectangular Plates," Amer. Soc. Mech. Eng. Paper A-71, J. Appl. Mech., 3, 2, (1936).

4. Holl, D. L., "Analysis of Thin Rectangular Plates Supported on Opposite Edges," Bulletin 129, Iowa Engineering Experimental Station, Iowa State College, Ames, Iowa, 100 pp. December 1936.

5. Bromwich, T. J. I'a, "An Introduction to the Theory of Infinite Series," Second Edition Revised, MacMillan, London, 1949.

6. Peirce, B. O., "A Short Table of Integrals," Third Revised Edition, Ginn and Company, Boston, 1929.

7. Knopp, K., "Theory and Application of Infinite Series," Second German Edition Translated and Revised, Hafner, New York, 1947.

8. Jahnke, E., and Emde, F., "Tables of Functions," Fourth Edition, Dover, New York, 1945.

Paper 1212 EM 2

Journal of the
ENGINEERING MECHANICS DIVISION
Proceedings of the American Society of Civil Engineers

PLATE BUCKLING IN THE STRAIN-HARDENING RANGE

Geerhard Haaijer[a]
(Proc. Paper 1212)

1. SYNOPSIS

The application of plastic design to continuous frames constructed of wide-flange shapes, imposes more severe limitations on the geometry of these shapes than conventional elastic design. In regions where yielding starts first, the flanges must be able to sustain strains considerably larger than the yield strain without the occurrence of local (plate) buckling.

With this practical application in mind, the problem of buckling of steel plates compressed beyond the yield strain is treated in the present paper. In the strain-hardening range the material is considered to be homogeneous. However, because of the yielding process the material cannot be expected to remain isotropic. Therefore, general expressions for the buckling strength are derived assuming the material to have become orthogonally anisotropic.

Orthogonal anisotropy in the case of plane stress is expressed mathematically by stress-strain relations involving five moduli. Numerical values of the moduli are estimated from the incremental theory of plasticity taking the second invariant of the deviatoric stress tensor as the loading function. The influence of initial imperfections is taken into account through proper adjustment of the values of the moduli. In selecting these values due consideration is given to the results of buckling tests.

In the yielding range the average strain in the direction of loading is between the strain at which yielding starts and the strain at the beginning of strain-hardening. For this case the material is considered to be partly elastic and partly strained up to the strain-hardening range.

Finally, theoretical estimates are compared with test results. It is considered that the theory adequately describes the behavior.

Note: Discussion open until September 1, 1957. Paper 1212 is part of the copyrighted Journal of the Engineering Mechanics Division of the American Society of Civil Engineers, Vol. 83, No. EM 2, April, 1957.

a. Fritz Eng. Lab., Dept. of Civ. Eng., Lehigh University, Bethlehem, Pa.

2. INTRODUCTION

Presently used steel wide-flange shapes are proportioned such that no local buckling occurs within the elastic range. Consequently they can safely be used for structures in which the design is based upon theoretical first yield as the limiting condition (conventional design). However, design based upon ultimate strength (plastic design) imposes more severe requirements on the sections with regard to local buckling. The structure will reach its full ultimate load only if those parts where yielding starts first, can undergo sufficiently large deformations. For framed structures constructed of wide-flange shapes the flanges at the above mentioned locations must then be able to sustain strains considerably larger than the yield strain. Consequently the flanges should be proportioned such that local (plate) buckling does not occur under this condition.

In order to solve problems of plate buckling the relationships between the increments of stresses and strains due to the deflection of the plate out of its plane must be known. Within the elastic range the assumption that the material is isotropic and homogeneous leads to predictions which are in good agreement with test results.(1) A satisfactory transition curve for the range from the elastic limit stress to the yield stress can easily be obtained by applying Bleich's semi-rational theory to an effective stress-strain curve.(2)

During the yielding process the material is heterogeneous. Yielding takes place in so-called slip bands and the strain jumps from its value at the elastic limit to that at the beginning of strain-hardening.(3) When all the material has been strained to the strain-hardening range the material again becomes homogeneous. In the strain-hardening range, stress-strain relations of different theories of plasticity could be applied. Such theories can be divided into two groups: deformation or total stress-strain relations and incremental stress-strain relations.

Bijlaard(4) was first to apply deformation stress-strain relations to the plate buckling problem. The theory was developed further by Ilyushin(5) and modified by Stowell.(6) Incremental stress-strain relations were applied by Handelman and Prager.(7) An extensive survey of stress-strain relations in the plastic range has been made by Drucker.(8) Although the necessity for an incremental type of mathematical theory of plasticity has been shown, the results of plastic buckling tests on aluminum plates are well correlated by a deformation theory and bear no resemblance to predictions of incremental theory. Onat and Drucker(9) investigated the influence of initial imperfections on torsional buckling for a simplified model of a cruciform section. For this case the paradox appears at its worst. Onat and Drucker showed that incremental plasticity leads to proper results when unavoidable initial imperfections are taken into account.

All theories of plate buckling in the plastic range imply orthotropic behavior of the material. This assumption seems to be very reasonable. Therefore, in the present report general expressions for the buckling strength of orthotropic plates are derived from general stress-strain relations involving five moduli (Chapter 3). Tests of steel tubes under combined compression and torsion showed that the behavior of the material is well described by the incremental theory with the second invariant of the deviatoric stress tensor as the loading function.(10) Consequently, this theory is used in order to obtain values of the moduli of the general stress-strain relations.

Generalities on stress and strain and incremental stress-strain relations

are summarized in Chapter 4. The influence of initial imperfections is illustrated in Chapter 5. From the results of coupon tests numerical values of the moduli are then obtained in Chapter 6. The influence of initial imperfections is taken into account through adjustment of the values of the moduli. Combining the results of Chapters 3 and 6 gives numerical solutions of the plate buckling problem which are compared with test results in Chapter 7.

In summary, then, the objective is to predict the strain at which buckling occurs in steel plate elements when the strain has exceeded the elastic limit.

3. Buckling of Rectangular Orthotropic Plates

3.1 General

Consider a rectangular steel plate taking the center plane of the plate as the x - y coordinate plane. Compressing the plate in the x - direction into the strain-hardening range may affect all deformation properties of the material. Hence the tangent moduli, E_x and E_y in the x - and y - direction respectively, are probably different. The same may hold for the coefficients of dilatation, ν_x and ν_y in the x - and y - direction. The shear modulus, G_t, may also be affected.

Thus

$$\left.\begin{aligned} \frac{\partial \epsilon_x}{\partial \sigma_x} &= \frac{1}{E_x} & \frac{\partial \epsilon_y}{\partial \sigma_y} &= \frac{1}{E_y} \\ \frac{\partial \epsilon_x}{\partial \sigma_y} &= -\frac{\nu_y}{E_y} & \frac{\partial \epsilon_y}{\partial \sigma_x} &= -\frac{\nu_x}{E_x} \\ \frac{\partial \gamma_{xy}}{\partial \tau_{xy}} &= \frac{1}{G_t} \end{aligned}\right\} \qquad (3.1)$$

where

ϵ = normal strain

γ = shear strain

σ = normal stress

τ = shear stress

Then the relations between the increments of strains and stresses can be written as follows:

$$\left.\begin{aligned} d\epsilon_x &= \frac{1}{E_x} d\sigma_x - \frac{\nu_y}{E_y} d\sigma_y \\ d\epsilon_y &= -\frac{\nu_x}{E_x} d\sigma_x + \frac{1}{E_y} d\sigma_y \\ d\gamma_{xy} &= \frac{1}{G_t} d\tau_{xy} \end{aligned}\right\} \qquad (3.2)$$

If equations (3.2) are valid for the entire cross-section the expressions for the bending and twisting moments in terms of the deflection, w, in the direction of the z-axis become

$$M_x = - \frac{E_x I}{1 - \nu_x \nu_y} \left[\frac{\partial^2 w}{\partial x^2} + \nu_y \frac{\partial^2 w}{\partial y^2} \right] \tag{3.3}$$

$$M_y = - \frac{E_y I}{1 - \nu_x \nu_y} \left[\frac{\partial^2 w}{\partial y^2} + \nu_x \frac{\partial^2 w}{\partial x^2} \right] \tag{3.4}$$

$$M_{xy} = - 2 G_t I \frac{\partial^2 w}{\partial x \partial y} \tag{3.5}$$

where

$I = \frac{t^3}{12}$

t = thickness of plate.

The condition that the bent position is in equilibrium can be expressed by the following differential equation:

$$D_x \frac{\partial^4 w}{\partial x^4} + 2H \frac{\partial^4 w}{\partial x^2 \partial y^2} + D_y \frac{\partial^4 w}{\partial y^4} = - \frac{t \sigma_x}{I} \cdot \frac{\partial^2 w}{\partial x^2} \tag{3.6}$$

where

$$D_x = \frac{E_x}{1 - \nu_x \nu_y}$$

$$D_y = \frac{E_y}{1 - \nu_x \nu_y}$$

$$D_{xy} = \frac{\nu_y E_x}{1 - \nu_x \nu_y}$$

$$D_{yx} = \frac{\nu_x E_y}{1 - \nu_x \nu_y}$$

$$2H = D_{xy} + D_{yx} + 4G_t$$

The derivation of these equations may be found in the pertinent literature.(11) Only if $H^2 = D_x D_y$, an assumption made by Bleich,(2) can solutions of this differential equation be easily obtained.

If the plate is initally perfectly plane the value of σ_x at which bifurcation of equilibrium occurs (the plane and the bent position are both equilibrium positions) is determined by equation (3.6). The condition that both the plane and the bent position are equilibrium positions can also be expressed in terms of work. The additional work done by the external forces due to bending of the plate must equal the change in internal energy of the plate.

This yields the following integral equation

$$\frac{\sigma_x t}{I}\iint\left(\frac{\partial w}{\partial x}\right)^2 dxdy = \iint\left[D_x\left(\frac{\partial^2 w}{\partial x^2}\right)^2 + \right.$$

$$+ D_y\left(\frac{\partial^2 w}{\partial y^2}\right)^2 + (D_{xy} + D_{yx})\left(\frac{\partial^2 w}{\partial x^2}\right)\cdot\left(\frac{\partial^2 w}{\partial y^2}\right) +$$

$$\left. + 4G_t\left(\frac{\partial^2 w}{\partial x \partial y}\right)^2\right] dxdy \qquad (3.7)$$

When external restraints are provided to the plate the right-hand side of equation (3.7) has to be supplemented by additional terms expressing the work done by these restraints.

By assuming an appropriate deflection surface, equation (3.7) gives an approximate solution. The degree of approximation depends upon the correctness of the assumed deflection surface. In any case the result will be conservative.

3.2 Plates with One Free Edge

For a rectangular plate with the loaded edges x = 0 and x = ℓ hinged, edge y = 0 restrained against rotation and edge y = b free (Fig. 1) the following deflection surface is assumed

$$w = \left[A\frac{y}{b} + B\left\{\left(\frac{y}{b}\right)^2 + a_1\left(\frac{y}{b}\right)^3 + a_2\left(\frac{y}{b}\right)^4\right\}\right]\sin\frac{\pi x}{\ell} \qquad (3.8)$$

The ratio B/A depends upon the amount of restraint. In the case of elastic restraint, where X = moment per unit length required for a unit rotation

$$\beta = \frac{B}{A} = \frac{\chi b}{2D_y I} \qquad (3.9)$$

Deflection surface (3.8) is similar to the one used by Lundquist and Stowell.[12] It can be shown[20] that better results are obtained with equation (3.8) if the following values for a_1 and a_2 are used

For $0 < \beta < 0.1$ $\quad a_1 = -0.7$, $\quad a_2 = 0.2$

and for $\beta = \infty$ $\quad a_1 = -1.10$, $\quad a_2 = 0.54$

Substituting w in equation (3.7) and integrating gives

$$\sigma_x = \frac{t^2}{12b^2}\left[D_x\left(\frac{\pi b}{\ell}\right)^2 + D_y\left(\frac{\ell}{\pi b}\right)^2 \frac{2B + B^2C_3}{\frac{1}{3} + BC_1 + B^2C_2} + \right.$$

$$- \left(D_{xy} + D_{yx}\right) \cdot \frac{BC_4 + B^2C_5}{\frac{1}{3} + BC_1 + B^2C_2} +$$

$$\left. + 4G_t \cdot \frac{1 + BC_6 + B^2C_7}{\frac{1}{3} + BC_1 + B^2C_2}\right] \qquad (3.10)$$

where

$$C_1 = 1/2 + 2/5\ a_1 + 1/3\ a_2$$

$$C_2 = 1/5 + 1/3\ a_1 + 1/7\ (a_1^2 + 2a_2) + 1/4\ a_1a_2 + 1/9\ a_2^2$$

$$C_3 = 4 + 12a_1^2 + 144/5\ a_2^2 + 12a_1 + 16a_2 + 36a_1a_2$$

$$C_4 = 1 + 2a_1 + 3a_2$$

$$C_5 = 2/3 + 2a_1 + 1/5\ (6a_1^2 + 14a_2) + 3a_1a_2 + 12/7\ a_2^2$$

$$C_6 = 2\ (1 + a_1 + a_2)$$

$$C_7 = 4/3 + 3a_1 + 1/5\ (9a_1^2 + 16a_2) + 4a_1a_2 + 16/7\ a_2^2$$

The minimum value, σ_{cr}, of σ_x is obtained for ℓ/b given by

$$\frac{\ell}{b} = \pi \sqrt{\frac{\frac{1}{3} + BC_1 + B^2C_2}{2B + B^2C_3}} \cdot \sqrt[4]{\frac{D_x}{D_y}} \qquad (3.11)$$

In the limiting cases when the edge y = 0 is hinged or completely fixed equation (3.10) reduces to

a.) Edge y = 0 hinged ($\beta = 0$) and $\ell = L$

$$\sigma_{cr} = \left(\frac{t}{b}\right)^2 \left[\frac{\pi D_x}{12}\left(\frac{b}{L}\right)^2 + G_t\right] \qquad (3.12)$$

For a long plate the first term can be neglected and

$$\sigma_{cr} = \left(\frac{t}{b}\right)^2 G_t \qquad (3.13)$$

b.) Edge y = 0 completely fixed ($\beta = \infty$)

The minimum value, σ_{cr}, of σ_x is obtained when the half-wave length ℓ satisfies

$$\frac{\ell}{b} = 1.46\sqrt[4]{\frac{D_x}{D_y}} \tag{3.14}$$

Then

$$\sigma_{cr} = \left(\frac{t}{b}\right)^2\left[0.769\sqrt{D_x D_y} - 0.270\,(D_{xy}+D_{yx}) + 1.712\,G_t\right] \tag{3.15}$$

3.3 Plates Supported Along All Four Edges

The loaded edges x = 0 and x = ℓ are hinged and the edges y = $\pm$ d/2 have equal restraint against rotation (Fig. 2). For this case the following deflection surface is used[13]

$$w = \left[B\pi\left(\frac{y}{d} - \frac{1}{4}\right) + (A+B)\cdot\cos\frac{\pi y}{d}\right]\sin\frac{\pi x}{\ell} \tag{3.16}$$

The ratio B/A depends on the amount of restraint. For elastic restraints with X = moment per unit length required for unit rotation

$$\beta = \frac{B}{A} = \frac{\chi d}{2D_y I} \tag{3.17}$$

Substituting w from equation (3.16) in equation (3.7) and integrating gives

$$\sigma_x = \frac{\pi^2 t^2}{12\,d^2}\left[D_x\left(\frac{d}{\ell}\right)^2 + D_y\left(\frac{\ell}{d}\right)^2 \frac{\frac{1}{4} + (c_1 + \frac{2}{\pi^2})\beta + \beta^2 c_3}{\frac{1}{4} + \beta c_1 + \beta^2 c_2} + \right.$$

$$+ (D_{xy} + D_{yx})\,\frac{\frac{1}{4} + \beta c_1 + \beta^2 c_4}{\frac{1}{4} + \beta c_1 + \beta^2 c_2} +$$

$$\left. + 4G_t \cdot \frac{\frac{1}{4} + \beta c_1 + \beta^2 c_4}{\frac{1}{4} + \beta c_1 + \beta^2 c_2}\right] \tag{3.18}$$

with

$$c_1 = 0.09472$$
$$c_2 = 0.00921$$
$$c_3 = 0.04736$$
$$c_4 = 0.01139$$

The minimum value of σ_x is obtained for ℓ given by

$$\frac{\ell}{d} = \sqrt[4]{\frac{D_x}{D_y}\,\frac{\frac{1}{4} + \beta c_1 + \beta c_2}{\frac{1}{4} + (c_1 + \frac{2}{\pi^2})\beta + \beta^2 c_3}} \tag{3.19}$$

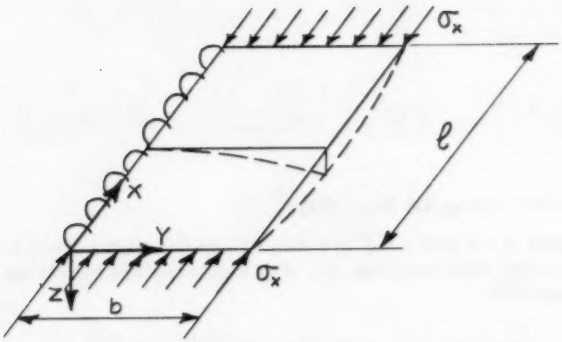

Fig. 1 - Plate with one free edge

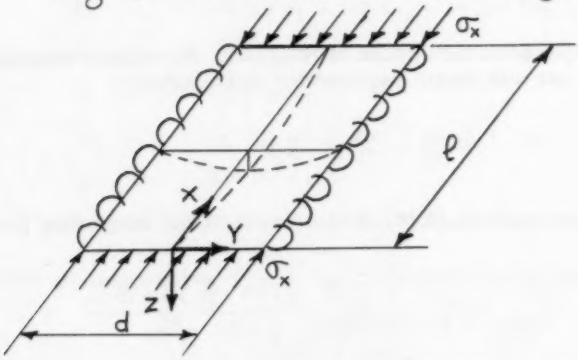

Fig. 2 - Plate supported at all four edges

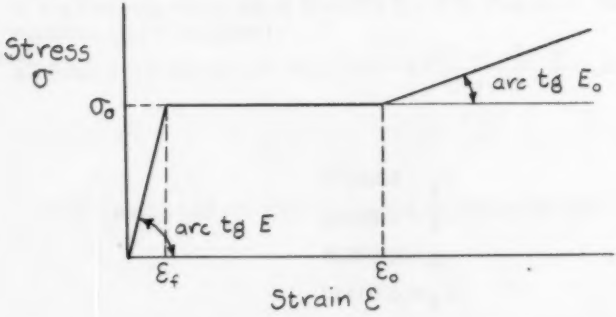

Fig. 3 - Simplified stress - strain curve

In the limiting cases, when the unloaded edges y = ± d/2 are hinged or completely fixed, the minimum values of σ_x are

a.) Edges y = ± d/2 hinged ($\beta = 0$)

$$\sigma_{cr} = \frac{\pi^2}{12}\left(\frac{t}{d}\right)^2 \left[2\sqrt{D_x D_y} + D_{xy} + D_{yx} + 4G_t\right] \tag{3.20}$$

where

$$\frac{\ell}{d} = \sqrt[4]{\frac{D_x}{D_y}} \tag{3.21}$$

b.) Edges y = ± d/2 completely fixed ($\beta = \infty$)

$$\sigma_{cr} = \frac{\pi^2}{12}\left(\frac{t}{d}\right)^2 \left[4.554\sqrt{D_x D_y} + 1.237\,(D_{xy} + D_{yx}) + 4.943\,G_t\right] \tag{3.22}$$

where

$$\frac{\ell}{d} = 0.664\sqrt[4]{\frac{D_x}{D_y}} \tag{3.23}$$

In the following chapters values of D_x, D_y, D_{xy} and G_t will be determined. On substituting these values in the above general expressions, numerical solutions to the local buckling problem will be obtained.

4. Incremental Stress-Strain Relations

4.1 General

It is commonly assumed that yielding occurs whenever some function of stress, f (σ_{ij}),* equals some number, k. If the material is originally isotropic this yield condition is independent of the orientation of the coordinate system. In this instance f must be a function of the stress invariants. An extension of the yield function is obtained by assuming the existence of a loading function, f (σ_{ij}), which depends upon the state of stress and strain and the history of loading. For ideally plastic materials plastic flow occurs whenever f equals some number k. For materials exhibiting strain-hardening plastic deformations occur when the loading function exceeds k.

Prager[15] proved that, if

* Tensor notation is used in referring to generalized stress and strain. Cartesian coordinates x_1, x_2, and x_3, corresponding to the x, y, and z axis of engineering notation are denoted by letter subscripts i, j, k, l, which take the values 1, 2, and 3. Thus the nine components of stress and strain tensors are represented by single symbols σ_{ij} and ϵ_{ij} respectively. Repeated subscripts indicate summation. See e.g. Ref. 14.

1. a loading function exists, and
2. the relation between infinitessimals of stress and strain in linear,

the only permissible stress-strain relation for strain-hardening material when loading is

$$d\epsilon_{ij}^{p} = F\frac{\partial f}{\partial \sigma_{ij}}\frac{\partial f}{\partial \sigma_{kl}}\,d\sigma_{kl} \tag{4.1}$$

and when unloading is

$$d\epsilon_{ij}^{p} = 0 \tag{4.2}$$

where ϵ_{ij}^{p} = plastic component of strain ϵ_{ij} and F and f are functions of stress and strain. The geometric proof of Prager's stress-strain law (equations 4.1 and 4.2) is also included by Drucker in his survey of stress-strain relations in the plastic range.(8)

As no information was available concerning the actual behavior of steel in the strain-hardening range a few tests were carried out on combined compression and torsion of steel tubes.(10) The tubes were compressed into the strain-hardening range and then subjected to torsion while keeping the axial load constant. It was found that for this particular loading path the behavior is very well described by Prager's incremental stress-strain relations taking $f = J_2$, where J_2 is the second variant of the deviatoric stress tensor.*

Although these tests are by no means a general verification of this theory they give some indication of its possible validity. In view of these results and on account of its simplicity, the loading function $f = J_2$ will be applied in the following derivations.

4.2 Loading Function $f = J_2$

Applying the loading function $f = J_2$ to equations (4.1) and (4.2) gives

$$d\epsilon_{ij}^{p} = F\,s_{ij}\,dJ_2 \tag{4.3}$$

when $dJ_2 > 0$
and

$$d\epsilon_{ij}^{p} = 0 \tag{4.4}$$

when $dJ_2 \leqslant 0$
The increments of the elastic components, ϵ_{ij}^{e}, of the strains are given by Hooke's law

---

* The state of stress, with components σ_{ij}, can be split into two parts: a uniform tension (or compression), s, and another state of stress, with components s_{ij}, having the same shear stress but zero mean normal stress. The latter is called the deviatoric stress tensor. Thus $\sigma_{ij} = s_{ij} + s\delta_{ij}$ with $s = 1/3\ \sigma_{ii}$. The second invariant is given by $J_2 = 1/2\ s_{ij}\ s_{ij}$.

$$d\epsilon_{ij}^{e} = \frac{1+\nu}{E} d\sigma_{ij} - \frac{\nu}{E} d\sigma_{kk} \delta_{ij} \quad (4.5)$$

where

E = modulus of elasticity

ν = Poisson's ratio

δ_{ij} = Kronecker delta, defined as unity for i = j and zero for i ≠ j

For the case of plane stress ($\sigma_z = \tau_{xz} = \tau_{yz} = 0$) the stress-strain relations, written in unabridged form, are

$$d\epsilon_x = \frac{1}{E} d\sigma_x - \frac{\nu}{E} d\sigma_y + \frac{1}{3} F (2\sigma_x - \sigma_y) dJ_2 \quad (4.6)$$

$$d\epsilon_y = -\frac{\nu}{E} d\sigma_x + \frac{1}{E} d\sigma_y + \frac{1}{3} F (2\sigma_y - \sigma_x) dJ_2 \quad (4.7)$$

$$d\epsilon_z = -\frac{\nu}{E} (d\sigma_x + d\sigma_y) - \frac{1}{3} F (\sigma_x + \sigma_y) dJ_2 \quad (4.8)$$

$$d\gamma = \frac{2(1+\nu)}{E} d\tau + 2F\tau dJ_2 \quad (4.9)$$

when

$$dJ_2 = \frac{1}{3} (2\sigma_x - \sigma_y) d\sigma_x + \frac{1}{3} (2\sigma_y - \sigma_x) d\sigma_y + 2\tau d\tau > 0 \quad (4.10)$$

and

$$d\epsilon_x = \frac{1}{E} d\sigma_x - \frac{\nu}{E} d\sigma_y \quad (4.11)$$

$$d\epsilon_y = -\frac{\nu}{E} d\sigma_x + \frac{1}{E} d\sigma_y \quad (4.12)$$

$$d\epsilon_z = -\frac{\nu}{E} (d\sigma_x + d\sigma_y) \quad (4.13)$$

$$d\gamma = \frac{2(1+\nu)}{E} d\tau \quad (4.14)$$

when

$$dJ_2 \leq 0$$

The function F can be obtained from the results of a simple coupon test for which $\sigma_y = \tau = d\sigma_y = d\tau = 0$

Denoting

$$\frac{d\sigma_x}{d\epsilon_x} = E_t \tag{4.15}$$

F is defined by equation (4.6) as

$$F = \frac{3}{4J_2}\left[\frac{1}{E_t} - \frac{1}{E}\right] \tag{4.16}$$

Because of unavoidable initial imperfections the above derived stress-strain relations cannot be applied without modification to the local buckling problem. After investigating the influence of initial imperfections on two simplified models in the next chapter effective stress-strain relations for the strain hardening range of steel will be derived in Chapter 6.

5. Influence of Initial Imperfections

5.1 General

A perfectly plane plate will remain plane if it is subjected to loads acting in its center plane which do not exceed the corresponding buckling loads. In the case of longitudinal loading in the x - direction producing a state of stress with σ_x as the only component, this state of stress will remain unchanged up to the point when buckling occurs. Consequently the buckling stress can be obtained from stress-strain relations (4.6) to (4.9) with $\sigma_y = \tau = 0$.

However, the buckling strength of actual plates with unavoidable imperfections does not agree with the predictions for perfectly plane plates. The main reason for the discrepancy seems to be equation (4.9) which predicts elastic behavior with regard to the superimposed shear stresses.

Applying a simplified stress-strain diagram to a simplified model of a cruciform section Onat and Drucker[9] have shown that small unavoidable imperfections may account for the difference between predicted and actual behavior. Apparently the influence of imperfections on sections which fail by torsional buckling is completely different from those which fail in bending. The latter case has been investigated by Wilder, Brooks and Mathauser.[16]

In the following, this difference in behavior will be illustrated for simplified models which buckle in the strain-hardening range. The applied simplified stress-strain curve with $n = E/E_t = 40$ is shown in Fig. 3. Reasons why the compressive stresses can exceed the yield stress, σ_o, will be discussed in Chapter 6.

5.2 Simplified WF Column

The simplified WF column consists of two thin flanges of equal area separated by a web of infinite shear stiffness and negligible area (Fig. 4). Instead of a true initial imperfection, the deflections at the beginning of strain-hardening ($\sigma = \sigma_o$ and $\epsilon = \epsilon_o$) are used in the computations.

Following the same approach as Wilder, Brooks and Mathauser the deflection curve is assumed to be

$$y = \bar{y} \sin \frac{\pi x}{\ell} \tag{5.1}$$

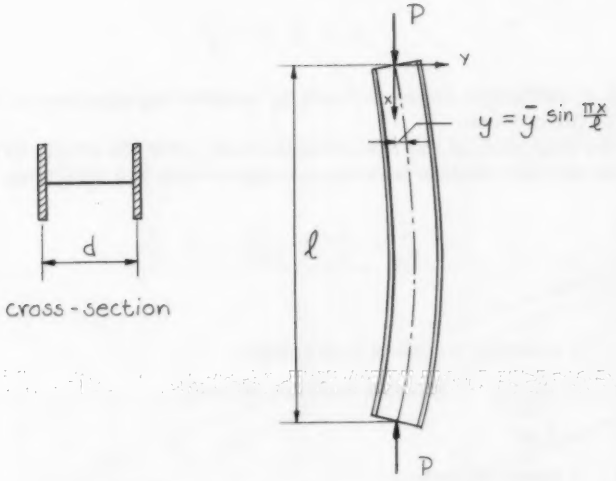

Fig. 4 - Simplified WF column

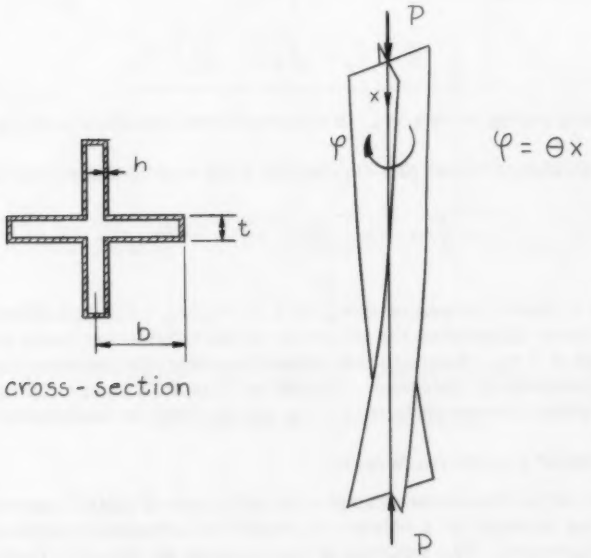

Fig. 5 - Simplified Cruciform Column

At the beginning of strain-hardening

$$y_o = \bar{y}_o \sin \frac{\pi x}{\ell} \tag{5.2}$$

The load vs deflection curve is found by considering equilibrium of the center section of the column.

For the first part of the load vs deflection curve the strain in both flanges increases and the relation between average stress and deflection is given by

$$\frac{\sigma}{\sigma_o} = \frac{\sigma_t}{\sigma_o} - \left(\frac{\sigma_t}{\sigma_o} - 1\right) \frac{f_o}{f} \tag{5.3}$$

where

σ = average stress of both flanges

$\sigma_t = \frac{\pi^2 E_t}{(\ell/r)^2}$ (tangent modulus stress)

$f = \bar{y}/d$

d = depth of section

f_o = value of f at beginning of strain-hardening.

Strain reversal occurs for

$$f = f_s = \sqrt{\tfrac{1}{2}\left(1 - \frac{\sigma_o}{\sigma_t}\right)}\ f_o \tag{5.4}$$

The corresponding stress, σ_s, is obtained from equation (5.3) by substituting $f = f_s$.

After strain-reversal has started the load vs deflection relation is given by

$$\frac{\sigma}{\sigma_o}\left[\frac{n-1}{2(n+1)} + f\right] = \frac{\sigma_s}{\sigma_o}\left[\frac{n-1}{2(n+1)} + f_s\right] + \frac{\sigma_t}{\sigma_o}\frac{2n}{n+1}(f - f_s) \tag{5.5}$$

Figure 6 shows curves of σ/σ_o vs f for $\sigma_t/\sigma_o = 1.2$ and different values of f_o. The figure illustrates the behavior of the column for loads corresponding to stresses $\sigma \cong \sigma_t$. Although the deflections start to increase more rapidly the load continues to increase. Therefore it is safe to use the tangent modulus load, which corresponds to $\sigma = \sigma_t$, as the limit of usefulness of the column.

5.3 Simplified Cruciform Section

In contrast to the above example the influence of initial imperfections on the buckling strength of a column of simplified cruciform cross-section will now be illustrated. The solution of the problem as given by Onat and Drucker[9] can be applied without modification to the simplified stress strain curve of Fig. 3.

The cross-section consists of a thin shell of constant thickness h (Fig. 5). The column which is loaded uniformly is assumed to fail by twisting. The ends are considered as providing no restraint, which considerably simplifies the kinematics of the problem and makes the state of stress and strain the

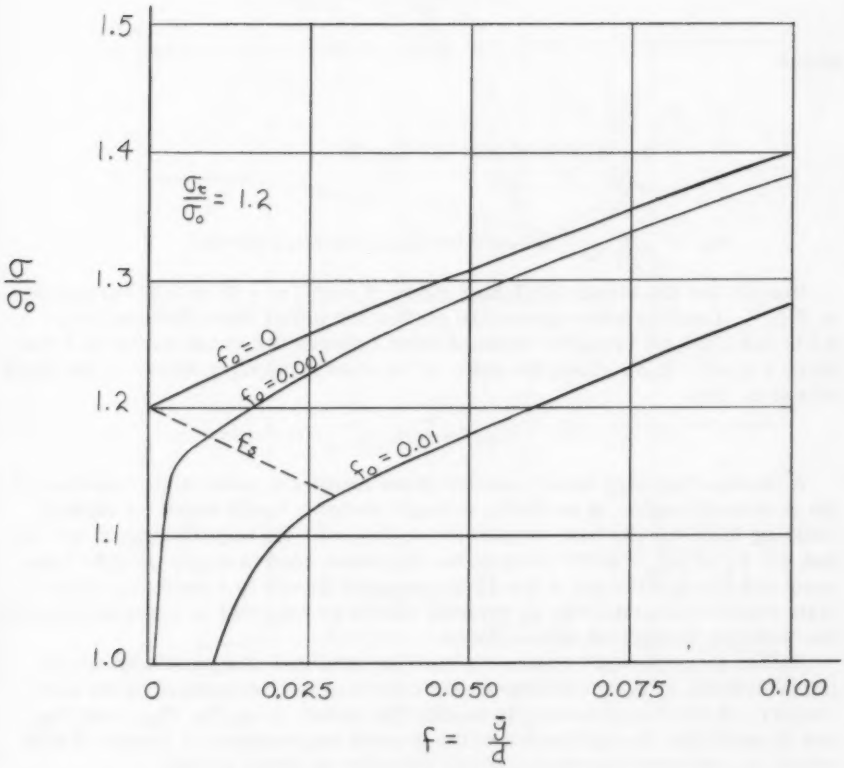

Fig. 6 - Effect of initial imperfections on a simplified WF section

same at each cross-section. An approximate solution for small values of X is given as

$$\sigma = \frac{\sigma_o \left(\frac{\gamma_o}{\gamma}\right)^{\frac{1}{2n'}} + \sigma_e \left[1 - \left(\frac{\gamma_o}{\gamma}\right)^{\frac{1}{2n'}}\right]}{1 + \frac{(n'-1)}{2n}(\gamma - \gamma_o)} \qquad (5.6)$$

where

$$X = \frac{b^4}{3t^2}\theta^2$$

θ = angle of twist per unit length

$$n' = \frac{3G}{E_t} + 1 - \frac{3G}{E}$$

$$\sigma_e = \frac{3t^2}{b^2}G \quad \text{(elastic torsional buckling stress)}$$

Results for the strain-hardening range of steel, n' = 46 (n = 40) are shown in Fig. 7. Load vs twist curves are plotted for initial imperfections $b\theta_o = 0$, 0.01^o and 0.1^o, $b\theta$ being the angle of twist between two cross-sections a distance b apart. In all cases the ratio of the elastic buckling stress to the yield stress is five.

$$(\sigma_e/\sigma_o = 5)$$

It is seen that very small imperfections cause a considerable reduction of the column strength. A perfectly straight member would reach its elastic buckling load, for the case considered $\sigma_e/\sigma_o = 5$. An imperfection at $\sigma = \sigma_o$ and $\epsilon = \epsilon_o$ of $b\theta_o = 0.01^o$ reduces the maximum load to $\sigma_m/\sigma_o = 1.4$. Consequently the application of the J2 incremental theory to a perfectly plane plate which fails primarily by twisting cannot be expected to correctly predict the buckling strength of actual plates.

Rather than attempt to solve the buckling problem of a plate with initial imperfections, effective stress-strain relations are determined in the next chapter. It will be necessary to modify the values of D_x, D_y, D_{xy}, and D_{yx}, and G_t such that the application to the general expressions of Chapter 3 will result in a correct description of the behavior of actual plates.

6. Stress-Strain Relations for the Strain-Hardening Range of Steel

6.1 Results of Coupon Tests

A simplified stress-strain curve obtained from a simple coupon test is shown in Fig. 3. It must be borne in mind that the strain represents an average strain measured over a certain gage length. It would be entirely erroneous to assume that the local strains within the plastic range from ϵ_f to ϵ_o are equal to the average strain. Yielding of mild steel occurs in small slip bands.(3) Slip takes place in a "jump" such that the strain across such a narrow band jumps from ϵ_f to ϵ_o. The first slip band originates at a weak point in the specimen, due to an inclusion, a stress concentration or other defects. From there on yielding will spread along the specimen.

This consideration leads to the conclusion that there is no material within the specimen at a strain between the yield strain, ϵ_f, and the strain-hardening

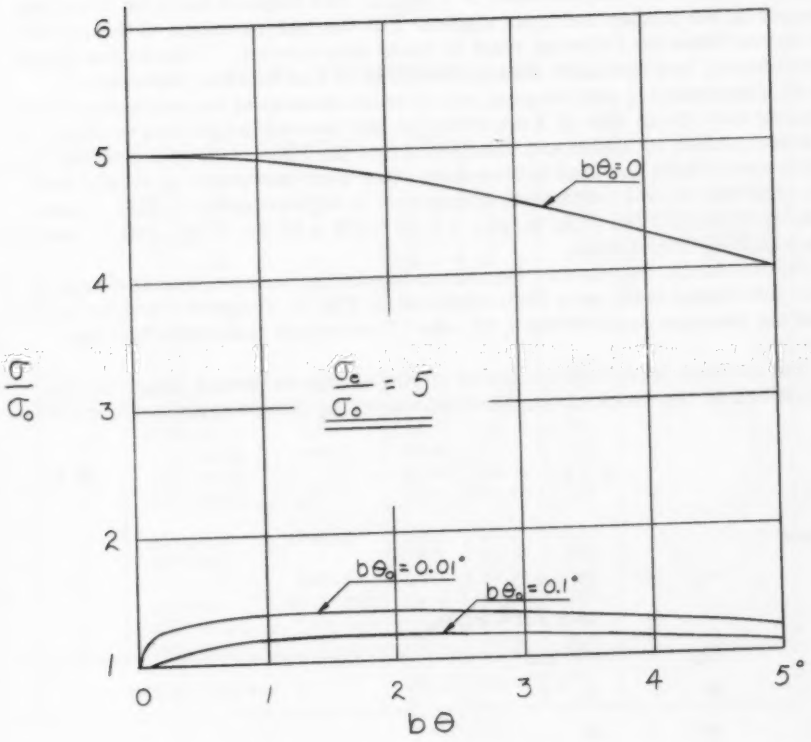

Fig. 7 - Influence of initial imperfections on a simplified cruciform section

strain, ϵ_0. Either the material is still elastic or it has reached the strain-hardening range.

In the strain-hardening range, $\epsilon > \epsilon_0$, the material is again homogeneous and in this range the "J_2 theory of plasticity" will be applied. In the intermediate range, $\epsilon_f < \epsilon < \epsilon_0$, the specimen can be considered to consist of two materials.

The results of 21 compression coupon tests carried out at Fritz Engineering Laboratory are summarized in Table 1. The coupons were cut from the flanges of WF shapes and from angles. For the interpretation of the results of coupon tests the following must be taken into account. Coupons are tested continuously in a hydraulic testing machine. It has become customary in Fritz Laboratory to test coupons with a valve opening of the machine corresponding to a strain rate of 1 micro in./in. per second in the elastic range. It has been shown by Huber and Beedle[17] that the ratio of the yield stress of a static test (where the load settles down after each increment of strain) and the yield stress of a continuous coupon test is approximately 0.925. Consequently a value of the yield stress, σ_0, of 0.925 x 39.2 = 36 ksi will be used in the following derivations.

Stress-strain curves for the strain-hardening range as obtained from 5 selected coupon tests have been replotted in Fig. 8. Coupons 9 and 18 represent the extreme cases while 5, 15, and 17 represent tests with "average" results.

The average stress-strain curve for the strain-hardening range can be expressed by the three parameters introduced by Ramberg and Osgood.[18]

$$\epsilon - \epsilon_o = \frac{\sigma - \sigma_o}{E_o} + K\left(\frac{\sigma - \sigma_o}{E_o}\right)^m \qquad (6.1)$$

where

σ_0 = 36 ksi

ϵ_0 = 14 x 10^{-3} in./in.

E_0 = 900 ksi*

K = 21

m = 2

Equation (6.1) is also plotted in Fig. 8.

The information now available is sufficient to determine F (J_2) defined by equation (4.16). From equations (4.16) and (6.1) it follows that

$$F = \left[67.357\frac{1}{\sqrt{J_2}} - 591.667\frac{1}{J_2}\right] \times 10^{-6}\ \frac{in^6}{kips^3} \qquad (6.2)$$

for $J_2 > 1/2\ \sigma_0^2 = 432\ kips^2/in.^4$

* The values of E_0 in Table 1 are taken from Fritz Laboratory reports in which they are usually not given as the slope of the stress-strain curve at the initiation of strain-hardening but as the slope at a strain somewhat larger than ϵ_0. Consequently E_0 as used in equation (6.1) is larger than the average value given in Table 1.

TABLE 1

RESULTS OF COMPRESSION COUPON TESTS

Coupon	Fritz Lab. Number	Section	σ_o ksi	ϵ_o x10^3	E_o ksi	Note
1	220A-UF3	14WF30	39.7	13.0	730	All WF section coupons taken from flanges
2	220A-UF4	"	41.5	14.6	690	
3	220A-LF1	"	42.5	14.6	650	
4	220A-LF2	"	39.0	12.5	790	
5	220A-LF3	"	39.7	12.5	730	
6	220A-LF4	"	42.0	13.0	670	
7	220A-A	"	40.8	15.0	640	
8	220A-B	"	40.8	12.5	675	
9	220A-D	"	40.3	15.5	650	
10	220A-E	"	39.6	14.5	650	
11	220A-F	"	35.3	(6.0)	780	
12	220A-G	"	36.2	(6.5)	700	
13	220A-B2F3	8WF31	40.0	17.4	770	
14	220A-B2F6	"	38.8	11.5	810	
15	220A-B2F7	"	39.0	14.8	730	
16	205E-C14	10WF33	40.0	14.5	855	
17	205E-C15	"	37.0	13.8	805	
18	205E-C2	8WF40	38.4	12.8	1060	
19	205E-C9	L6.6.3/8	39.0	12.8	710	
20	205E-C12	"	37.6	14.3	906	
21	205E-C13	"	35.1	14.6	845	
Average Values*			39.2	13.9	755	

* Numbers in parentheses not used for determining average value

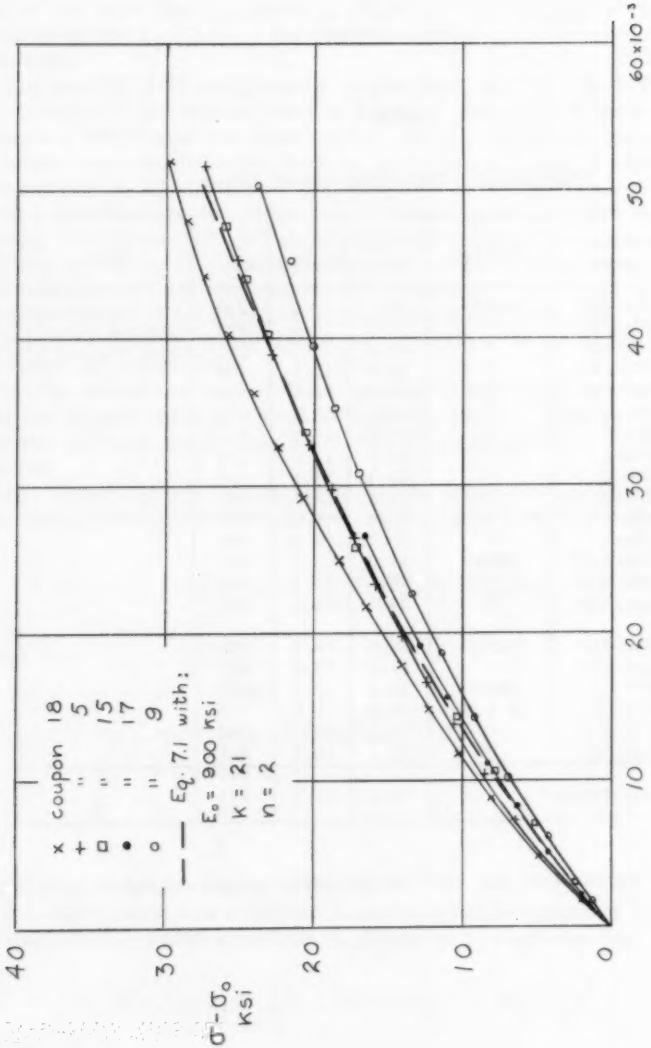

Fig. 8 - Results of Compression Coupon Tests in the Strain - Hardening Range

6.2 The Tangent-Modulus in Shear

Consider the case where shear stresses, τ, are superimposed on a constant normal stress, σ_x, taking $\sigma_y = 0$ and $d\sigma_x = d\sigma_y = 0$. The relations between the increments of stress and strain given by equations (4.6) and (4.9) reduce to

$$d\epsilon_x = \frac{4}{3} F \sigma_x \tau d\tau \tag{6.3}$$

$$d\gamma = \frac{2(1+\nu)}{E} d\tau + 4F\tau^2 d\tau \tag{6.4}$$

Integrating equation (6.4) gives the relationship between τ and γ as shown in Fig. 9 for $\sigma_x = 36$ ksi and $\sigma_x = 48$ ksi. The corresponding slope

$$G_t = \frac{d\tau}{d\gamma} \tag{6.5}$$

is plotted in Fig. 10.

It is seen from Fig. 10 that the value of G_t drops rapidly for small values of γ. However, in the region 2,000 ksi $< G_t <$ 3,000 ksi the decrease becomes slower. Consequently any value in this region could be selected as a useful value of G_t for the strain-hardening range of steel. On account of the results of torsional buckling tests on angle specimens presented in Chapter 7, the value G_t = 2,400 ksi is selected as being applicable to the strain-hardening range. From Fig. 9 it follows that the influence of the magnitude of the normal stress can be neglected for that part of the strain-hardening range under consideration.

6.3 Bi-Axial Normal Stresses

For regions of a plate in which cross bending is of importance the shear stresses are zero or very small, e.g. the center of plates supported along all four edges or the fixed edge of a clamped outstanding flange.

In this case equations (4.6) and (4.7) reduce to

$$d\epsilon_x = \left[\frac{1}{E} + \frac{1}{9} F (2\sigma_x - \sigma_y)^2\right] d\sigma_x + \\ - \left[\frac{\nu}{E} - \frac{1}{9} F (2\sigma_x - \sigma_y)(2\sigma_y - \sigma_x)\right] d\sigma_y \tag{6.6}$$

$$d\epsilon_y = \left[\frac{1}{E} + \frac{1}{9} F (2\sigma_y - \sigma_x)^2\right] d\sigma_y + \\ - \left[\frac{\nu}{E} - \frac{1}{9} F (2\sigma_x - \sigma_y)(2\sigma_y - \sigma_x)\right] d\sigma_x \tag{6.7}$$

Comparing equations (6.6) and (6.7) with equations (3.2) gives

$$\frac{1}{E_x} = \frac{1}{E} + \frac{1}{9} F (2\sigma_x - \sigma_y)^2 \tag{6.8}$$

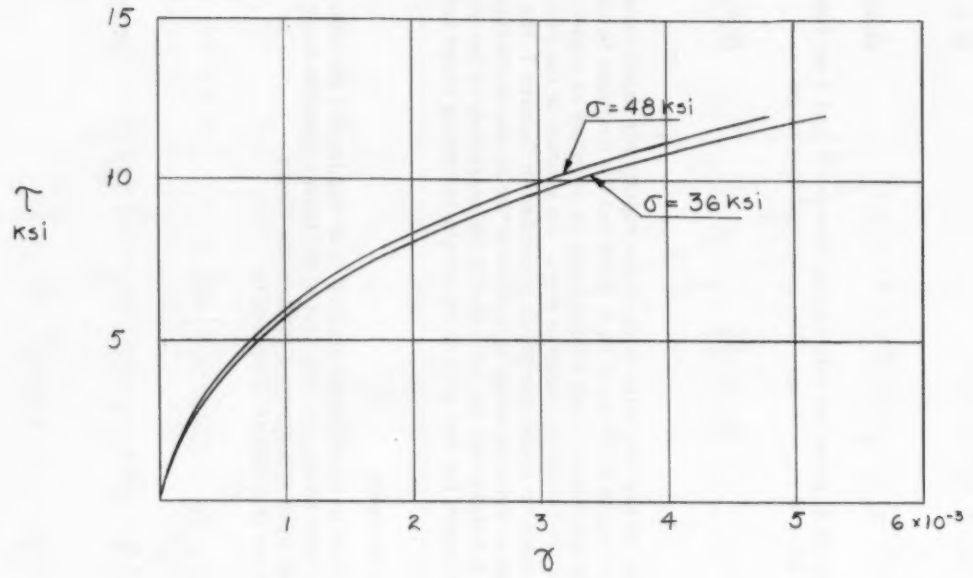

Fig. 9 - Superposition of Shear Stress on Constant Normal Stress

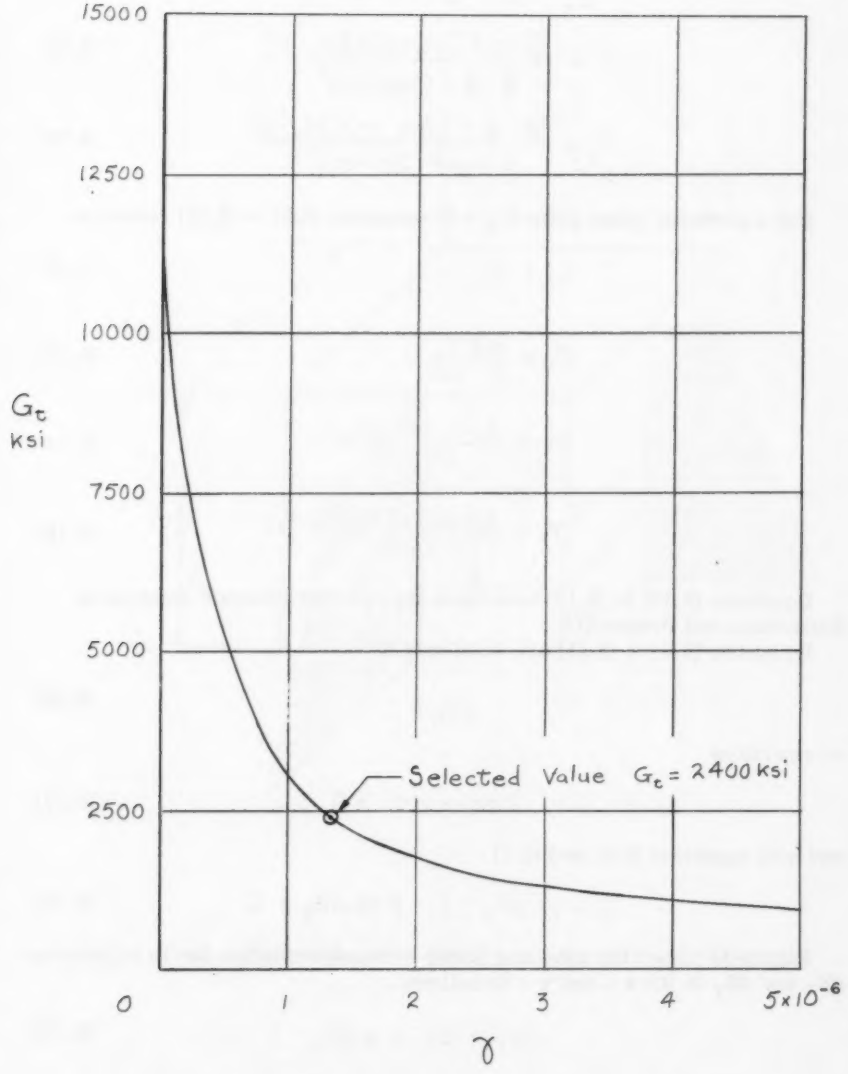

Fig. 10 - The Tangent Shear Modulus

$$\frac{1}{E_y} = \frac{1}{E} + \frac{1}{9} F (2\sigma_y - \sigma_x)^2 \tag{6.9}$$

$$\nu_x = \frac{\frac{\nu}{E} - \frac{1}{9} F (2\sigma_x - \sigma_y)(2\sigma_y - \sigma_x)}{\frac{1}{E} + \frac{1}{9} F (2\sigma_x - \sigma_y)^2} \tag{6.10}$$

$$\nu_y = \frac{\frac{\nu}{E} - \frac{1}{9} F (2\sigma_x - \sigma_y)(2\sigma_y - \sigma_x)}{\frac{1}{E} + \frac{1}{9} F (2\sigma_y - \sigma_x)^2} \tag{6.11}$$

For a perfectly plane plate ($\sigma_y = 0$) equations (6.8) to (6.11) reduce to

$$E_x = E_t \tag{6.12}$$

$$E_y = \frac{4 E E_t}{E + 3 E_t} \tag{6.13}$$

$$\nu_x = \frac{E - (1 - 2\nu) E_t}{2E} \tag{6.14}$$

$$\nu_y = \frac{2E - (1 - 2\nu) E_t}{E + 3 E_t} \tag{6.15}$$

Equations (6.12) to (6.15) have been applied with different notation by Handelman and Prager.(7)

Equations (6.9) to (6.11) are valid only if

$$dJ_2 > 0 \tag{6.16}$$

or rewritten

$$2 d\sigma_x - d\sigma_y > 0 \tag{6.17}$$

and with equations (6.6) and (6.7)

$$(2 - \nu)\, d\epsilon_x - (1 - 2\nu)\, d\epsilon_y > 0 \tag{6.18}$$

Figure 11 shows the assumed linear strain distribution due to curvatures dK_x and dK_y in the x - and y - directions.

$$d\epsilon_x = d\epsilon_1 + z\, dK_x \tag{6.19}$$

$$d\epsilon_y = d\epsilon_2 + z\, dK_y \tag{6.20}$$

where $d\epsilon_1$ and $d\epsilon_2$ are strain increments of the central plane in the x - and y - direction and z is the distance to the central plane.

The condition that all of the section is deformed plastically is obtained by substituting equations (6.19) and (6.20) in equation (6.18)

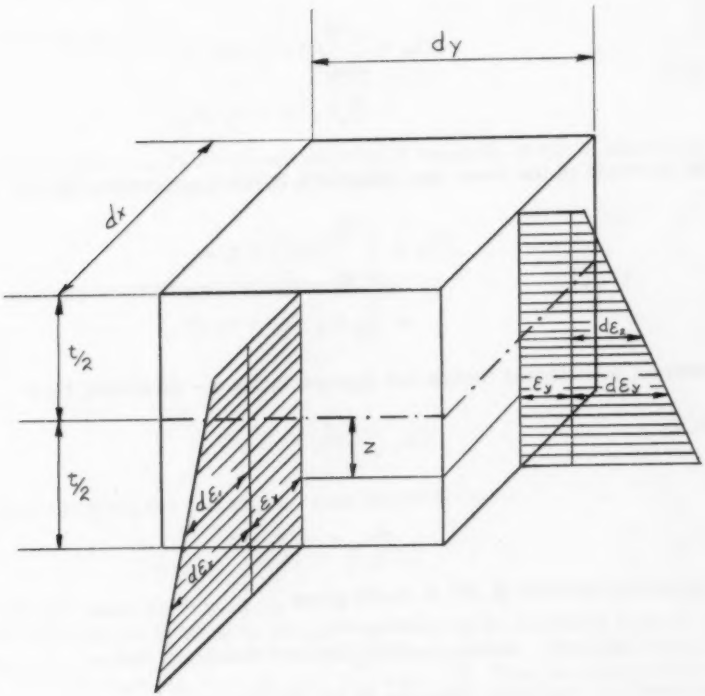

Fig. 11 - Assumed linear strain distribution

$$(2-\nu)(d\epsilon_1 + z\,dK_x) - (1-2\nu)(d\epsilon_2 + z\,dK_y) > 0 \qquad (6.21)$$

for $-t/2 \leq z \leq t/2$

The increase of the force per unit width in the x - direction, N_x, is found by rearranging equation (3.2) and integrating over the thickness of the plate

$$dN_x = \int_{-t/2}^{t/2} (d\sigma_x)\,dz = \qquad (6.22)$$
$$= D_x t\,(d\epsilon_1 + \nu_y\,d\epsilon_2)$$

The increase of the force per unit width in the y - direction is

$$dN_y = \int_{-t/2}^{t/2} (d\sigma_y)\,dz = \qquad (6.23)$$
$$= D_y t\,(d\epsilon_2 + \nu_x\,d\epsilon_1)$$

However, no external forces are applied in the y - direction, thus

$$dN_y = 0 \qquad (6.24)$$

or

$$d\epsilon_2 = -\nu_x\,d\epsilon_1 \qquad (6.25)$$

Substituting equation (6.25) in (6.22) gives

$$dN_x = E_x t\,d\epsilon_1 \qquad (6.26)$$

The plasticity condition, equation (6.21), then becomes

$$\left[2-\nu+(1-2\nu)\nu_x\right]d\epsilon_1 + (2-\nu)\,z\,dK_x - (1-2\nu)\,z\,dK_y > 0 \qquad (6.27)$$

for $-t/2 \leq z \leq t/2$

If the neutral zone between loading and unloading zones is at $z = t/2$, equation (6.27) gives

$$d\epsilon_1 = \frac{t/2\left\{(2-\nu)\,dK_x - (1-2\nu)\,dK_y\right\}}{2-\nu+(1-2\nu)\nu_x} \qquad (6.28)$$

Obviously $d\epsilon_1 > 0$ only if

$$dK_y < \frac{2-\nu}{1-2\nu}\,dK_x \qquad (6.29)$$

Checking the plasticity condition (6.27) for $d\epsilon_1$ given by equation (6.21) shows

that condition (6.27) is not violated if (6.29) is satisfied.

If the neutral zone is at z = - t/2 equation (6.27) gives

$$d\epsilon_1 = \frac{t/2\{(1-2\nu)\,dK_y - (2-\nu)\,dK_x\}}{2-\nu+(1-2\nu)\,\nu_x} \tag{6.30}$$

and $d\epsilon_1 > 0$ only if

$$dK_y > \frac{2-\nu}{1-2\nu}\,dK_x \tag{6.31}$$

The plasticity condition (6.27) is not violated if equation (6.31) is satisfied.

From equations (6.28) and (6.30) it is seen that

$$d\epsilon_1 = 0$$

and consequently according to equation (6.26)

$$dN_x = 0$$

for

$$dK_y = \frac{2-\nu}{1-2\nu}\,dK_x \tag{6.32}$$

Furthermore $dJ_2 = 0$ for the entire cross-section. Thus

$$d\sigma_x = \tfrac{1}{2}\,d\sigma_y \tag{6.33}$$

for an initially plane plate with $\sigma_y = 0$.

In this case, since bending is not accompanied by an increase in axial load the influence of initial imperfections will be the greatest. Suppose biaxial loading starts at $\sigma_x = \sigma_x^*$, $\sigma_y = 0$, $\epsilon_x = \epsilon_x^*$, $\epsilon_y = \epsilon_y^*$. Then it follows from equation (4.10) with equation (6.33) that initially

$$dJ_2 = \tfrac{1}{2}\sigma_y\,d\sigma_y \tag{6.34}$$

If during biaxial loading the ratio of $d\sigma_x$ and $d\sigma_y$ is taken according to equation (6.33), then integrating equation (6.34) gives

$$J_2 = J_2^* + \sigma_y^2 = \tfrac{1}{3}\sigma_x^{*2} + \sigma_y^2 \tag{6.35}$$

Applying equations (6.8) to (6.11) to the computation of the moduli D_x, D_y and D_{xy} as defined by equation (3.6) gives:

$$D_x = \frac{S}{RS-T^2} \tag{6.36}$$

$$D_y = \frac{R}{RS-T^2} \tag{6.37}$$

$$D_{xy} = D_{yx} = \frac{T}{RS - T^2} \tag{6.38}$$

where

$$R = \frac{1}{E} + \frac{4}{9} F \sigma^{*2} \tag{6.39}$$

$$S = \frac{1}{E} + \frac{1}{9} F \left(\frac{3}{2}\sigma_y - \sigma_x^*\right)^2 \tag{6.40}$$

$$T = \frac{\nu}{E} - \frac{2}{9} F \sigma_x^* \left(\frac{3}{2}\sigma_y - \sigma_x^*\right) \tag{6.41}$$

The results are shown graphically in Fig. 12 for $\sigma_x^* = 36$ ksi and $\sigma_x^* = 54$ ksi. From these results it can be concluded that the influence of the magnitude of σ_x^* is negligibly small. It is not obvious, however, which values of D_x, D_y and D_{xy} should be selected as being applicable in the strain-hardening range. Fortunately, compression tests on wide-flange sections presented in Chapter 7 reveal that the ratios of the half-wave length of the buckled shape over the depth of the section for the cases of web buckling are 0.55 and 0.54 (Tests D4 and D6 respectively). According to equation (3.21) this ratio is equal to $\sqrt[4]{D_x/D_y}$ if the small restraining effects of the flanges are neglected. Figure 13 shows the influence of σ_y/σ_x^* on $\sqrt[4]{D_x/D_y}$. On account of the results of the web buckling tests the values of D_x, D_y and D_{xy} corresponding to $\sigma_y/\sigma_x^* = 0.34$. Have been selected as applicable to the strain-hardening range.

Thus

D_x = 3,000 ksi

D_y = 32,800 ksi

$D_{xy} = D_{yx}$ = 8,100 ksi

7. Comparison with Test Results

For the selection of applicable values of D_x, D_y, D_{xy}, D_{yx} and G_t use has been made of the results of local (plate) buckling tests. The results are summarized here and are presented in more detail in another paper.(19)

7.1 Compression Tests on Angles

A number of compression tests on angles were performed with the purpose of checking the theoretical estimates developed above. Angle specimens have better known boundary conditions than WF sections and therefore give a more positive check. When buckling torsionally under the action of an axial load, the flanges of the angle act as two plates each with one free and one hinged edge, the heel forming the hinged edge. The loaded ends of the column were fixed against rotation in the testing machine. The dimensions of all specimens are given in Table 2. Besides the longitudinal strains at the flange tips and

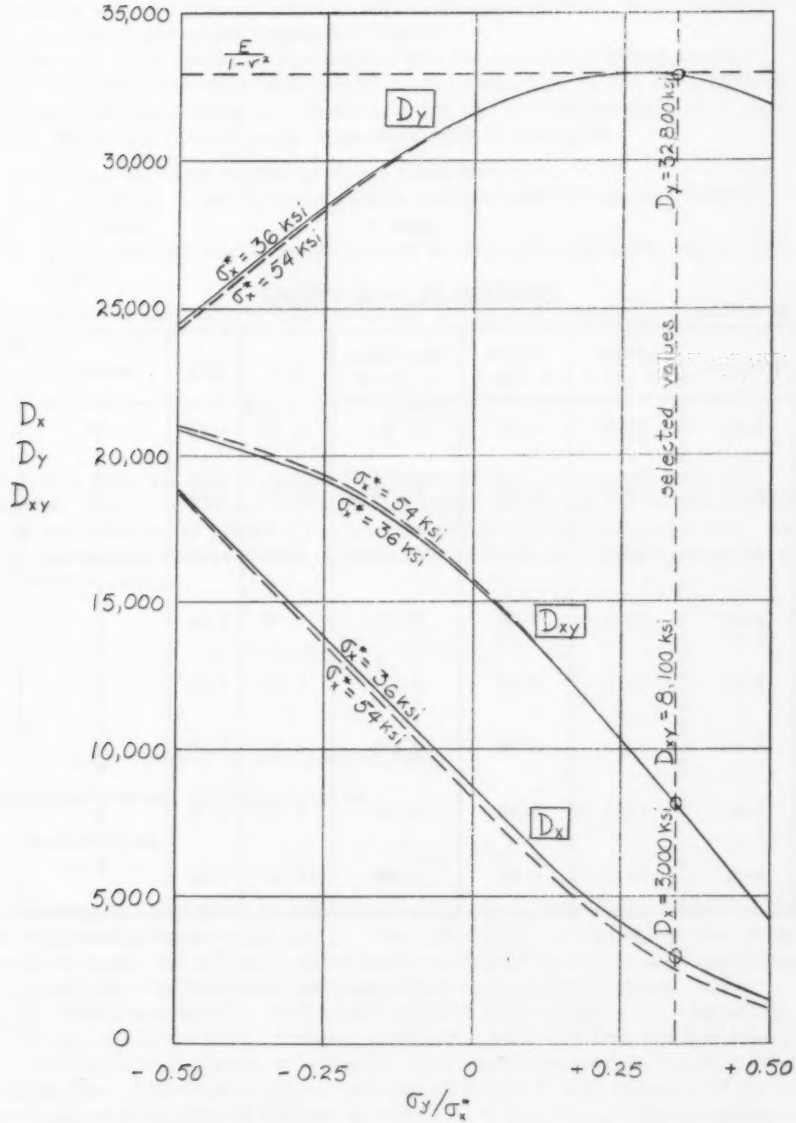

Fig. 12 – Influence of σ_y/σ_x^* on D_x, D_y, and D_{xy}

TABLE 2

DIMENSIONS OF ANGLE SPECIMENS

Specimen	Length 2L (in.)	Width b (in.)	Thickness t (in.)	b/t	2L/b	Material
A-21	25.0	4.87	0.383	12.70	5.14	↑
A-22	25.0	4.79	0.381	12.60	5.21	
A-31	17.9	3.27	0.370	8.85	5.48	Annealed
A-32	17.9	3.28	0.374	8.79	5.46	
A-41	12.5	2.31	0.377	6.13	5.41	
A-42	12.5	2.34	0.371	6.36	5.35	↓
A-33	17.5	3.30	0.378	8.73	5.30	↑
A-51	21.2	4.07	0.380	10.70	5.21	As-Delivered ↓

the heel, the rotation of the center section was measured. From the rotation measurements the critical average strain was determined. The results of the angle tests are summarized in Table 3.

When all of the material is strained into the strain-hardening range ($\epsilon_{cr} \geq \epsilon_o$) the theoretical solution is given by equation (3.12), the length of the angle specimen being 2L. A solution for the yielding range ($\epsilon_f < \epsilon_{cr} < \epsilon_o$) can be derived if the following three assumptions are made:

1. The material is elastic up to the yield stress.
2. In the yield range the specimen is partly elastic and partly strain-hardened.
3. The strain-hardening zones initiate at both ends and move toward the middle.

From the first assumption it follows that, if $\sigma_{cr} \leq \sigma_o$ the critical stress is given by

$$\sigma_{cr} = \left(\frac{t}{b}\right)^2 \left[\frac{\pi^2 E}{12(1-\nu^2)} \left(\frac{b}{L}\right)^2 + G\right] \tag{7.1}$$

When σ_{cr} obtained from equation (7.1) exceeds σ_o yielding will have commenced. From the second assumption it then follows that the middle section, being still elastic, is practically rigid compared with the yielded zones. Assuming that only the latter will deform results in the following expression for the buckling stress

$$\sigma_{cr} = \sigma_o = \left(\frac{t}{b}\right)^2 \left[\frac{\pi^2 D_x}{12} \left(\frac{b}{\zeta L}\right)^2 + G_t\right] \tag{7.2}$$

where

ζL = length of each yielded zone

The corresponding critical strain is

$$\epsilon_{cr} = (1-\zeta)\epsilon_f + \zeta\epsilon_o \tag{7.3}$$

Substituting in equation (7.2) the values of D_x and G_t this equation determines the relationship between b/t and ζ. For L/b = 2.65, the average value of the tested sections, the b/t vs ζ curve has been plotted in Fig. 14 as a solid line. As elastic deformations have been neglected in equation (7.2) b/t = ∞ for ζ = 0. For this case b/t = 20.7 which is found from equation (7.1) by taking σ = 36 ksi and L/b = 2.65. Knowing the rigid plastic solution and the point for ζ = 0 of the elastic-plastic solution the latter has been sketched in Fig. 14 as a dotted line. The elastic-plastic solution of b/t vs ζ with equation (7.3) gives ϵ_{cr} as a function of b/t for the range $\epsilon_f < \epsilon_{cr} < \epsilon_o$. The complete theoretical curves are shown in Fig. 15 for L/b = ∞ and L/b = 2.65, and are compared with the test results. The theoretical curves give a good description of the buckling strength.

7.2 Tests on Wide-Flange Shapes

In order to investigate the actual behavior of WF shapes with regard to

TABLE 3

RESULTS OF ANGLE TESTS

Test	σ_o ksi	$\epsilon_{cr} \cdot 10^3$	σ_{cr} ksi	Type of Buckling
A-22	--	3.0	32.2	torsional
A-31	34.9	16.5	35.8	torsional
A-32	34.6	16.5	35.6	torsional
A-41	35.3	--	--	bending
A-42	34.1	--	--	bending
A-33	41.3	16.0	46.4	torsional
A-51	41.0	6.0	41.2	torsional

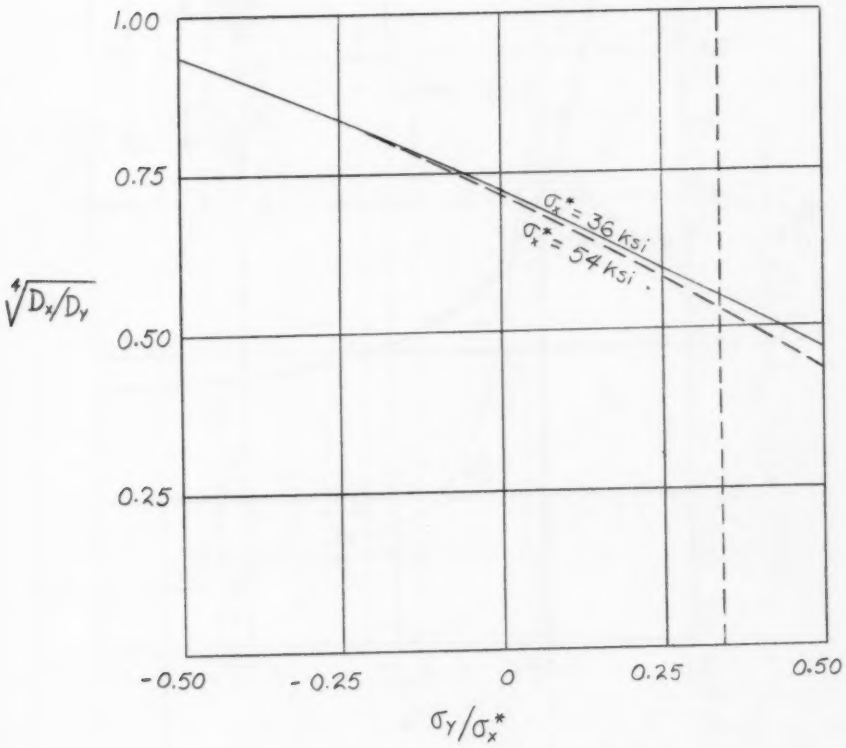

Fig. 13 – Influence of σ_Y/σ_x^* on $\sqrt[4]{D_x/D_y}$

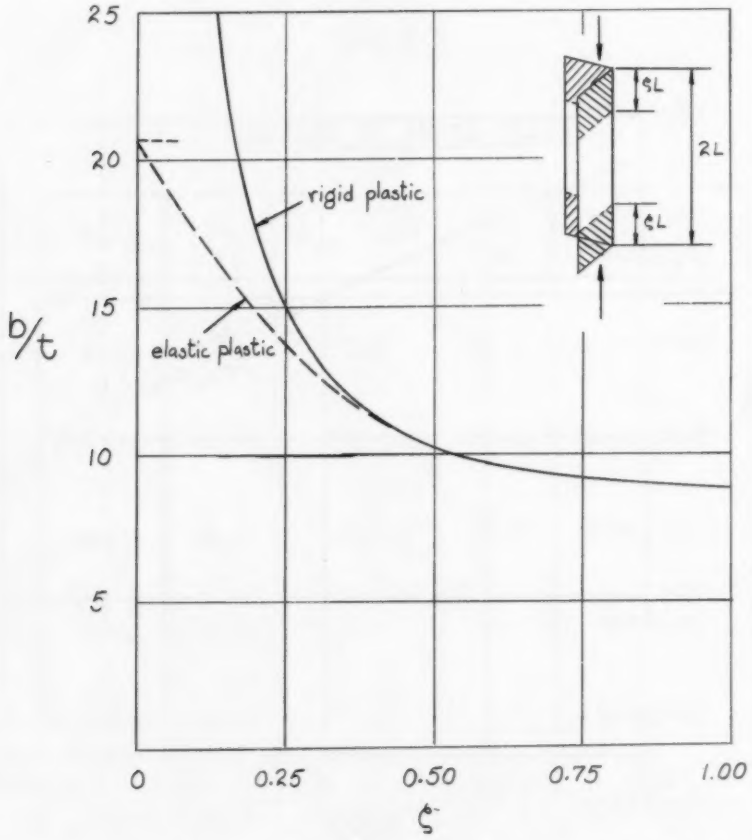

Fig. 14 – Yield Penetration ζ as a Function of b/t for $L/b = 2.65$

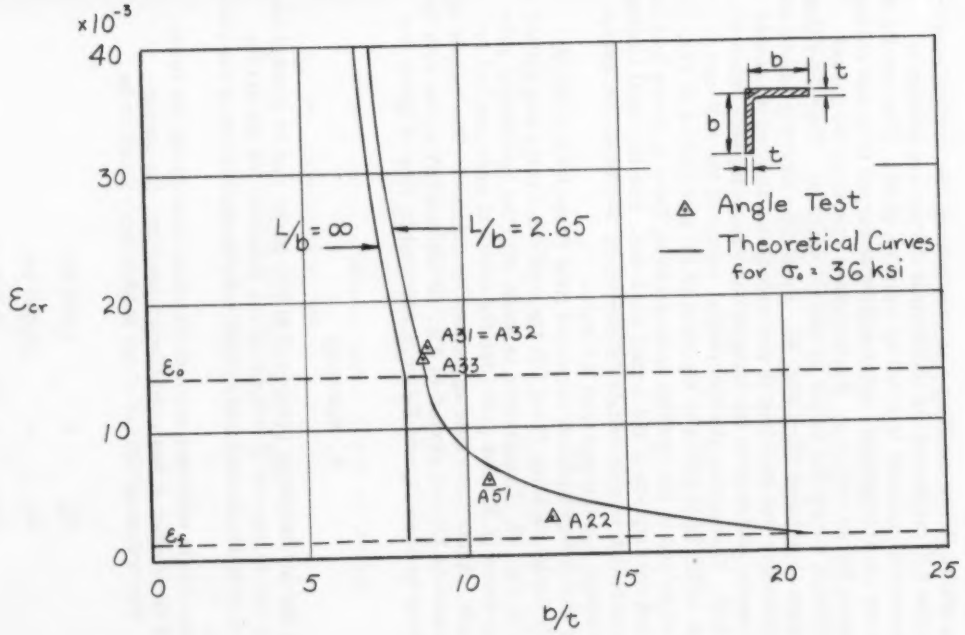

Fig. 15 – Comparison of Results of Torsional Buckling Tests on Angles with Theoretical Curves

local buckling, six different shapes were each tested under two loading conditions:

a) Axial compression (Test D1, D2, D3, D4, D5, D6)
b) Pure Bending (Test B1, B2, B3, B4, B5, B6)

The dimensions of all WF specimens are given in Table 4 and the test results are summarized in Table 5.

For the cases where flange buckling was predominant the critical strains of the flanges vs the b/t ratios and the theoretical curves are plotted in Fig. 16. The theoretical solution is given by equation (3.10). The results of tests D4 and D6 are omitted because web buckling occurred first and obviously caused premature flange buckling. Furthermore specimen B4 did not develop a major flange buckle but failed by lateral buckling. Therefore this result has also been eliminated from Fig. 16. From this figure it can be concluded that, if premature web buckling is prevented, the webs of the tested sections provide some restraint to the flanges corresponding to a value of β from 0 to about 0.05. Comparing the theoretical values of the half-wave length over flange width ratio given by equation (3.11) and plotted in Fig. 17, with the measured values of the bending tests given in Table 5 shows that the theory gives a good description of the actual behavior. For the axial loading tests the half-wave length was obviously influences by web buckling, except for specimen D5 which had the smallest d/t ratio.

For the cases where web buckling occurred first (Test D4 and D6) or simultaneous with flange buckling (Test D2) the critical strains are plotted vs the d/t ratios as in Fig. 18. Comparison is made with the theoretical solutions given by equations (3.20) and (3.22) for the cases of zero and full restraint respectively. Again favorable agreement is obtained. The values of ℓ/d given by equation (3.21) and plotted in Fig. 19 necessarily agree with the experimental values because D_x and D_y were selected in view of these test results.

8. Summary

The results of the investigation presented in this paper can be divided into two parts: firstly the derivation of stress-strain relations for the strain-hardening range of structural steel and secondly their application to the plate buckling problem.

Effective stress-strain relations were determined describing the orthotropic behavior of steel after it has been compressed into the strain-hardening range. The following values of the moduli were found to be applicable:

$$D_x = 3{,}000 \text{ ksi}$$

$$D_y = 32{,}800 \text{ ksi}$$

$$D_{xy} = D_{yx} = 8{,}100 \text{ ksi}$$

$$G_t = 2{,}400 \text{ ksi}$$

It is considered that the agreement between theory and test results (Figs. 15, 16, and 18) justifies this approach to the problem.

A direct practical application of the findings presented in this paper is the prevention of local buckling of outstanding flanges in continuous frames, in

TABLE 4

DIMENSIONS OF WF SPECIMENS

Spec.	Shape	2b in	t_f in	d in	t_w in	L in	L^1 in	b/t_f	d/t_w
B1 D1	10WF33	7.95	0.429	9.37	0.294	32	32	9.2	31.9
B2 D2	8WF24	6.55	0.383	7.63	0.236	26	26	8.6	32.3
B3 D3	10WF39	8.02	0.512	9.37	0.328	32	32	7.8	28.6
B4 D4	12WF50	8.18	0.620	11.57	0.351	32	32	6.6	33.0
B5 D5	8WF35	8.08	0.476	7.65	0.308	32	32	8.5	24.8
B6 D6	10WF21	5.77	0.318	9.56	0.232	23	26	9.1	40.9

2b = width of flange

t_f = thickness of flange

d = distance between center planes of flanges

t_w = thickness of web

L = length of compression specimen

L^1 = length of part of bending specimen subjected to pure bending

TABLE 5

RESULTS OF WF TESTS

Test	σ_o ksi	$\epsilon_{cr} \cdot 10^3$		σ_{cr} ksi		Flange ℓ/b	Web ℓ/d	Type of Buckling
		Flange	Web	Flange	Web			
D1	34.4	8.5	8.5	34.2	34.2	1.8	0.56	flange
D2	34.0	13.5	12.7	34.0	34.0	1.5	0.50	flange & web
D3	35.2	19.0	19.0	39.0	39.0	1.5	0.46	flange
D4	35.0	18.5	5.0	36.8	35.4	1.5	0.55	web
D5	36.6	17.0	17.0	38.0	38.0	2.1	0.56	flange
D6	38.0	4.3	1.6	33.8	37.2	--	0.54	web
B1	--	7.0	--	--	--	2.4	--	flange
B2	--	23.0	--	--	--	2.0	--	flange & lateral
B3	--	22.5	--	--	--	2.2	--	flange & lateral
B4	--	29.0	--	--	--	--	--	lateral
B5	--	22.0	--	--	--	2.0	--	flange & lateral
B6	--	14.0	--	--	--	2.4	--	flange & lateral

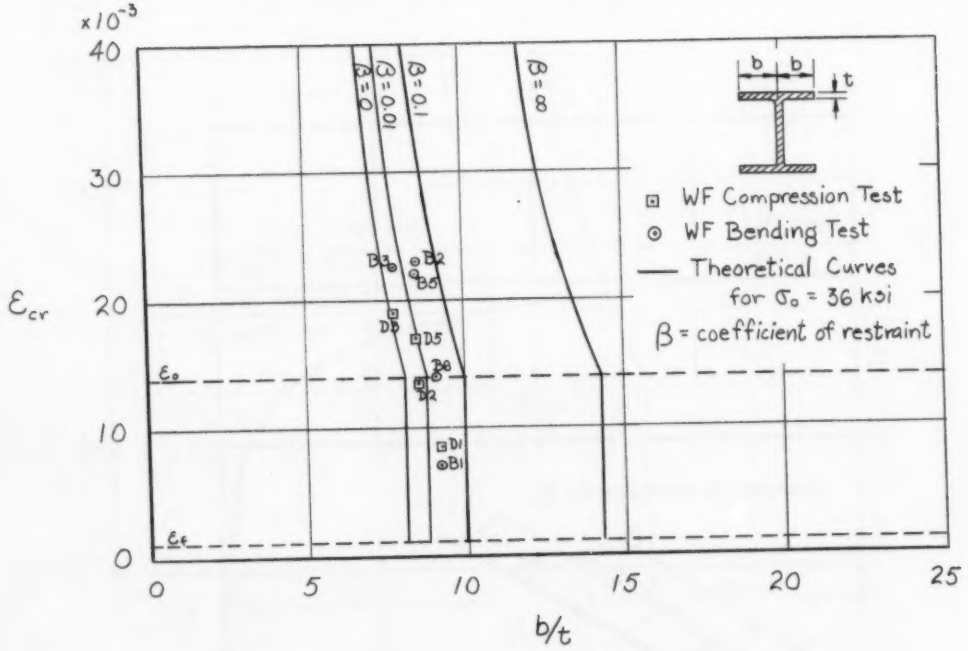

Fig. 16 - Buckling of Wide - Flange Shapes

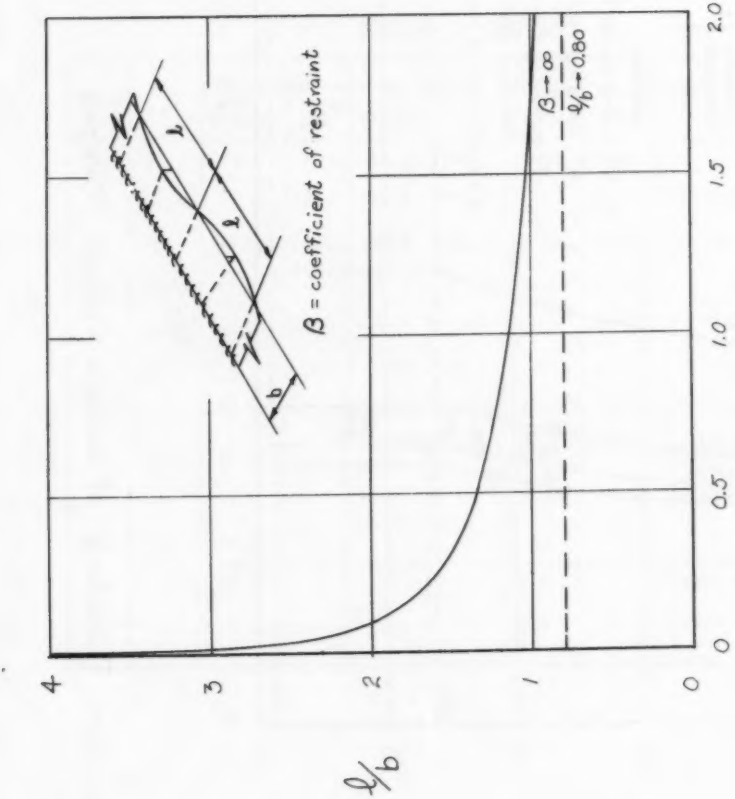

Fig. 17 - Half-Wave Length of Outstanding Flanges

Fig. 18 - Buckling of Webs of Wide-Flanged Shapes (Uniform Compression)

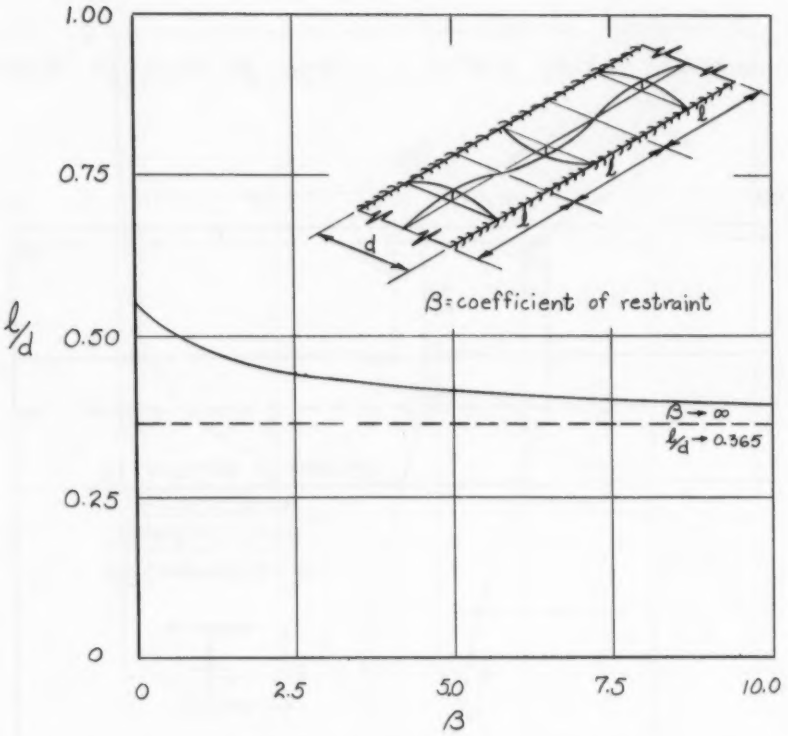

Fig. 19 – Half-wave length of webs

which the design is based upon ultimate strength. From the required rotation capacity of the plastic hinges the strains of the flanges can be determined. Fig. 16 then gives the required b/t ratio, for $\beta = 0.01$.

These stress-strain relations could equally well be applied to other problems involving the occurrence of shear and biaxial stresses and strains in the strain-hardening range of steel.

9. Acknowledgments

This paper is based on a Ph.D. dissertation presented to the Graduate Faculty of Lehigh University. The author is greatly indebted to Dr. Bruno Thürlimann who supervised the research project. His advice and suggestions are sincerely appreciated.

The project was part of the research program "Welded Continuous Frames and Their Components," carried out at Fritz Engineering Laboratory, Lehigh University, Bethlehem, Pennsylvania under the general direction of Dr. Lynn S. Beedle; the investigation is sponsored jointly by the Welding Research Council and the Department of the Navy with funds furnished by the American Institute of Steel Construction, American Iron and Steel Institute, Column Research Council (Advisory), Office of Naval Research (Contract 39303), Bureau of Ships and Bureau of Yards and Docks. Professor William J. Eney is Director of Fritz Engineering Laboratory and Head of the Department of Civil Engineering.

10. References

1. Timoshenko, S., "THEORY OF ELASTIC STABILITY," McGraw-Hill, New York, 1936.
2. Bleich, F., "BUCKLING STRENGTH OF METAL STRUCTURES," McGraw-Hill, New York, 1952.
3. Nadai, A., "THEORY OF FLOW AND FRACTURE OF SOLIDS," McGraw-Hill, New York, 1950.
4. Bijlaard, P. P., "SOME CONTRIBUTIONS TO THE THEORY OF ELASTIC AND PLASTIC STABILITY," International Association for Bridge and Structural Engineering, Vol. VIII, 1947.
5. Ilyushin, A. A., "STABILITY OF PLATES AND SHELLS BEYOND THE PROPORTIONAL LIMIT," (Translated from Russian), NACA TM-116, October, 1947.
6. Stowell, E. Z., "A UNIFIED THEORY OF PLASTIC BUCKLING OF COLUMNS AND PLATES," NACA Report 898, 1948.
7. Handelman, G. H. and Prager, W., "PLASTIC BUCKLING OF A RECTANGULAR PLATE UNDER EDGE THRUSTS," NACA TN-1530, August, 1948.
8. Drucker, D. C., "STRESS-STRAIN RELATIONS IN THE PLASTIC RANGE—A SURVEY OF THEORY AND EXPERIMENT," Report All S1, Graduate Division of Applied Mathematics, Brown University, December, 1950.
9. Onat, E. T. and Drucker, D. C., "INELASTIC INSTABILITY AND INCREMENTAL THEORIES OF PLASTICITY," Journal of the Aeronautical Sciences, Vol. 20, No. 3, March, 1953.

10. Haaijer, G. and Thürlimann, B., "COMBINED COMPRESSION AND TORSION OF STEEL TUBES IN THE STRAIN-HARDENING RANGE," Fritz Laboratory Report 241.2, Lehigh University (in preparation).

11. Girkmann, K, "FLACHENTRAGWERKE," 2nd Edition, Springer Verlag, Vienna, 1948.

12. Lundquist, E. E. and Stowell, E. Z., "CRITICAL COMPRESSIVE STRESS FOR OUTSTANDING FLANGES," NACA Report 734, 1942.

13. Lundquist, E. E. and Stowell, E. Z., "CRITICAL COMPRESSIVE STRESS FOR FLAT RECTANGULAR PLATES SUPPORTED ALONG ALL EDGES AND ELASTICALLY RESTRAINED AGAINST ROTATION ALONG THE UNLOADED EDGES," NACA Report No. 733, 1942.

14. Sokolnikoff, I. S., "MATHEMATICAL THEORY OF ELASTICITY," McGraw-Hill, New York, 1946.

15. Prager, W., "RECENT DEVELOPMENTS IN THE MATHEMATICAL THEORY OF PLASTICITY," Journal of Applied Physics, Vol. 20, Nr 3, 1949.

16. Wilder, T. W., III; Brooks, W. A., Jr.; and Mathauser, E. E., "THE EFFECT OF INITIAL CURVATURE ON THE STRENGTH OF AN INELASTIC COLUMN," NACA TN 2872, January, 1953.

17. Huber, A. W. and Beedle, L. S., "RESIDUAL STRESS AND THE COMPRESSIVE STRENGTH OF STEEL," Welding Journal, 33 (12), December, 1954.

18. Ramberg, W. and Osgood, R., "DESCRIPTION OF STRESS-STRAIN CURVES BY THREE PARAMETERS," NACA TN 902, 1943.

19. Haaijer, G. and Thürlimann, B., "ON INELASTIC LOCAL BUCKLING IN STEEL," A Theoretical and Experimental Study with Recommendations for the Geometry of Wide-Flange Shapes in Plastic Design, Fritz Laboratory Report 205E.8, Lehigh University, August, 1956.

20. Haaijer, G. "LOCAL BUCKLING OF WIDE FLANGE SHAPES," Ph.D. Dissertation 1956, Lehigh University.

11. Nomenclature

Tensor Notation

F = function defined by equation (4.1)

f = yield and loading function

i, j, k, ℓ, m - are letter subscripts taking the values 1, 2, and 3

J_2 = second invariant of deviatoric stress tensor

k = constant

s = mean normal stress

s_{ij} = components of deviatoric stress tensor

x_i = coordinate axis

δ_{ij} = Kronecker delta

ϵ_{ij} = components of strain tensor

ϵ^{e}_{ij} = elastic strain component

ϵ^{p}_{ij} = plastic strain component

σ_{ij} = components of stress tensor

Engineering Notation

A, a_1, a_2 - are constants

B = constant

b = width of plate with one free edge

C_1, C_2, C_3, C_4, C_5, C_6, C_7 - are constants

$D_x = \frac{E_x}{1 - \nu_x \nu_y}$

$D_y = \frac{E_y}{1 - \nu_x \nu_y}$

$D_{xy} = \nu_y D_x$

$D_{yx} = \nu_x D_y$

d = width of plate supported along all four edges

E = modulus of elasticity

E_t = tangent modulus

E_x = tangent modulus in x - direction

Ey = tangent modulus in y - direction

E_o = strain-hardening modulus

f = ratio of $\bar{y}$ over depth of simplified column

f_o = value of f at initiation of strain-hardening

f_s = value of f at which strain reversal takes place

G = modulus of elasticity in shear

G_t = tangent modulus in shear

H = function defined by equation (3.6)

h = thickness of sheet forming simplified cruciform section

I = moment of inertia per unit width of plate

K = constant

K_x = curvature of plate in x - direction

K_y = curvature of plate in y - direction

K_{xy} = twist of plate

ℓ = half-wave length of buckled shape

M_x = bending moment per unit width of plate in x - direction

M_y = bending moment per unit width of plate in y - direction

M_{xy} = torsional moment per unit width of plate in

N_x = axial force per unit width of plate in x - direction

N_y = axial force per unit width of plate in y - direction

m = exponent in equation (6.1)

n = ratio of modulus of elasticity over tangent modulus

n' = ratio defined by equation (5.6)

R = function defined by equation (6.39)

S = function defined by equation (6.40)

T = function defined by equation (6.41)

t = thickness of plate

w = deflection of plate

x = coordinate axis

y = coordinate axis

y = deflection of simplified column

$\bar{y}$ = maximum value of y

z = coordinate axis

β = B/A = coefficient of restraint

γ_{xy} = angular strain in xy plane

ϵ_{cr} = critical strain corresponding to σ_{cr}

ϵ_f = yield strain

ϵ_o = strain at initiation of strain-hardening

ϵ_x = normal strain in x - direction

ϵ_x^* = value of ϵ_x at which biaxial loading starts

ϵ_y = normal strain in y - direction

ϵ_y^* = value of ϵ_y at which biaxial loading starts

ζ = coefficient determining length of yielded zone

θ = angle of twist per unit length

ν = Poisson's ratio

ν_x = coefficient of dilatation for stress increment in x - direction

ν_y = coefficient of dilatation for stress increment in y - direction

σ_{cr} = critical (buckling) stress

σ_e = elastic buckling stress

σ_o = yield stress

σ_s = value of σ at which strain reversal takes place

σ_x = normal stress in x - direction

σ_x^* = value of σ_x at which biaxial loading starts

σ_y = normal stress in y - direction

τ_{xy} = shear stress

X = function defined by equation (6.10)

ψ = edge moment per unit length to produce unit rotation of edge

Journal of the
ENGINEERING MECHANICS DIVISION
Proceedings of the American Society of Civil Engineers

INELASTIC RESPONSE OF COLUMNS TO DYNAMIC LOADINGS

B. J. Hartz,* J.M. ASCE, and R. W. Clough,** A.M. ASCE
(Proc. Paper 1213)

SYNOPSIS

An analytical investigation of the response of columns to single compressive loadings of arbitrary time history such that the material of the column is strained into the inelastic range is presented in this paper. The column is assumed to have pinned-ends and to have a slight initial curvature or to have the loading applied slightly eccentric to the axis of the column.

The modal superposition approach is used to obtain the equations for the elastic response while an idealized, one-degree of freedom, rigid-plastic system is used to obtain the equations for the ensuing inelastic response, after the strain at some point in the column exceeds the yield strain for the material. Numerical integration is used to obtain solutions for both the elastic response and the inelastic response. A numerical example is worked out and the results compared to the experimentally determined response of an actual column.

INTRODUCTION

If a compressive force is applied slowly to a column, the classical stability analysis may be used to obtain the static stability load in the case of a concentrically loaded member. However, if the load is applied rapidly, the dynamic equilibrium of the column must be considered. As the load is applied and the column deflects laterally, inertia forces tend to resist the lateral deflection and have the effect of stiffening the column, so that, if the load is removed before the column attains a large lateral deflection or velocity, the column may be able to support loads much in excess of the static loads for this short period.

Note: Discussion open until September 1, 1957. Paper 1213 is part of the copyrighted Journal of the Engineering Mechanics Division of the American Society of Civil Engineers, Vol. 83, No. EM 2, April, 1957.

* Asst. Prof., Dept. of Civ. Eng., Univ. of Washington, Seattle, Wash.
** Associate Prof., Div. of Civ. Eng., Univ. of California, Berkeley, Calif.

If the column is a very long, slender member, the stresses due to a dynamic loading will generally remain below the yield point for the material throughout the entire response. This problem of elastic buckling of columns subjected to dynamic loadings has been treated by several previous investigators; Koning and Taub[1] followed by others[2,3,4] have investigated the elastic response due to a given applied loading and Hoff and others[5,6] have investigated the response due to a given time varying displacement of the end of the column.

However, most practical columns have a slenderness ratio such that they buckle only after the stresses in the column exceed the yield point. Two previous investigators[7,8] have discussed the inelastic response in the case of a given time varying displacement of the end of the column. The purpose of this paper is to present a method of analysis for the inelastic response of a column to an arbitrary dynamic loading. The numerical method of integration presented may also be used for obtaining the complete elastic response to an arbitrary dynamic loading in the case when the column does not yield. In addition the method may be adapted readily to obtain the elastic or inelastic response of certain types of beams subjected to dynamic loadings or to specified initial displacement and velocity distributions.

Equations for Elastic Response

The initial response to a dynamic loading will be elastic in all cases except the idealized case of a suddenly applied load equal to the dynamic yield strength of the column. Therefore, the first part of the analysis is devoted to obtaining the elastic response from which can be determined the instant of yielding and the initial conditions for the inelastic response.

Consider the column shown in Fig. 1, in which $y(x,t)$ is the deflection of the column at time t and $y_o(x)$ is the initial deflection of the column due to either initial curvature or end eccentricity, e, or a combination of these. The differential equation of equilibrium of this column for constant stiffness, EI, and mass per unit length, m, and neglecting rotatory inertia and shear effects is:

$$EI\left[\frac{\partial^4 y(x,t)}{\partial x^4} - \frac{\partial^4 y_o(x)}{\partial x^4}\right] + P(t)\frac{\partial^2 y(x,t)}{\partial x^2} + m\frac{\partial^2 y(x,t)}{\partial t^2} = 0 \qquad (1)$$

Assuming, for pinned-end columns,

$$y(x,t) = \sum_{n=1}^{\infty} u_n(t) \sin\frac{n\pi x}{L} \qquad (2)$$

and

$$y_o(x) = \sum_{n=1}^{\infty} u_{on} \sin\frac{n\pi x}{L} \qquad (3)$$

where

$$u_{on} = \frac{2}{L}\int_0^L y_o(x) \sin\frac{n\pi x}{L}\,dx \tag{4}$$

and substituting into Eq. 1 yields:

$$\sum_{n=1}^{\infty}\left[EI\left(\frac{n^4\pi^4}{L^4}u_n(t) - \frac{n^4\pi^4}{L^4}u_{on}\right) - P(t)\frac{n^2\pi^2}{L^2}u_n(t) + m\frac{d^2u_n(t)}{dt^2}\right]\sin\frac{n\pi x}{L} = 0 \tag{5}$$

But since the terms of this series are all linearly independent, in order for the sum to be zero the coefficients of each term must be zero, or

$$EI\frac{n^4\pi^4}{L^4}\left[u_n(t) - u_{on}\right] - P(t)\frac{n^2\pi^2}{L^2}u_n(t) + m\frac{d^2u_n(t)}{dt^2} = 0 \tag{6}$$

Rewriting this differential equation for the "generalized coordinates," $u_n(t)$ gives, (using dots to represent differentiation with respect to time)

$$\ddot{u}_n(t) + \frac{n^2\pi^2}{mL^2}\left[\frac{n^2\pi^2 EI}{L^2} - P(t)\right]u_n(t) = \frac{n^2\pi^2}{mL^2}\left(\frac{n^2\pi^2 EI}{L^2}u_{on}\right); \qquad n = 1, 2, \cdots \infty. \tag{7}$$

Eq. 7 can be simplified by introducing

$$P_{En} = \frac{n^2\pi^2 EI}{L^2} \tag{8}$$

and the non-dimensional parameters

$$v_n(t) = \frac{u_n(t)}{u_{on}} \tag{9}$$

$$\lambda_n(t) = \frac{P(t)}{P_{En}} \tag{10}$$

and

$$\tau = t\omega \tag{11}$$

where

$$\omega = \frac{\pi^2}{L^2}\sqrt{\frac{EI}{m}} \tag{11a}$$

Eq. 7 then becomes

$$\ddot{v}_n(\tau) + n^4\left[1 - \lambda_n(\tau)\right] v_n(\tau) = n^4 \; ; \; n = 1, 2, \cdots \infty \tag{12}$$

The initial conditions are:

$$y(x,0) = y_0(x) \text{ and } \frac{\partial y(x,0)}{\partial t} = 0 \tag{13}$$

or

$$v_n(0) = 1 \text{ and } \dot{v}_n(0) = 0 \tag{14}$$

Eq. 12 with the initial conditions (Eq. 14) are an infinite system of linear, second-order differential equations for the quantities $v_n(t)$ from which the deflection can be obtained using Eqs. 9 and 12. The solution of these equations for constant $\lambda_n(t)$ (i.e., constant P(t) are well known (three solutions exist, one each for $\lambda_n<1$, $\lambda_n = 1$, and $\lambda_n>1$). It should be noted that the series of Eq. 2 will not converge to the correct moments at the end in the eccentrically loaded case and, in general, will converge only slowly near the ends in this case. Pian & Siddall[3] have given a form of the solution with more rapid convergence which corresponds to subtracting the Fourier sine expansion for a parabola and adding the equation of a parabola to this series.

Equations for End of Elastic Response

The equations derived above are valid until the strain in some fiber of the column exceeds the yield strain. The strain in an outside fiber of the column is given by (c is its distance from the neutral axis)

$$\epsilon = \frac{P(t)}{AE} \pm c\,\frac{\partial^2 y(x,t) - y_0(x)}{\partial x^2} \tag{15}$$

where y(x,t) and $y_0(x)$ are given by Eqs. 2 and 3. For symmetrical initial shapes subjected to loads of not too short duration ($>0.3T_N$, where T_N is the natural period of vibration), the onset of yielding may be defined with sufficient accuracy by using only the 1st and 3rd modes of the response, and the maximum strain will be at the center. However, very rapidly applied eccentric loads will cause yielding at the end of the column if the strain at the end, given by the expression

$$\epsilon = \frac{P(t)}{AE} + \frac{P(t)ec}{EI} \tag{16}$$

exceeds the yield point. In the case of unsymmetrical initial shapes, the 1st and 2nd modes of the response would generally be required to determine satisfactorily the location and instant of first yielding. The strain at which yielding occurs would, of course, depend on the rate of straining of the mate-

rial but within a certain range of loading, a satisfactory single value probably could be established for all cases. It should be noted that even though only one mode may be required to define the deflections, more than one mode may be required to determine adequately the instant of yielding.

Equations for Inelastic Response

As soon as yielding commences in the column, a rigid-plastic type of action is assumed in which a hinge develops at the point of yielding and the segments of the column on either side of the hinge are "frozen" in the deflected shape which existed at the instant of yielding. Such a system is shown in Fig. 2 for a hinge located a distance x_0 from the left end of the column. The dynamic moment equilibrium condition of the left segment of the column provides the equation

$$P \cdot u - \frac{m\ddot{u}}{6}(2L - x_o)x_o + \frac{m\ddot{u}}{2}x_o\frac{x_o}{3} - M_I = 0 \tag{17}$$

or simplifying

$$\frac{mx_o}{3}(L - x_o)\ddot{u}(t) = P(t)u(t) - M_I \tag{18}$$

where M_I is the internal plastic moment resistance of the hinge. For the ordinary symmetrical case of a hinge at the center of the column this equation becomes

$$\frac{mL^2}{12}\ddot{u}(t) = P(t)u(t) - M_I \tag{19}$$

The initial conditions for the inelastic response are obtained from continuity of displacements at the position of the hinge, and from continuity of momentum from the elastic motion to the rigid-plastic motion. For the case of a hinge at the center, these initial conditions for the inelastic response are

$$u_{o\ inelastic} = u(t_i)_{elastic} \tag{20}$$

and

$$\dot{u}_{o\ inelastic} = \frac{4}{\pi}\dot{u}(t_i)_{elastic} \tag{21}$$

where t_i is the time at the instant of yielding.

Eqs. 18 or 19 for the inelastic response require an expression for the inelastic moment M_I in terms of t. This inelastic moment for a column will be a function of the shape of the cross-section, the properties of the material, the axial force, and the curvature, which is in turn a function of the deflection. In general, the true relationship between moment (M), axial force (P) and curvature (ϕ) in the inelastic range can be approximated by one or more linear relationships such as

$$M_I = M_a\left(1 - \frac{P(t)}{P_a} - \frac{\phi(t)}{\phi_a}\right) \tag{22}$$

where M_a, ϕ_a, and P_a are constants to be determined for the particular cross-section and material properties. It may also be possible to find an approximate linear relationship between ϕ and u in the inelastic range of the form

$$\phi(t) = k\,u(t) + C \tag{23}$$

which would correspond to a yield zone of fixed length. It should be noted here that although it was possible to put the equations for the elastic response (Eq. 7) in the non-dimensional form of Eq. 12, the equations for the end of the elastic response and for the inelastic response do not depend on these same non-dimensional parameters, hence the total response cannot be put in non-dimensional form. For this reason, the total response will be a function of the actual dimensions as well as of the initial deflections of the column and the loading.

Numerical Integration of the Equations

In the case when P(t) is a constant, Eq. 12 may be solved explicitly for the elastic deflection. A solution in terms of Mathieu functions is available for the case of a sinusoidal loading. It is not likely that a solution of Eq. 18 for the inelastic response could be found except in the special case of constant load and for a particular form of internal moment, M_I. For arbitrary P(t) and for more general forms of M_I, numerical integration of the equations must be used to obtain solutions of the equations. For dynamic equations similar to these, other investigators have used various step-by-step, collocation and finite differences methods.(3,7,9) The method chosen here is a step-by-step iterative method which has been applied to dynamics equations by Newmark.(10) This method has the advantages that relatively large time intervals may be used, that the initial conditions enter in a simple manner, and that quantities such as accelerations and velocities do not lose their physical significance.

The method of numerical integration used here consists of assuming that the second derivative of the displacement varies linearly over a small time interval, Δt, from the known initial value, $\ddot{u}_b$, to an assumed final value $\ddot{u}(t_b + \Delta t)$. Integration of this twice yields the displacement at the end of the time interval. This value of the displacement at the end of the time interval can then be used in the equations for the response of the column to obtain a value for $\ddot{u}(t_b + \Delta t)$ which should check the assumed value. The assumed and computed values of $\ddot{u}(t_b + \Delta t)$ at the end of the interval are made to agree by iteration at each time interval. The method is portrayed in Fig. 3. The equations for $\dot{u}$ and u for an assumed value of $\ddot{u}(t_b + \Delta t)$ are

$$\dot{u}(t_b + \Delta t) = \frac{\ddot{u}(t_b + \Delta t)}{2}\Delta t + \frac{\ddot{u}_b}{2}\Delta t + \dot{u}_b \tag{24}$$

and

$$u(t_b+\Delta t) = \frac{\ddot{u}(t_b+\Delta t)}{6}(\Delta t)^2 + \frac{\ddot{u}_b}{3}(\Delta t)^2 + \dot{u}_b \Delta t + u_b \qquad (25)$$

Since either Eq. 7 for the elastic response or Eq. 19 for the inelastic response gives $\ddot{u}(t)$ as a function of $u(t)$ and $P(t)$, the appropriate equation can then be used to compute $\ddot{u}(t_b + \Delta t)$ from Eq. 25 and $P(t_b + \Delta t)$ from the given load function $P(t)$. If this computed value is not the same as the value assumed for computing $\ddot{u}(t_b + \Delta t)$ from Eq. 25, this new value can be used as an assumed value for repeating the process. If the time interval Δt is small enough the process will converge quickly to the correct acceleration. Newmark indicates that satisfactory convergence will be obtained if the time interval of integration is less than 1/10th the period of vibration for simple vibration problems. The time interval used in this investigation was less than 1/10th the period of vibration of the unloaded column. The convergence was checked using an interval half as large and was found to give the same results (within one percent). In some cases the maximum usable time interval may be the largest value that would satisfactorily approximate either the load curve or the instant at which the column yielded.

Numerical Example and Comparison with Test Results

Test results were available for about 80 dynamic loading tests performed by the authors on columns in which the response was in the inelastic range. The analysis presented in this paper is now applied to one of these tests.

The column considered was an annealed mild steel tube, 1 inch square outside with a wall thickness of 0.11 inch and a length of 44.5 inches. The L/r ratio was 124, the Euler buckling load was 7.2 kips, and the fundamental period of free lateral vibration was 0.0198 sec. The static yield load for the section was 12.8 kips (32.0 ksi). The test results indicated that the upper dynamic yield point loading was about 23.6 kips (62.0 ksi) giving a dynamic yield strain of 2100 microinches/inch. The lower dynamic yield point was estimated to be 17.7 kips (46.5 ksi) at a strain of 7350 microin./in. Stress-strain properties of the material are depicted in Fig. 4. Using these dynamic stress-strain properties and the dimensions of the cross-section gives the dynamic moment-curvature-axial force relationship shown in Fig. 5. The relationship used for M_I in the analysis is shown by the dotted lines, and is of the form of Eq. 22, with the constants defined as follows. From the instant of yielding (which is assumed to occur at $\phi = 4.90 \times 10^{-3}(1 - \frac{P}{23.6})$) until the curvature reaches the value $\phi = 11 \times 10^{-3}$ in/in/in, the constants are taken as $P_a = 23.6$ kips, $M_a = 8$ kip-inches, and $\phi_a = 44 \times 10^{-3}$ in/in/in. For curvatures greater than $\phi = 11 \times 10^{-3}$ in/in/in, they were taken as $P_a = 17.7$ kips, $M_a = 6$ kip-inches and $\phi_a = \infty$. The relationship between deflection and curvature for use in Eq. 22 was found to be given by an equation of the form of Eq. 23 as follows

$$\phi = \phi_i + 1.8\frac{\pi^2}{L^2}(u - u_i) \qquad (26)$$

assuming a hinge to develop at the center, where ϕ_i and u_i are the values of ϕ and u at the instant of yielding. This corresponds to a uniform yielded length of 10 inches.

The column was concentrically loaded and, since its initial shape was primarily a first mode deflection, only one elastic mode was used for the analysis. The initial first mode deflection was 0.043 inches. The loading and the measured and computed center deflections plotted as functions of time, are shown in Fig. 6. The time interval of integration was one-half millisecond (0.0005 second). On this figure is indicated the instant at which the column was found to yield in the analysis, according to the criterion established above. Values of the Euler buckling load, the static yield load, and the fundamental period of free vibration are also shown.

CONCLUSIONS

The method of analysis presented gave a very good approximation to the actual response of the column considered, even though only one mode was used in calculating the elastic response. This column had a dynamic loading applied during an interval equal to 0.6 times the fundamental period of vibration of the unloaded column (T_N).

The method was found to give good results when applied to any of the columns tested for which the duration of the loading was from 0.3 to 0.9 times the fundamental period of vibration. However, if the period of loading were quite short (i.e., $< 0.3\ T_N$) it would be expected that more modes would be required to determine satisfactorily the position and instant of yielding, even for columns containing relatively small amounts of higher modes in the initial shape. This is because the short duration loading would be more effective, relatively, in exciting the short period modes of vibration. On the other hand, if the period of loading were relatively long (i.e., $> 0.9\ T_N$), it would be expected that a better approximation of the inelastic moment resistance and the dynamic yield point would be required to give a satisfactory approximation of the actual deflection, because the time during which dynamic yielding took place would occupy a more significant portion of the total response. Both of these expectations were substantiated by the results of the test program. If proper consideration is given to these factors, the method presented may be applied to columns subjected to any type of dynamic loading, subject only to the limitation that the columns considered form a single, reasonably concentrated, plastic hinge during yielding so that the inelastic response may be approximated by a rigid-plastic column.

REFERENCES

1. Koning, C. and Taub, J., "Impact Buckling of Thin Bars in the Elastic Range," NACA Technical Memorandum 748, 1934.

2. Meier, J. H., "On the Dynamics of Elastic Buckling," Jour. of The Aeronautical Sciences, Vol. 12, Oct. 1945, p. 433.

3. Pian, T. H. H. and Siddall, J. N., "Dynamic Buckling of Slender Struts," ONR Tech. Report, MIT, 1950.

4. Davidson, J. F., "Buckling of Struts under Dynamic Loads," Jour. Mech. and Physics of Solids, Vol. 2, No. 1, 1953, p. 54.

5. Hoff, N. J., "The Dynamics of the Buckling of Elastic Columns," Jour. of Appl. Mechanics, Vol. 18, No. 1, p. 68, Mar. 1951.

6. Hoff, N. J., Nardo, and Erickson, "The Maximum Load Supported by an Elastic Column in a Rapid Compression Test," Proc. 1st U.S. Nat'l. Congress of Appl. Mechanics, 1951, p. 419.

7. Chawla, J. P., "Numerical Analysis of the Process of Bucklong of Elastic and Inelastic Columns," Proc. 1st U.S. Nat'l. Congress of Appl. Mechanics, 1951, p. 435.

8. Brooks, W. A., Jr. and Wilder, T. W., III, "The Effects of Dynamic Loading on the Strength of an Inelastic Column," NACA Tech. Note 3077, 1954.

9. Fraenkel, S. J. and Grinter, L. E., "Non-Elastic Behavior of Bridges Under Impulsive Loading," ASCE Proc. Vol. 79, Separate No. 185, 1953.

10. Newmark, N. M., "Method of Analysis for Structures Subjected to Dynamic Loading," Report to the Directorate of Intelligence, Headquarters USAF, Washington, D. C., 1949.

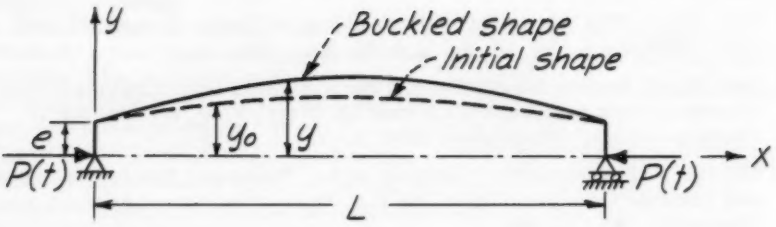

Fig. 1.-- Elastic Column.

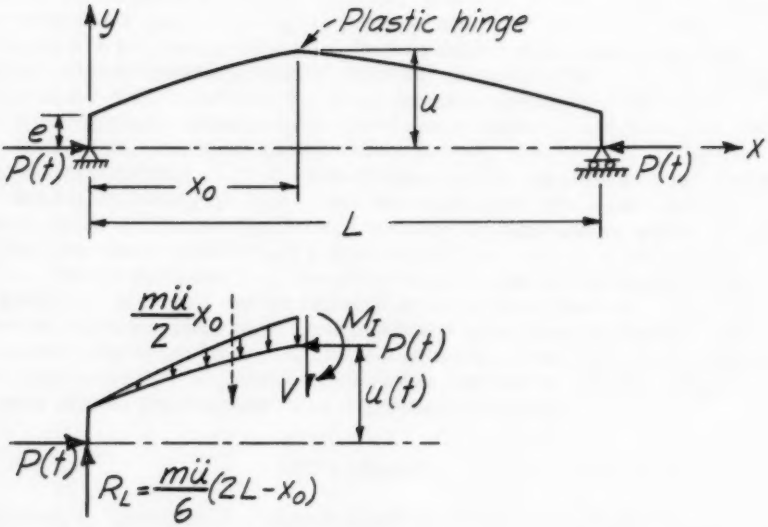

Fig. 2.-- Inelastic Column.

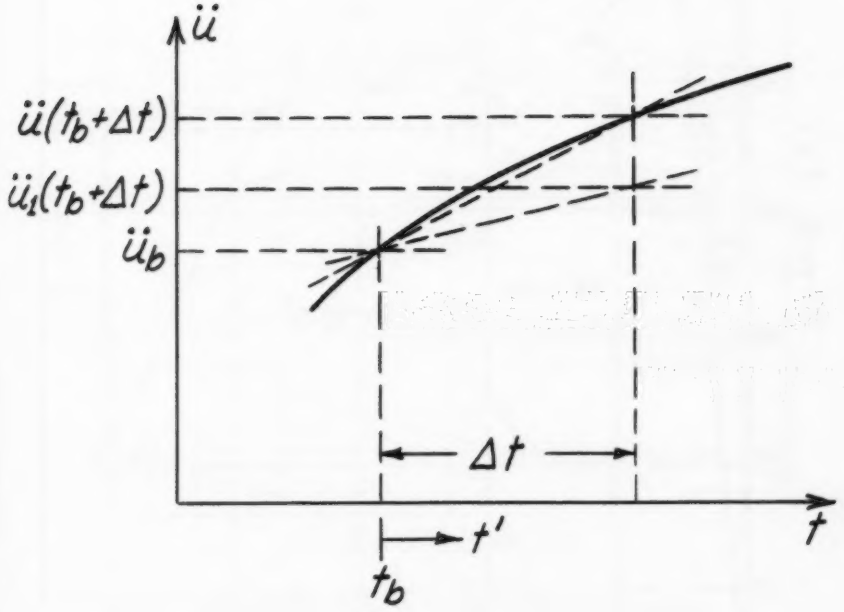

Fig.3.-- Numerical Integration.

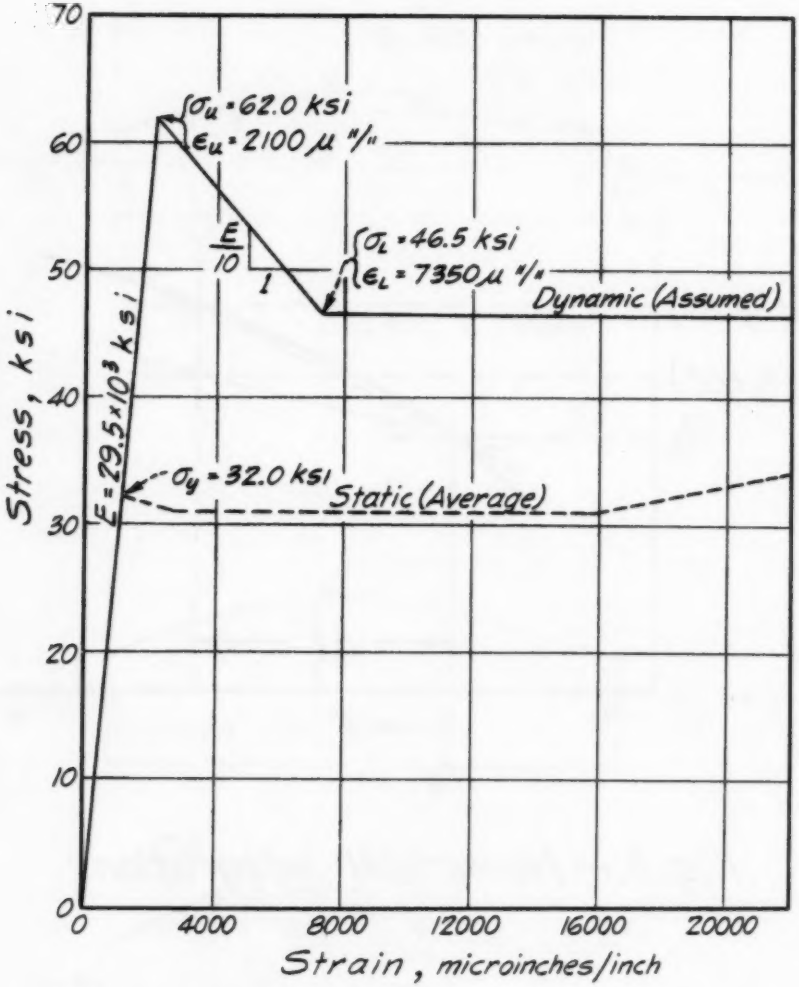

Fig. 4.--Static and Dynamic Stress-Strain Curves.

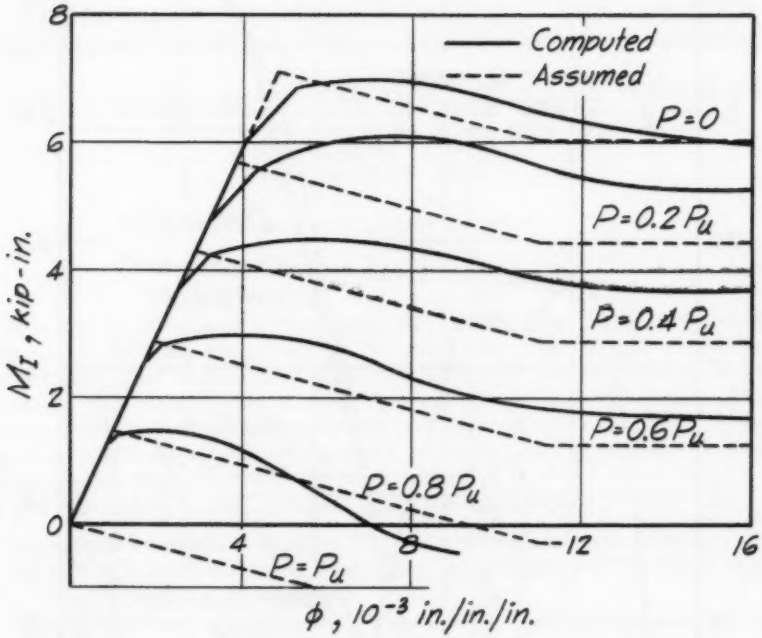

Fig.5.--Moment-Curvature Relationship.

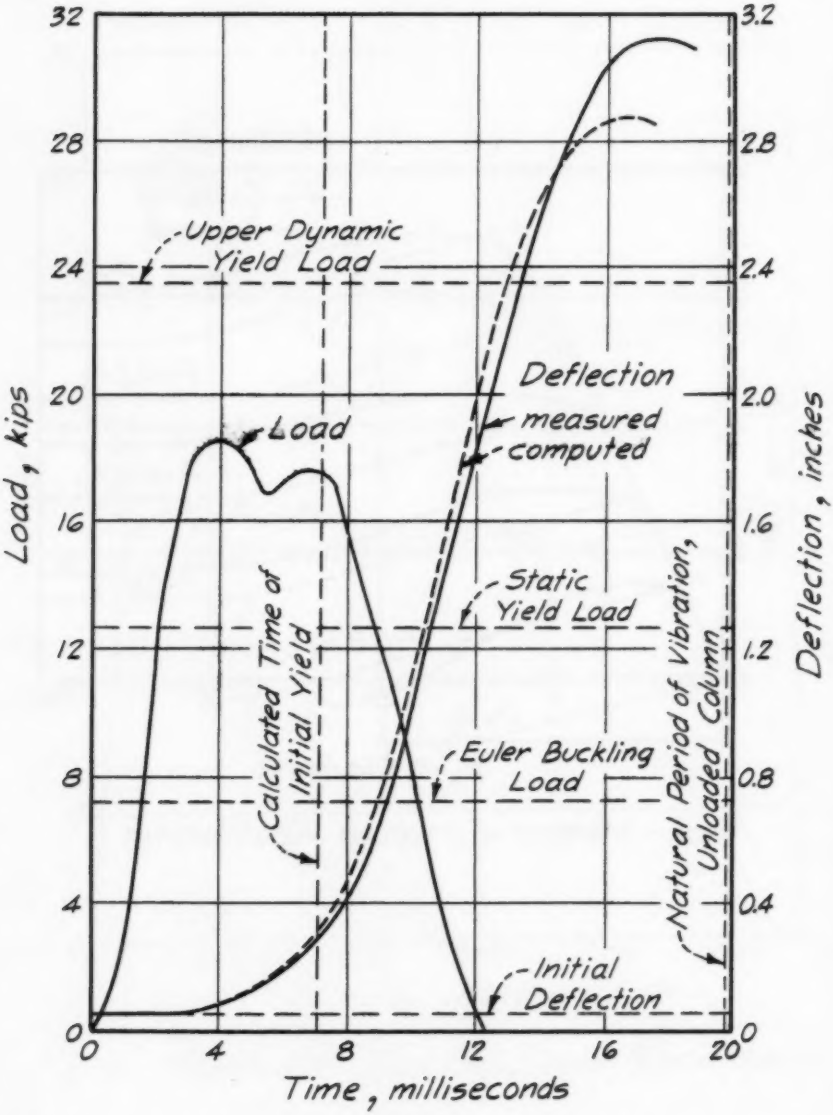

Fig.6.--Load and Deflection for Test Column.

Journal of the
ENGINEERING MECHANICS DIVISION
Proceedings of the American Society of Civil Engineers

SOME CONTRIBUTIONS TO THE WEDGE-WATER ENTRY PROBLEM

Sidney F. Borg,* A.M. ASCE
(Proc. Paper 1214)

SYNOPSIS

Some of the results of a theoretical and experimental study of the wedge-water entry problem are presented.(1) The study is based upon a new formulation of the basic equations of hydrodynamics especially applicable to this problem. The development is given first for the compressible case. This is then specialized to the incompressible (water) case and a study of the resulting equations leads to various relations and properties governing the general straight-sided wedge water entry phenomenon.

The new theory is then applied to give the following:

(a) An exact relaxation solution for an unsymmetrical entry case.
(b) A closed form analytical expression for the approximate shape of the free surface for a thin wedge.
(c) An approximate solution for blunt-nosed wedges.

In addition, the theoretical results of (a) and (b) are compared with experimental results.

NOTATION

a, b	dimension parameters for blunt-nosed bodies
n	direction of normal
p	pressure
$\bar{q}$	(u, v), physical (actual) velocity
$\bar{r}$	$(\xi, \eta) = (\frac{x}{t}, \frac{y}{t})$, distance in the conical (ξ, η) plane
s	subscript, "steady state"

Note: Discussion open until September 1, 1957. Paper 1214 is part of the copyrighted Journal of the Engineering Mechanics Division of the American Society of Civil Engineers, Vol. 83, No. EM 2, April, 1957.

*Prof. and Head of Civ. Eng., Stevens Inst. of Technology, Hoboken, N.J.

t	time
u, v	components of the physical (actual) velocity
x, y	physical (actual) coordinates of a point
F. S.	free streamline, free surface
$\bar{Q}$	$\bar{q} - \bar{r}$, "reduced" velocity
R	$\frac{S}{Qe^{-i\theta}}$, a term introduced in a transformation of the flow field
S	distance along free streamline, entropy
U	constant blunt-nosed body velocity
V_o	constant water velocity for wedge immersion (wedge stationary)
α line,	a curve in the (ζ, η) plane parallel to $\bar{Q}$, hence a particle path
β line,	a curve in the (ζ, η) plane along which $\frac{Q^2}{2} + \frac{p}{\rho}$ = constant
ζ, η	conical coordinates
δ	half wedge angle
μ	$\sigma + i\lambda$, a plane of transformation
φ	potential function
ψ	stream function
ρ	density of water
ν	$Q^{\rho - i\theta}$, a term introduced for thin wedge, free streamline analysis
θ	angle of Q line
ω	$\left(\frac{\partial u}{\partial y} - \frac{\partial v}{\partial x}\right)$, the physical vorticity
∇	$\left(\frac{\partial}{\partial \zeta}, \frac{\partial}{\partial \eta}\right)$, the vector operator "del"
∇^2	$\left(\frac{\partial^2}{\partial \zeta^2} + \frac{\partial^2}{\partial \eta^2}\right)$, the Laplacian operator
Ω	$\left(\frac{\partial u}{\partial \eta} - \frac{\partial v}{\partial \zeta}\right)$, the "reduced" vorticity

INTRODUCTION

The wedge-water entry problem was studied first by Wagner[2] who established the similarity property and obtained an approximate solution based upon an "expanding plate" analysis. He also gave one value for a total force which, presumably, was obtained by an iterative method but no details were given. Since then, with one exception, all work on the wedge-entry problem has essentially been either an extension or filling-in of Wagner's original presentation (Pierson,[3] Cooper,[4] Karzas,[5] Bisplinghoff and Doherty,[6] Schiffman and Spencer[7]). The exception is Garabedian,[8] who utilizes a set of Kirchhoff type transformations to obtain a solution for an oblique entry subject to unusual initial and boundary conditions.

In this report, a procedure is used which differs from all of the above. It

leads to a new set of equations governing the phenomena. A study of these gives various relations and properties for the wedge-entry problem and these are presented in this report. Following this, various applications of the new theory are given and an experimental verification of some of these results is also described.

The Two Dimensional Unsteady, Non-Viscous, Non-Heat Conducting Flow in Conical Coordinates

It will be shown that the non-viscous, non-heat conducting unsteady flow equations, in two dimensions, can be given in terms of new variables,

$$\xi = \frac{x}{t} \quad , \quad \eta = y/t$$

The flow equations in this form do not contain the length dimensions alone and in the (ξ, η) field the flow is represented by a single map which represents the flow at all times. This implies that such time dependent flow fields grow uniformly with time. If, in addition, the boundary does not specifically contain a length parameter, then the field may be called "conical" and the entire phenomenon may be called one of "unsteady conical flow." Examples of flows which satisfy all of the above conditions are:

(a) A shock striking an infinite straight sided wedge.
(b) An infinite straight sided wedge travelling with constant velocity and entering an infinite ocean, or conversely, an infinite ocean travelling with constant velocity and engulfing an infinite straight-sided wedge.

The case (a) will be discussed first. This corresponds to compressible flow conditions. The equations will then be specialized to incompressible flows and will therefore be the equations governing the phenomena of type (b).

Consider the two dimensional, unsteady, non-heat conducting non-viscous compressible flow, with

$$u = u(x, y, t)$$
$$v = v(x, y, t)$$

If it is assumed that u and v can be given in terms of the new variables (ξ, η) defined by

$$u = u(\xi, \eta)$$
$$v = v(\xi, \eta)$$

then

$$\xi = x/t$$
$$\eta = y/t$$

and it will be found that the equations are independent of x, y and t. Because the boundary is also independent of any length parameter, it follows that the flow pattern can be represented in the (ξ, η) plane.

The basic equations are

conservation of mass

$$\begin{cases} \rho_t + u\rho_x + v\rho_y + \rho u_x + \rho v_y = 0 \\ \text{or} \qquad \rho_t + (\rho u)_x + (\rho v)_y = 0 \end{cases} \tag{1}$$

conservation of momentum

$$\begin{cases} (\rho u)_t + (\rho u^2)_x + \rho(uv)_y + p_x = 0 \\ (\rho v)_t + (\rho vu)_x + \rho(v^2)_y + p_y = 0 \end{cases} \tag{2}$$

equation of state

$$p = p(\rho, S) \tag{3}$$

and for changes of state which are adiabatic, an equation of conservation of energy, in terms of entropy S,

$$S_t + u S_x + v S_y = 0 \tag{4}$$

Hence, corresponding to five unknowns, u, v, ρ, p, and S there are five independent equations.

Now introducing the coordinates (ξ, η) and noting that

$$\left.\begin{aligned} \frac{\partial}{\partial t} &= -\frac{\xi}{t}\frac{\partial}{\partial \xi} - \frac{\eta}{t}\frac{\partial}{\partial \eta} \\ \frac{\partial}{\partial x} &= \frac{1}{t}\frac{\partial}{\partial \xi} \\ \frac{\partial}{\partial y} &= \frac{1}{t}\frac{\partial}{\partial \eta} \end{aligned}\right\} \tag{5}$$

and defining a "reduced velocity," $\bar{Q}$, by means of

$$\left.\begin{aligned} \bar{Q} &= (u - \xi, v - \eta) \\ &= \bar{q} - \bar{r} \end{aligned}\right\} \tag{6}$$

the five equations become

conservation of mass, $$\nabla \cdot (\rho \bar{Q}) + 2\rho = 0 \tag{7}$$

conservation of momentum, $$\bar{Q} \cdot \nabla \bar{Q} + \bar{Q} = -\frac{1}{\rho} \nabla p \tag{8}$$

state, $$p = p(\rho, S) \tag{9}$$

conservation of energy, $$\bar{Q} \cdot \nabla S = 0 \tag{10}$$

where $$\nabla = \left(\frac{\partial}{\partial \xi}, \frac{\partial}{\partial \eta} \right)$$

Equations (7) through (10) are the general compressible flow form of the basic equations in terms of the reduced velocity $\bar{Q}$, and the variables (ξ, η).

Some Properties of the Wedge Water Entry Flow Field in Conical Coordinates

For the incompressible flow, with which this report shall hereafter be concerned, the above five equations specialize to three equations in terms of u, v, and p. The first of these, the conservation of mass, leads to

I—The conservation of mass equations becomes, in terms of Q and (ξ, η),

$$\nabla \cdot Q + 2 = 0 \tag{11}$$

This follows directly from equation (7) with constant ρ.

The second and third of the basic incompressible equations are the conservation of momentum equations. Eq. (8) becomes, for constant density

$$\rho \bar{Q} \cdot \nabla \bar{Q} + \rho \bar{Q} = -\nabla p \tag{12}$$

Using the familiar vector identity

$$\bar{Q} \cdot \nabla \bar{Q} = \nabla \left(\frac{Q^2}{2} \right) - \bar{Q} \times (\nabla \times \bar{Q}) \tag{13}$$

equation (12) becomes, upon collecting terms

$$\nabla \left(\frac{Q^2}{2} + \frac{p}{\rho} \right) - \bar{Q} \times (\nabla \times \bar{Q}) + \bar{Q} = 0 \tag{14}$$

For an irrotational motion $\nabla \times \bar{Q} = 0$. Hence

II—The conservation of momentum equation for the incompressible fluid in irrotational motion is given by

$$\nabla\left(\frac{Q^2}{2}+\frac{p}{\rho}\right)+\bar{Q}=0 \tag{15}$$

A stream function, ψ, may be defined as follows

$$\left.\begin{aligned} u &= \frac{\partial \psi}{\partial \eta} \\ v &= -\frac{\partial \psi}{\partial \xi} \end{aligned}\right\} \tag{16}$$

which identically satisfies Eq. (11) as may easily be verified. Taking $\nabla\times$ of Eq. (14) and using Eq. (16), there follows

III—The incompressible fluid in rotational motion satisfies the equation

$$\left(\frac{\partial \psi}{\partial \eta}-\xi\right)\frac{\partial}{\partial \xi}(\nabla^2\psi)+\left(-\frac{\partial \psi}{\partial \xi}-\eta\right)\frac{\partial}{\partial \eta}(\nabla^2\psi)-\nabla^2\psi=0 \tag{17}$$

where

$$\nabla^2=\frac{\partial^2}{\partial \xi^2}+\frac{\partial^2}{\partial \eta^2}$$

This is equivalent to

$$\bar{Q}\,\nabla(\nabla^2\psi)-\nabla^2\psi=0 \tag{18}$$

Also, if we define a "reduced vorticity" by $\Omega=\nabla\times\bar{Q}$ then

$$\nabla^2\psi=2\Omega \tag{19}$$

and it follows from Eq. (18) that

IV—The incompressible fluid in rotational motion also satisfies the equation

$$\bar{Q}\cdot\nabla\Omega-\Omega=0 \tag{20}$$

Note that Ω is equal to the physical vorticity, ω, multiplied by t. Also,

V—If an incompressible, conical fluid motion has Ω at any time, the fluid motion is always irrotational. This is the Helmholz vorticity statement for the incompressible, conical flow.

If the fluid motion is irrotational, then it follows from Eq. (16) that

VI—The stream function, ψ, satisfies the Laplace equation in (ξ, η) coordinates everywhere in the field, or

$$\nabla^2 \psi = 0 \tag{21}$$

and Eq. (17) is identically satisfied.

In the present study, the fluid motion is irrotational before wedge entry. Therefore it is also irrotational after wedge entry. Because the motion is irrotational, there exists a potential, ϕ, such that

$$\left.\begin{aligned} \frac{\partial \phi}{\partial \xi} &= -u \\ \frac{\partial \phi}{\partial \eta} &= -v \end{aligned}\right\} \tag{22}$$

Eq. (15) can also be stated in the form

$$\nabla\left(\frac{Q^2}{2} + \frac{p}{\rho}\right) + \bar{g} - \bar{r} \tag{23}$$

or

$$\nabla\left(\frac{Q^2}{2} + \frac{p}{\rho} - \frac{r^2}{2}\right) + \bar{g} = 0 \tag{24}$$

Therefore

$$\phi = \frac{Q^2}{2} + \frac{p}{\rho} - \frac{r^2}{2} \tag{25}$$

and from Eq. (22) and because of irrotationality

$$\nabla^2 \phi = 0 \tag{26}$$

Also, in the (ξ, η) plane, lines of constant ϕ are perpendicular to lines of constant ψ. All of the above is stated as

VII—In the (ξ, η) plane there exists a potential function defined by

$$\phi = \frac{Q^2}{2} + \frac{p}{\rho} - \frac{r^2}{2} \tag{25}$$

such that

$$\left.\begin{aligned} \frac{\partial \varphi}{\partial \xi} &= -u \\ \frac{\partial \varphi}{\partial \eta} &= -v \end{aligned}\right\} \tag{22}$$

and

$$\nabla^2 \varphi = 0 \tag{26}$$

Also, lines of φ = constant are normal to lines of ψ = constant.

In analogy to streamlines of steady flow we can introduce, in the (ξ, η) plane, the concept of $\overline{Q}$ lines. These lines, which are everywhere tangent to the direction of $\overline{Q}$, may be defined as a family of lines

$$\alpha(\xi,\eta) = \text{constant} \tag{27}$$

This being so, it follows from Eq. (15) that

VIII—In the (ξ, η) plane, if we define

$$\frac{Q^2}{2} + \frac{p}{\rho} = \beta(\xi,\eta) \tag{28}$$

then there are lines

$$\beta(\xi,\eta) = \text{constant} \tag{29}$$

which are everywhere perpendicular to the lines

$$\alpha(\xi,\eta) = \text{constant} \tag{27}$$

Thus, up to this point, two mutually perpendicular sets of curves in the (ξ, η) plane have been defined for the general non-viscous, non-heat conducting, incompressible fluid in irrotational motion. These are

SET I	POTENTIAL CURVES	φ = CONSTANT
	"STREAMLINES"	ψ = CONSTANT

and

SET II	$\overline{Q}$ LINES	$\alpha(\xi,\eta)$ = CONSTANT
	LINES	$\beta(\xi,\eta)$ = CONSTANT

Also, up to this point the equations and relations obtained are perfectly general and held without regard to origin of coordinates. The discussion will now be tied into the particular problem being considered. The major portion of this report is concerned with the behavior of an infinite straight sided wedge travelling with constant vertical velocity V_o, and entering an infinite ocean with undisturbed surface horizontal and extending to infinity in both directions. The pressure in the air and in the ocean before immersion is zero.

For our purposes, it will be convenient to assume the problem in the following equivalent form (see Fig. 1). The wedge is stationary, the infinite ocean is moving vertically upward with a constant velocity V_o and engulfs the wedge. The origin of the (ξ, η) coordinates will be taken at the point of the wedge. After engulfing the wedge, the ocean has free surfaces AB and A' B' which attach to the wedge at points A,A' as shown, which are at zero pressure and which approach the undisturbed surface position at infinity tangentially. The velocity and pressure of the ocean at infinity are V_o and zero. Along the wedge face, the fluid velocity is tangent to the wedge surface. Hence the wedge face is a $\bar{Q}$ line. The motion is irrotational. It may also be noted that continuity of mass requires that the volume of fluid displaced above the initial position of the free surface must equal the immersed volume of the wedge. Unless otherwise stated all of the following developments refer to the conical (ξ, η) plane.

IX—From Eq. (15) it follows that a Bernoulli type equation in the (ξ, η) plane for the flows being considered, is (S being the distance measured along $\bar{Q}$ lines),

$$\frac{\partial}{\partial S}\left(Q^2 + \frac{p}{\rho}\right) = |Q| \tag{30}$$

This is an expression for the variation of $Q^2/2 + p/\rho$ along a $\bar{Q}$ line. The corresponding steady state Bernoulli equation is (S being the distance measured along streamlines in the physical (x,y) plane),

$$\frac{\partial}{\partial S}\left(\frac{q^2}{2} + \frac{p}{\rho}\right) = 0 \tag{31}$$

The following is an important relation:

X—In the (ξ, η) plane, $\bar{Q}$ lines are particle paths.

The proof follows: The particle path as defined in the physical plane, $\bar{R}(x,y)$, with $\bar{q}(u,v)$ is given by

$$\frac{d\bar{R}}{dt} = \bar{q}$$

But if $\bar{r}$ is (ξ, η), then $\bar{R} = \bar{r}\,t$ and therefore

$$\frac{d\bar{R}}{dt} = t\frac{d\bar{\lambda}}{dt} + \bar{\lambda}$$

or

$$t\frac{d\bar{\lambda}}{dt} = \bar{q} - \bar{\lambda} = \bar{Q}$$

Thus, in the (ξ, η) plane, $\bar{Q}$ lines are the particle paths. It is interesting to note that if, in addition,

$$\tau = \log t$$

then

$$\frac{d\bar{\lambda}}{d\tau} = \bar{Q}$$

so that in the time distorted τ plane, the $\bar{Q}$ lines are not only the particle paths, but the particles move along them with velocity $\bar{Q}$.

The three statements which follow immediately have been proven elsewhere (as noted) and are included herein because they are utilized in proving some of the relations which come after.

Several proofs have been given for XI. See, for example, Garabedian.[8] XII was proved by Cooper[4] and XIII is a classical result given, for example, in Lamb.[9]

XI—The distance between particles on the free surface, in the (x,y) plane remains constant with time.

XII—The free surface particle in contact with the wedge face at the initial instant of immersion is always in contact with the wedge face.

XIII—For the flow conditions considered herein, a particle which is in the free surface at any time is always in the free surface. Hence, the free surface is a particle path, or a Q line, and we shall speak of it as the "free streamline," i.e., F.S.

It can now be shown that

XIV—The free streamline in the (ξ, η) plane attaches to the wedge at a finite distance from the wedge point.

The proof is as follows:

(1) The wedge is stationary and the infinite ocean is travelling upward with uniform velocity V_o at infinity.
(2) The conical property requires that the complete flow field be established at the instant after immersion, $t = 0^+$, and that this field be similar to itself at all times thereafter.

(3) According to XI, the distance between any two particles on the free streamline is constant, starting from the time $t = 0$ when the wedge begins immersing. Also, according to XII, a particle in the free streamline at any time is always in the free streamline.

(4) If the free streamline does not attach to the wedge at a finite distance from the wedge point (i.e., attaches at infinity), then because of (a) above, at least one particle on the free streamline must have had an infinite velocity at the instant of immersion $t = 0$.

(5) If one particle had an infinite velocity, then because of (3) all particles in the free streamline have an infinite velocity at the instant of immersion and therefore at all times. This violates the boundary condition in (1) and is therefore not possible. Hence the free streamline must attach to the wedge at a finite distance from the wedge point.

From XIV and because of XII and the property of the conical flow plane, it follows that

XV—The free streamline particle at the wedge attachment point, A, travels with a constant velocity $\bar{q}_A$, which is equal to $\bar{r}_A$, the distance of this particle from the wedge point in the (ξ, η). Therefore, for this particle $\bar{Q}_A = 0$.

It is now possible to derive the boundary condition which must be satisfied by $\bar{Q}$ along the free streamline. The complete statement is

XVI—At any point on the free streamline in the (ξ, η) plane

$$\left|Q_{F.S.}\right| = S_{F.S.} \tag{32}$$

where $\left|Q_{F.S.}\right|$ is the value of Q at this point on the free streamline, and $S_{F.S.}$ is the distance, measured along the free streamline, from the wedge attachment point to the point in question. In addition, of course, the vector $\bar{Q}$ is everywhere tangent to the free streamline.

The last part of XVI follows at once because of XIII. The proof for the first part follows—see Fig. 2.

(1) At point A, $\bar{q}_A = \bar{r}_A$

(2) At point B, $\bar{r} = \bar{r}_B$ as shown

(3) Between A and B, $\Delta\bar{q}$ must be perpendicular to $\Delta\bar{r}$ as shown in the figure. This is so because the pressure gradient on the free streamline is perpendicular to the free streamline

(4) Hence $\bar{q}_B \neq \bar{r}_B$, since from (1) above, $\bar{q}_B$ will equal $\bar{r}_B$ only if $(\Delta\bar{r})_{AB} = (\bar{q})_{AB}$

(5) Hence $\bar{Q}_B \neq 0$

(6) On the free streamline, $p = 0$, and therefore from Eq. (15)

$$Q(dQ/dS + 1) = 0$$

everywhere along the free streamline, where S is in the direction tangent to the free streamline.

(7) At B, $\bar{Q}_B \neq 0$, so that from (6) above, $|Q_B| = |\Delta r|$ and continuing along the free streamline to any point on the free streamline, we obtain

$$|Q_{FS}| = S_{FS}$$

A result of some interest is

XVII—Throughout the (ξ, η) plane flow field the function $\beta(\xi, \eta)$ satisfies the equation

$$\nabla^2 \beta = 2 \tag{33}$$

This follows from

I $$\nabla \cdot \bar{Q} + 2 = 0 \tag{11}$$

and II $$\nabla \beta + \bar{Q} = 0 \tag{15}$$

Take $\nabla \cdot$ (15) and using Eq. (11), Eq. (33) is obtained at once.
Also, we may show that

XVIII—In the (ξ, η) plane, along the wedge face, the pressure will be a maximum or a minimum only if

$$\text{either} \begin{cases} Q = 0 \\ dq = 0 \end{cases} \quad \text{or}$$

Proof: From II

$$\nabla\left(\frac{Q^2}{2} + \frac{p}{\rho}\right) + \bar{Q} = 0 \tag{15}$$

and because the wedge face is a Q line, this becomes, along the wedge

$$d\left(\frac{Q^2}{2} + \frac{p}{\rho}\right) + Q\, dS = 0 \tag{34}$$

or

$$\frac{dp}{\rho} + Q\, dQ + Q\, dS = 0 \tag{35}$$

or

$$\frac{dp}{\beta} + Q\,(dQ + dS) = 0 \tag{36}$$

From this

$$dp = 0 \quad , \quad \text{IF} \quad \begin{cases} Q = 0 \\ dQ + dS = 0 \end{cases} \quad \text{or} \tag{37}$$

But, along the wedge

$$\left.\begin{aligned} Q &= q - s \\ dQ &= dq - ds \end{aligned}\right\} \tag{38}$$

so that Eq. (37) becomes,

$$dp = 0 \quad , \quad \text{IF} \quad \begin{cases} Q = 0 \\ dq = 0 \end{cases} \tag{39}$$

An Exact Relaxation Solution for an Unsymmetrical Wedge

In view of equations (22), (25) and (26), it is possible to set up a numerical relaxation procedure for obtaining exact solutions to wedge-water entry problems.

The solution requires finding a $\phi(\xi, \eta)$ which satisfies

$\nabla^2 \phi = 0$, everywhere in the field and

the following boundary conditions:

$\phi = Q^2/2 - r^2/2$ along the free streamline

(It can be noted at this point that the free streamline at infinity has a value for ϕ given by $\phi_{\text{F.S. } \infty} = -\frac{V_0^2}{2}$)

$\frac{\partial \phi}{\partial n} = 0$ along the wedge face, n being the direction of the normal to the wedge

$\frac{\partial \phi}{\partial \eta} = -V_0$ at infinity

The problem is complicated by the fact that the free streamline is not known beforehand. In this respect the difficulty is similar to the one which appears in the problem of percolation of a fluid through a porous medium, which was solved by relaxation methods by Shaw and Southwell.[10] In essence, the procedure in these cases is to assume a free surface and to obtain a solution which satisfies the field equation and the boundary conditions subject to the assumed free surface. Then, using this known solution, there will

be another equation or relation which leads to an independent check of the assumed surface shape. In general, the assumed shape will not check out, so that another shape must be assumed and the process repeated.

In the present problem, the procedure formalizes to the following:

(1) Assume a free streamline shape.

(2) Calculate ϕ along the free streamline, using

$$\phi = Q^2/2 - r^2/2$$

(3) Obtain a relaxation solution of the Laplace equation subject to the given boundary conditions.

(4) Having obtained ϕ everywhere, it is now possible to determine the physical velocity, $\bar{q}$, along the free streamline. Hence, at all points on the free streamline, $\bar{Q} = \bar{q} - \bar{r}$ can be obtained. These values of $\bar{Q}$ must check the actual assumed values of $\bar{Q}$. If they do not check, then the free streamline shape must be altered and the entire process repeated.

(5) Having the correct solution for ϕ, it is now possible to obtain values of p/ρ along the wedge face, since

$$\phi = Q^2/2 + p/\rho - r^2/2$$

and ϕ, Q and r are known.

This method is now applied to the unsymmetrical entry of a 90^0 wedge as shown in Fig. 3. Because the Laplacian is invariant with respect to rotation of axes and because the relaxation numerical work is simplified thereby, the net lines are taken parallel and perpendicular to the wedge face as shown.

As initial guides for the assumed free streamline, the two continuity conditions on displaced volume and free streamline length are used. In the beginning, rather coarse nets are used. These permit checks on the F.S. and they are used until an acceptable check is obtained. Then the net is made finer and the process repeated.

In one of the early solutions, it was found that the fluid along the wedge face OA, in the neighborhood of 0 is moving in the direction of 0. This implied the existence of an infinite velocity singularity at 0 corresponding to flow about a sharp corner. Methods of handling this are described by Motz[11] and these were used. In the present problem, it was found necessary to use a fine net in the neighborhood of the sharp bend of the free streamline. The final solution is shown in Fig. 3, which shows

(a) The distribution of $p/\frac{1}{2}\rho V_0^2$ along each wedge face.

(b) The free streamlines

(c) The network used in the relaxation solution.

An experiment was performed to check the results. A wedge with plastic end plates (to simulate two-dimensional effects) was dropped into a tank of water at constant velocity and a high speed flash photograph was taken of the resulting disturbance. For the case under consideration, the photograph is shown in Fig. 4.

In connection with this photograph, it must be remembered that the theory assumed a perfect fluid in which gravity effects were neglected. For the most part these assumptions are reasonable for the experiment performed. However, in the neighborhood of the free streamline-wedge attachment point,

it is obvious that gravity has caused "fall back" of the particles. It is, however, still possible to obtain a comparison between the theoretical shape of the free streamline and the experimental shape, if the photographic free streamline is simply corrected for its gravity trajectory fall back at its outer end to give the wedge attachment point. This has been done, and the resulting free streamlines are shown in Fig. 5.

It will be recalled that the theoretical solution called for an infinite velocity (and hence negative infinite pressure) at the wedge point. These are, of course, impossible to obtain experimentally. Thus, some disagreement between theory and experiment is to be expected on this score.

Also, the photograph Fig. 4 clearly shows leakage of fluid between the plastic end plate and the wedge on the high pressure side of the wedge. This would reduce the amount of fluid on this side of the wedge and the comparison between theoretical and experimental free streamlines at this face clearly shows this effect.

On the whole, however, the agreement between theory and experiment for this unsymmetrical wedge is good.

The Free Streamline Shape for the Thin Wedge

The theory of this study may be utilized in obtaining an approximate solution for the thin wedge free streamline shape. The method is analogous to Kirchhoff's free streamline theory of steady incompressible flows. The solution which will be obtained satisfies the following conditions:

(1) The boundary condition on Q along the free streamline
(2) The F.S. will be tangent to the wedge at its attachment point.
(3) The free streamline asymptotic condition, i.e., the physical requirement that at infinity the free streamline approaches the undisturbed surface level asymptotically.
(4) The volume displacement condition, i.e., the requirement that the immersed volume of the wedge must be equal to the volume of the fluid displaced above the initial horizontal water surface.
(5) Because in the limit as the wedge angle becomes zero the radius of curvature at the free streamline wedge attachment point is zero, the solution which will be obtained is one for which the radius of curvature will be zero at this point.

Let (see Fig. 6)

δ = the half angle of a symmetrical thin wedge

θ = inclination of the Q lines with respect to vertical axis.

Introduce the quantity

$$\nu = Qe^{-i\theta} \tag{40}$$

Consider the term

$$R = \frac{S}{\nu} \tag{41}$$

in which S is the distance measured along each Q line from the point where each line intersects the wedge.

Then

$$\log R = \log \frac{S}{Q} + i\theta \tag{42}$$

Along the free streamline, S = Q exactly, and therefore along the free streamline

$$\log R = i\theta \tag{43}$$

The actual flow field of Fig. 6 will now be approximated on a log R plane as shown in Fig. 7.

AB represents the free streamline exactly as $\zeta \longrightarrow 0$. BE_∞ represents the flow at infinity between B and some point E_∞ such that between these points

(1) $\theta = \pi/2$ and
(2) S/Q goes from unity to ∞ between B and E_∞. Between E_∞ and D_∞ it is assumed that
  (1) θ changes from $\pi/2$ to 0 and
  (2) S/Q remains infinite.

The entire half flow field thus lies within the rectangle E_∞ BAD$_\infty$ in the approximation assumed here.

Transform the log R plane of Fig. 7 into a $\mu = \sigma + i\lambda$ plane, Fig. 8, such that E_∞ BAD$_\infty$ lies on the real axis, $\lambda = 0$, and so that B is at $\sigma = 0$ and A is at $\sigma = +1$. The transformation that accomplishes this is

$$\log R = K \cosh^{-1} \mu + L \tag{44}$$

in which K and L are constants which determine the origin and the scale of the transformation. Using the μ plane values for the locations of A and B, this becomes

$$\log R = \cosh^{-1} \mu \tag{45}$$

Also, along AB, $\log R = i\theta$, so that along AB this becomes

$$i\theta = \cosh^{-1} \mu \tag{46}$$

or

$$\mu = \cos \theta \tag{47}$$

$$d\mu = -\sin \theta \, d\theta \tag{48}$$

Also, along AB

$$\left.\begin{aligned} d\xi &= \cos \theta \, dS \\ d\eta &= \sin \theta \, dS \end{aligned}\right\} \tag{49}$$

In order to obtain an equation for the free streamline AB which is consistent with all the above, it is necessary that some relation be established between S and μ. In particular, the relation will be given in terms of $dS/d\mu$.

First note,

$$dS/d\mu = \frac{dS/d\theta}{d\mu/d\theta} \tag{50}$$

and from (47)

$$d\theta/d\mu = -1/\sin\theta \begin{cases} -\infty \text{ at A} \\ -1 \text{ at B} \end{cases} \tag{51}$$

Also, it is necessary that

$$dS/d\theta = \begin{cases} 0 \text{ at A, in order that the radius of the curvature be zero here} \\ \infty \text{ at B, in order to satisfy the asymptotic condition} \end{cases} \tag{52}$$

All these are satisfied by taking for $dS/d\mu$ the simple relation

$$dS/d\mu = M/\mu = M/\cos\theta \tag{53}$$

where M is some constant which will be determined in order that the constancy of volume condition be satisfied. See Fig. 9. Note also from Eq. (57) which follows that M represents the maximum rise of the free surface.

From (49) through (53)

$$\left.\begin{aligned} d\xi &= M \sin\theta \, d\theta \\ d\eta &= M \sin\theta \tan\theta \, d\theta \end{aligned}\right\} \tag{54}$$

Also, the displaced half-wedge volume is $V_0^2 \delta/2$.

Now equating the volume under the free streamline and above the undisturbed free streamline to the displaced half-wedge volume, one obtains

$$\int_0^\infty (M - \xi) d\eta = V_0^2 \delta/2 \tag{55}$$

or, substituting the values from (54) and integrating,

$$M = -V_0 \sqrt{2\delta/\pi} \tag{56}$$

Integrating the expressions for $d\xi$ and $d\eta$, the parametric equations of the free streamline are finally obtained as

$$\xi = - V_o \sqrt{2\delta/\pi} \; (1 - \cos\theta)$$

$$\eta = - V_o \sqrt{2\delta/\pi} \; (1/2 \log \frac{1 + \sin\theta}{1 - \sin\theta} - \sin\theta) \qquad (57)$$

in which ξ and η are here measured from the origin as shown in Fig. 9.

An experiment was performed to obtain a check on this result. A thin wooden wedge, of total angle 20^0, with plastic side plates, was dropped into a tank of water with constant velocity V_o. Photographs were taken of the resulting disturbance. In Fig. 10, the experimental free streamline for this wedge angle is compared to the theoretical free streamline given by Eq. (57).

In connection with this figure, it must again be recalled that the basic theory of this investigation assumed a perfect fluid—i.e., a non-viscous, gravity free, surface tension free fluid. For the most part, these assumptions are reasonable. However, in the neighborhood of the free streamline attachment point it would be expected that viscosity and surface tension effects might be important. In the present case, the experimental free streamline had a reversal of curvature near the attachment point—which is impossible in a perfect fluid and is probably due to surface tension effects.

On the whole, however, the agreement between the theoretical and experimental free streamline shapes is good.

Blunt-Nosed Wedge Water Entry

Because of equations (22), (25) and (26) it is possible to obtain approximate solutions for straight-sided wedge entry problems as follows:

We require a $\phi(\xi, \eta)$ function which satisfies

(1) $\nabla^2\phi = 0$, everywhere in the field

(2) $u = - \frac{\partial\phi}{\partial\xi}$, $v = - \frac{\partial\phi}{\partial\eta}$ } everywhere in the field

(3) $\phi = \frac{Q^2}{2} - \frac{r^2}{2}$ along the F.S.

(4) $\phi = - \frac{V_o^2}{2}$ at infinity on the F.S.

(5) $\frac{\partial\phi}{\partial n} = 0$ along the wedge face.

(6) $\frac{\partial\phi}{\partial\eta} = - V_o$ at infinity.

ϕ functions which satisfy all of the above except (3) may be obtained by utilizing the known results of steady-state potential flow theory of classical hydrodynamics. Having ϕ everywhere in the flow field, we can use equation (25) to find the pressure along the wedge face or any other desired property.

This method will give rapid, approximate solutions for straight-sided wedges such as were considered in the previous portions of this paper. We

need only use the known potential solutions for steady flow about diamond shape wedges.

It is possible to apply this method to obtain approximate solutions for unsteady water entry flows for two dimensional blunt-nosed bodies, for which the classical theory of potential flow will permit the development of practically any desired shape.[12] Typical results obtained using this approximation are:

(1) Fig. 11 shows the pressure distribution along a blunt-nosed wedge shape developed by a vortex pair in a uniform flow field.[13] The region of negative pressure will exist only in an ideal fluid. We may consider it as a cavitation or separated region for the real fluid.

(2) A blunt-nosed body may be developed by a steady potential flow source-sink pair in a uniform field.[14] One half of this immersing symmetrical body could be the nose of a two dimensional projectile or similar body. When this nose is just fully immersed, there is an unsteady state pressure, p, at the nose tip which is greater than the steady potential flow stagnation pressure, p_s. The amount of this excess is given by

$$\frac{p - p_s}{\frac{1}{2}\rho U^2} = \frac{b^2 - a^2}{ab} \log\left(\frac{b + a}{b - a}\right) \tag{58}$$

If $a/b \rightarrow 0$, then the nose shape becomes a semi-circle and the expression becomes

$$\frac{p - p_s}{\frac{1}{2}\rho U^2} = 2 \tag{59}$$

The same method can be used to give approximate solutions for unsymmetrical two dimensional blunt-nosed body entry and for three dimensional shapes as well. An extension of the method permits one to obtain approximate solutions when the entry velocity is variable.

CONCLUSION

The paper presented some of the results of a study of the wedge-water entry problem based upon a new formulation of the basic equations of hydrodynamics applicable to this problem. Included were

(a) a development of the equations and the various relations and properties which follow from these.
(b) an exact relaxation solution for an unsymmetrical wedge.
(c) a closed form analytical solution for the approximate shape of the free streamline for a thin wedge.
(d) an approximate solution for blunt-nosed wedges.
(e) comparisons between theory and experiment for cases (b) and (c).

ACKNOWLEDGMENT

The author wishes to thank Drs. Francis Clauser and V. Morkovin of the Aeronautics Department of Johns Hopkins University for many helpful discussions dealing with this research. The work on blunt-nosed wedges was supported by a National Science Foundation Research Grant.

REFERENCES

1. The major portion of this paper is based upon a doctoral dissertation, Department of Aeronautics, Johns Hopkins University, 1956.
2. Wagner, H. "Über Stoss und Gleitvorgange unter Oberflache fur Flussigkeiten," ZAMM, 1932.
3. Pierson, J. D. "The Penetration of a Fluid Surface by a Wedge," Stevens Institute of Technology ETT Report 381, 1950.
4. Cooper, E. P. "Theory of Water Entry of Missiles with Flat Noses," NOTS 208, Inyokern, Cal. 1949.
5. Karzas, W. J. "The Vertical Water Entry of a Wedge," TM 576, China Lake, Cal. 1952.
6. Bisplinghoff, R. L. and Doherty, C. S. "A Two Dimensional Study of the Impact of Wedges on a Water Surface," MIT, Dept. of Aero. Engrg., March 1951.
7. Schiffman, M. and Spencer, D. C. "The Force of Impact on a Cone Striking a Water Surface (Vertical Entry)," Comm. on Pure and Appl. Math., November 1951.
8. Garabedian, P. R. "Oblique Water Entry of a Wedge," Stanford University Report, July 1952.
9. Lamb, H. "Hydrodynamics," Cambridge University Press, 1924.
10. Shaw, F. S. and Southwell, R. V. "Relaxation Methods Applied to Engineering Problems. Part VII—Problems Relating to the Percolation of Fluids through Porous Materials," Proc. Royal Soc. Series A, 1941.
11. Motz, H., "The Treatment of Singularities of Partial Differential Equations by Relaxation Methods," Quarterly of Applied Mathematics, Vol. IV, 1947.
12. S. F. Borg and P. N. Hu. "Blunt-Nosed Wedge Water Entry," Stevens Institute of Technology, ETT NOTE 412, Jan. 1957.
13. The steady flow potential function for this case may be found in L. M. Milne-Thomson, "Theoretical Hydrodynamics," Second Edition, The MacMillan Co., New York, 1950, Art. 13.30.
14. Ibid., Art. 8.30. The notation used is that of the reference.

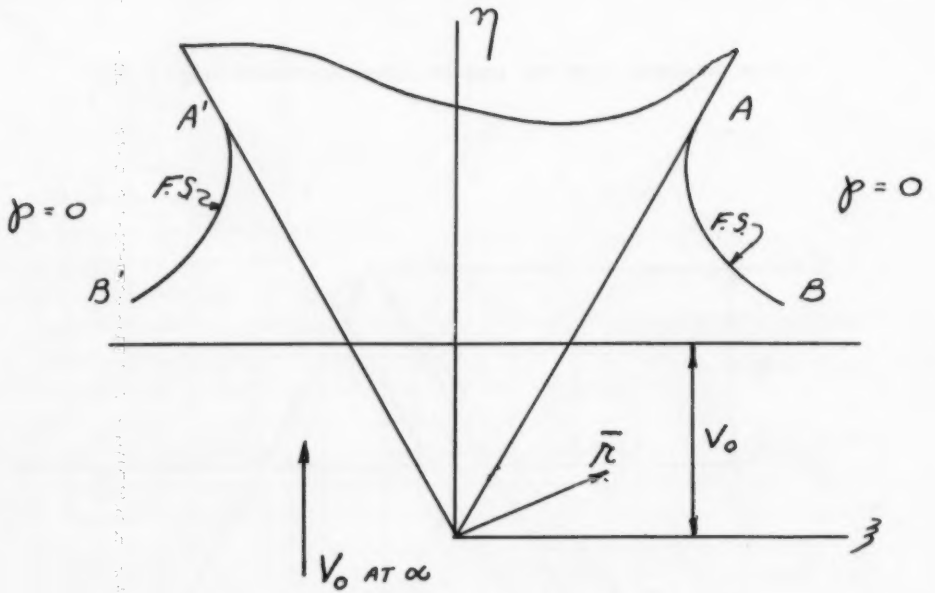

Fig. 1 The geometry of the immersing wedge in the (ξ, η) plane

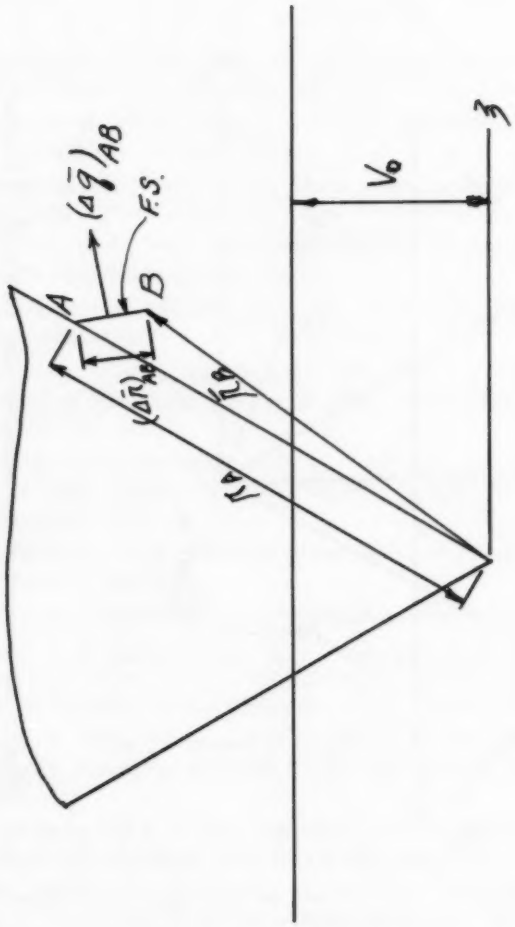

Fig. 2 Free streamline conditions near the wedge attachment point

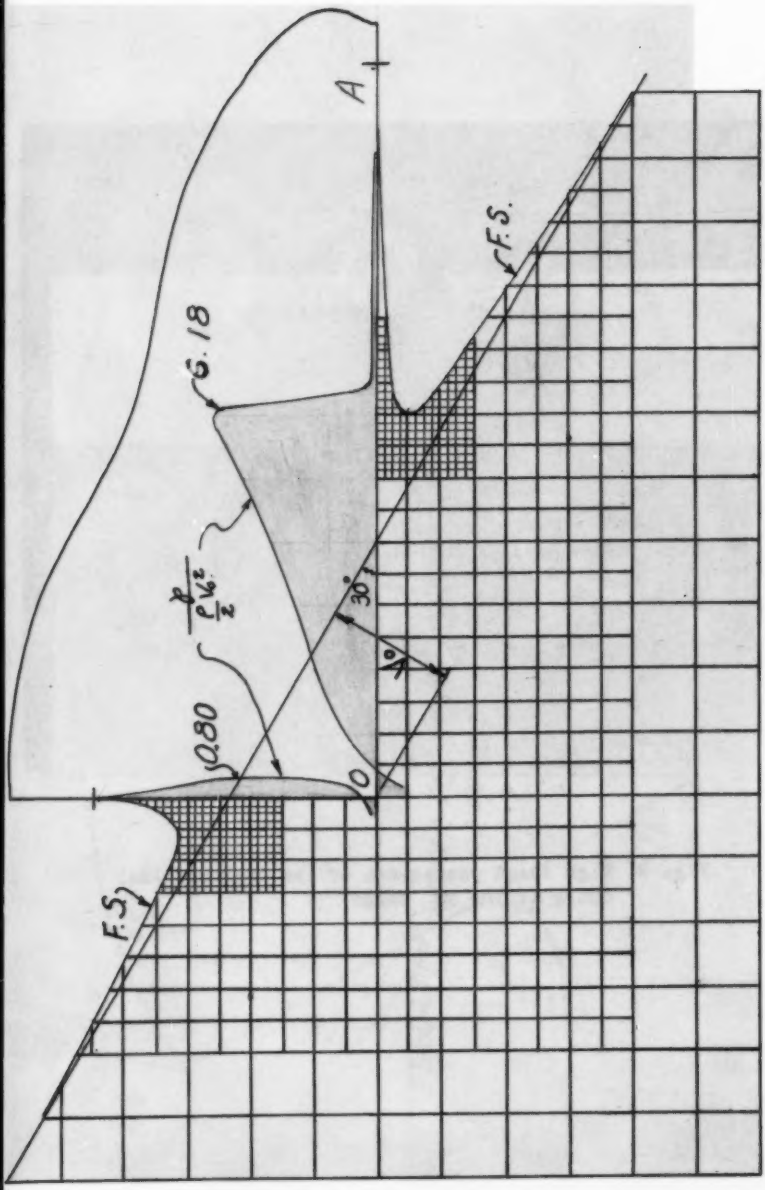

Fig. 3 The relaxation solution for the unsymmetrical entry of a 90° wedge.

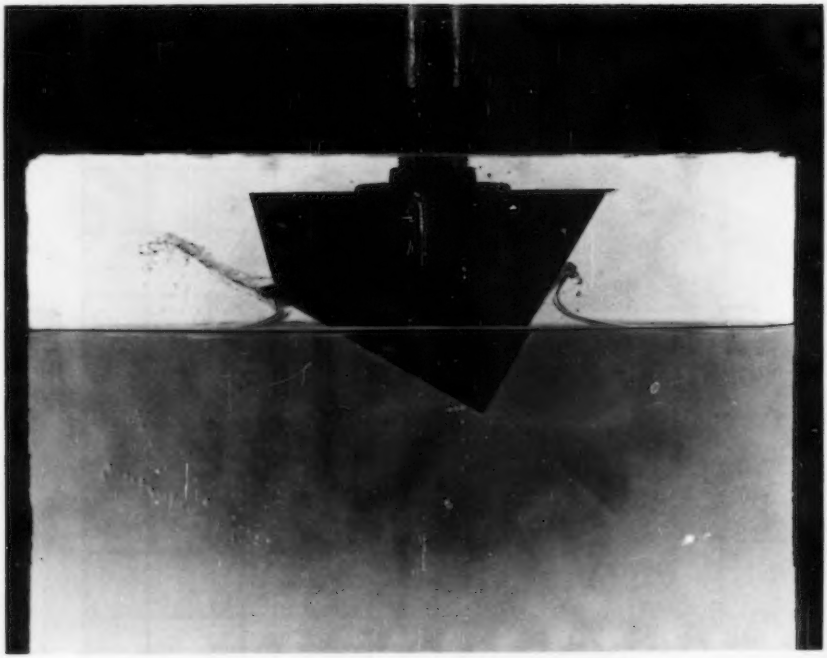

Fig. 4 High speed photograph of the unsymmetrical entry of the 90° wedge

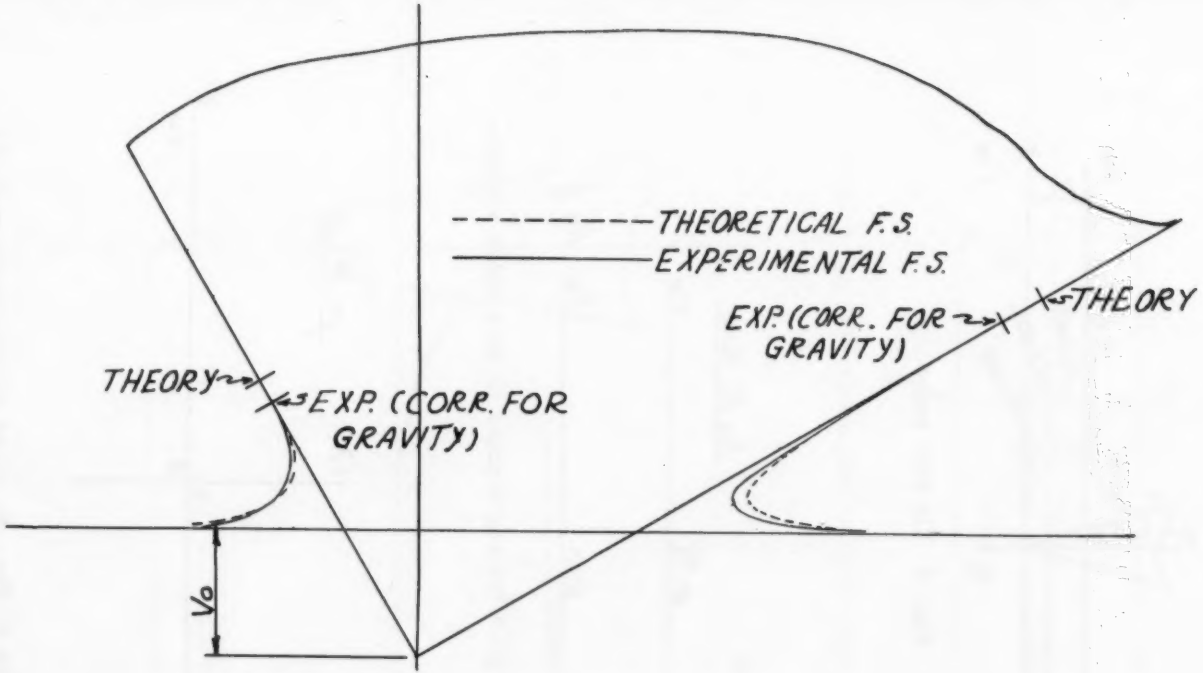

Fig. 5 Comparison of theoretical and experimental free streamline shapes for the unsymmetrical entry case

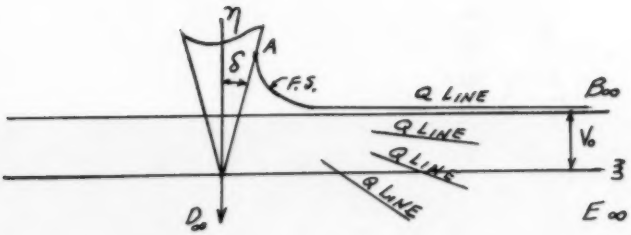

Fig. 6 The thin wedge

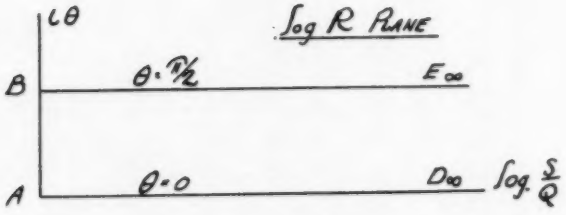

Fig. 7 The log R plane in thin wedge analysis

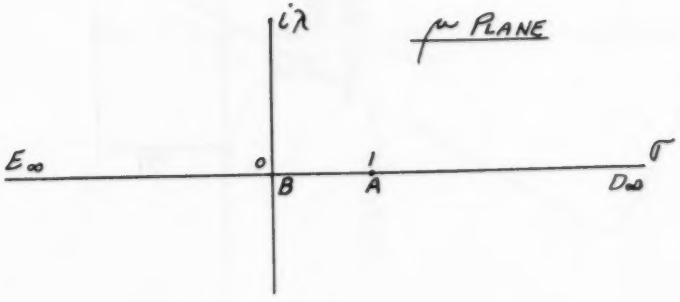

Fig 8 The μ plane in thin wedge analysis

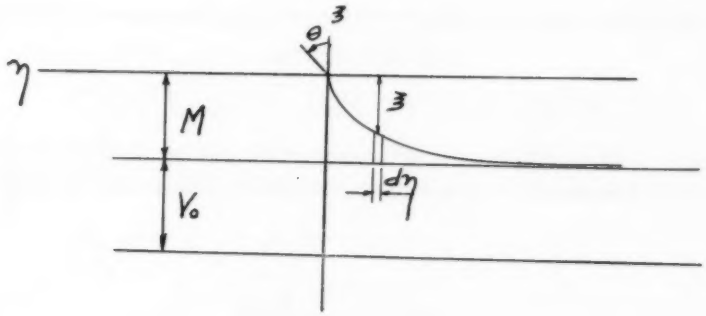

Fig. 9 The free streamline in thin wedge analysis

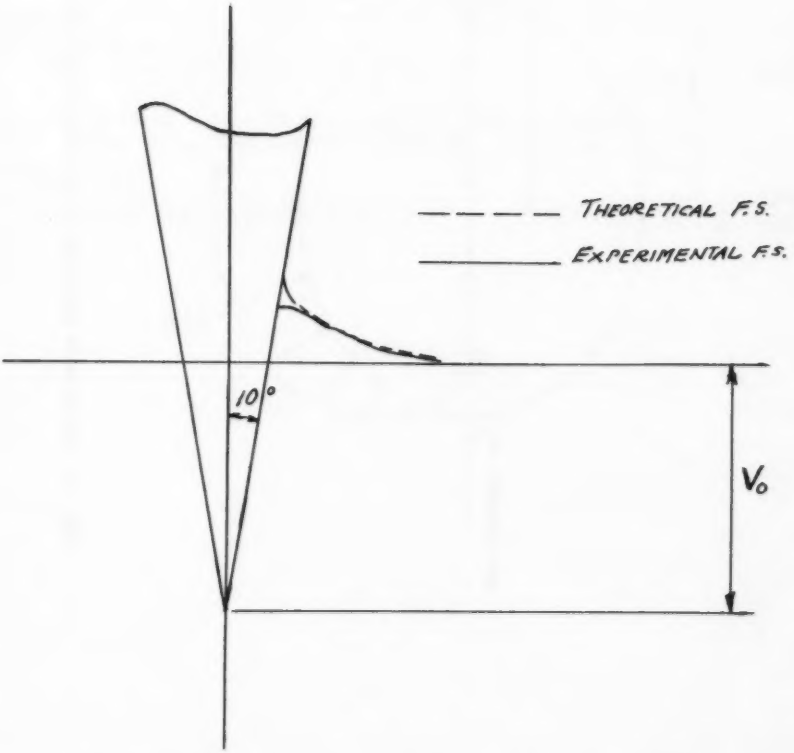

Fig. 10 Comparison of theoretical and experimental free streamlines for the thin (20°) wedge

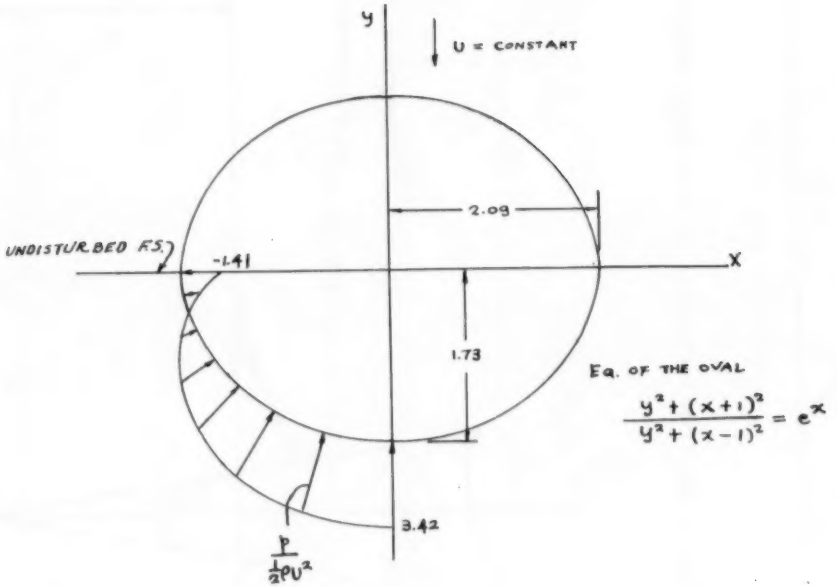

Fig. 11 Approximate solution for an immersing blunt-nosed wedge

Journal of the
ENGINEERING MECHANICS DIVISION
Proceedings of the American Society of Civil Engineers

CONTENTS

DISCUSSION
(Proc. Paper 1229)

Discussion of
"THE VISCOUS SUBLAYER ALONG A SMOOTH BOUNDARY"

by H. A. Einstein and Huon Li
(Proc. Paper 945)

H. A. EINSTEIN,[1] M. ASCE, and HUON LI.—Both discussers, Messrs. E. Silberman and N. N. Ambraseys have helped the writers in one vital point. They made it very clear that the problem is difficult to handle experimentally and theoretically alike. The experimental difficulty is caused predominantly by the turbulence outside the sublayer which moves past any place of observation at high velocity and causes pressure fluctuations of equal magnitude but with higher frequency then these developed in the sublayer itself. The theoretical difficulty is caused by the fact that the sublayer should constitute a transition between the still boundary and the turbulent velocity profiles while a mathematical solution for the transition could be found only between the still boundary and a uniform flow of constant velocity.

No objections were voiced against the main ideas of the paper:

1) that the sublayer was interpreted as a non-steady flow with an average flow pattern rather than as a steady flow with superimposed fluctuations.

2) that in areas of predominantly viscous character turbulent effects may be neglected (build-up phases) and that in areas of turbulent character the viscous effects are negligible (mixing with main flow).

These two ideas appear to be basic and new and may prove to be helpful in the description of other similar phenomena, too.

Mr. Silberman proposes the use of another definition for the effective sublayer thickness. He is welcome to change that definition at will since the choice is completely arbitrary. The proposed use of dye was actually applied by the authors to show that at some instances a distinctly laminar flow pattern exists near the wall while at some other instances turbulence appears to reach all the way to the wall. The processes are too fast for visual observation but show up very well in high speed photography.

Mr. Ambraseys' observations of the statistical flow description in the range of the sublayer seem to be most interesting. Unfortunately, no observations are available from the experiments described in this paper that would permit to check Mr. Ambraseys' results.

In conclusion, the writers like to extend the heartiest thanks to the discussers for their help and suggestions and they hope that more measurements may become available soon that will permit a more detailed description of the sublayer with the help of the proposed theory.

1. Associate Prof. of Mechanical Eng., Univ. of California, Berkeley, Calif.

Discussion of
"LATERAL BRACING FORCES ON BEAMS AND COLUMNS"

by William Zuk
(Proc. Paper 1032)

CORRECTIONS.—Figs. A and B to which Prof. Posey referred in his discussion of this paper were omitted from Proc. Paper 1154. These figures are reproduced herewith:

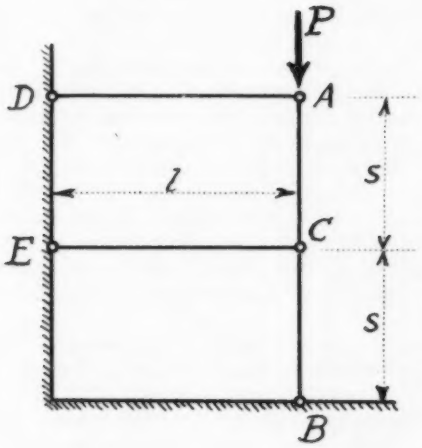

Fig. A

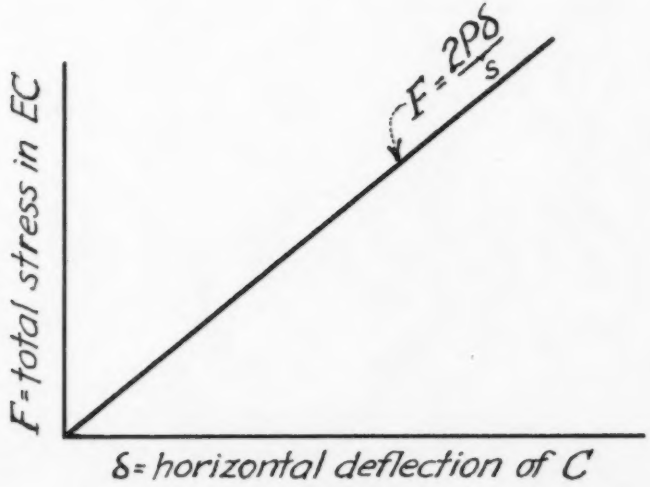

Fig. B

WILLIAM ZUK,[1].—The writer wishes to thank Messrs. Hauer, Posey, and Segedin for their interest in commenting on the subject of lateral bracing.

Both Messrs. Hauer and Posey noted a lack of discussion on the stiffness factor in connection with elastic bracing. The writer is quite aware of the role of stiffness and has studied the subject at length, even though it was only briefly mentioned in the paper. Stiffness was deliberately de-emphasized in the paper because, as Mr. Hauer himself pointed out, "the stiffness requirement for the bracing member is not hard to fulfill." This conclusion was also reached by the writer for many other practical examples. It was felt therefore that a force analysis would more adequately serve the needs of the practicing engineer. Stiffness, of course, has no meaning for cases of immovable supports, where forces themselves must be had.

Another comment of Mr. Hauer concerning the doubtfulness of using a crookedness parameter calls for reply. To those familiar with the buckling phenomena, it is clear that the initial imperfection is one of the most fundamental parameter. As uncertain as this crookedness may be, it nevertheless—in an analytical study—must be presented as the parameter it is. Reference is made to the classic "Secant Column Formula" for column buckling which also has in it an imperfection parameter. The "Secant Formula" stands as one of our most accurate column formulas.

Unfortunately, Mr. Posey's drawings were accidentally omitted from his discussion but are shown just prior to this closure. Nevertheless, the writer would like to make a side note that in a continuous column with a brace at mid height, the true position of the flex point is not exactly at the center. Mr. Posey's analysis however gives a very simple and effective picture of column-bracing action.

To Mr. Segedin, the writer is endebted for his refinement of the solution of Case I and to his very interesting extension to the case of moment bracing of a column.

In closing, the writer wishes to emphasize the importance of the portion of the paper on beam bracing which is the more difficult subject and on which experimental work should be done.

---

1. Associate Prof. of Civ. Eng., Univ. of Virginia, Charlottesville, Va.

PROCEEDINGS PAPERS

The technical papers published in the past year are identified by number below. Technical-divisional sponsorship is indicated by an abbreviation at the end of each Paper Number, the symbols referring to: Air Transport (AT), City Planning (CP), Construction (CO), Engineering Mechanics (EM), Highway (HW), Hydraulics (HY), Irrigation and Drainage (IR), Power (PO), Sanitary Engineering (SA), Soil Mechanics and Foundations (SM), Structural (ST), Surveying and Mapping (SU), and Waterways and Harbors (WW) divisions. Papers sponsored by the Board of Direction are identified by the symbols (BD). For titles and order coupons, refer to the appropriate issue of "Civil Engineering." Beginning with Volume 82 (January 1956) papers were published in Journals of the various Technical Divisions. To locate papers in the Journals, the symbols after the paper numbers are followed by a numeral designating the issue of a particular Journal in which the paper appeared. For example, Paper 1112 is identified as 1112 (HY6) which indicates that the paper is contained in the sixth issue of the Journal of the Hydraulics Division during 1956.

VOLUME 82 (1956)

APRIL: 926(WW2), 926(WW2), 927(WW2), 928(SA2), 929(SA2), 930(SA2), 931(SA2), 932(SA2)[c], 941
933(SM2), 934(SM2), 935(WW2), 936(WW2), 937(WW2), 938(WW2), 939(WW2), 940(SM2), 941
(SM2), 942(SM2)[c], 943(EM2), 944(EM2), 945(EM2), 946(EM2)[c], 947(PO2), 948(PO2), 949(PO2),
950(PO2), 951(PO2), 952(PO2)[c], 953(HY2), 954(HY2), 955(HY2)[c], 956(HY2), 957(HY2), 958
(SA2), 959(PO2), 960(PO2).

MAY: 961(IR2), 962(IR2), 963(CP2), 964(CP2), 965(WW3), 966(WW3), 967(WW3), 968(WW3), 969
(WW3), 970(ST2), 971(ST3), 972(ST3)[c], 973(ST3), 974(ST3), 975(WW3), 976(WW3), 977(IR2),
978(AT2), 979(AT2), 980(AT2), 981(IR2), 982(IR2)[c], 983(HW2), 984(HW2), 985(HW2)[c], 986(ST3),
987(AT2), 988(CP2), 989(AT2).

JUNE: 990(PO3), 991(PO3), 992(PO3), 993(PO3), 994(PO3), 995(PO3), 996(PO3), 997(PO3), 998
(SA3), 999(SA3), 1000(SA3), 1001(SA3), 1002(SA3), 1003(SA3)[c], 1004(HY3), 1005(HY3), 1006
(HY3), 1007(HY3), 1008(HY3), 1009(HY3), 1010(HY3)[c], 1011(PO3)[c], 1012(SA3), 1013(SA3),
1014(SA3), 1015(HY3), 1016(SA3), 1017(PO3), 1018(PO3).

JULY: 1019(ST4), 1020(ST4), 1021(ST4), 1022(ST4), 1023(ST4), 1024(ST4)[c], 1025(SM3), 1026
(SM3), 1027(SM3), 1028(SM3)[c], 1029(EM3), 1030(EM3), 1031(EM3), 1032(EM3), 1033(EM3)[c].

AUGUST: 1034(HY4), 1035(HY4), 1036(HY4), 1037(HY4), 1038(HY4), 1039(HY4), 1040(HY4),
1041(HY4)[c], 1042(PO4), 1043(PO4), 1044(PO4), 1045(PO4), 1046(PO4)[c], 1047(SA4), 1048
(SA4)[c], 1049(SA4), 1050(SA4), 1051(SA4), 1052(HY4), 1053(SA4).

SEPTEMBER: 1054(ST5), 1055(ST5), 1056(ST5), 1057(ST5), 1058(ST5), 1059(WW4), 1060(WW4),
1061(WW4), 1062(WW4), 1063(WW4), 1064(SU2), 1065(SU2), 1066(SU2)[c], 1067(ST5)[c], 1068
(WW4)[c], 1069(WW4).

OCTOBER: 1070(EM4), 1071(EM4), 1072(EM4), 1073(EM4), 1074(HW3), 1075(HW3), 1076(HW3),
1077(HY5), 1078(SA5), 1079(SM4), 1080(SM4), 1081(SM4), 1082(HY5), 1083(SA5), 1084(SA5),
1085(SA5), 1086(PO5), 1087(SA5), 1088(SA5), 1089(SA5), 1090(HW3), 1091(EM4)[c], 1092
(HY5)[c], 1093(HW3)[c], 1094(PO5)[c], 1095(SM4)[c].

NOVEMBER: 1096(ST6), 1097(ST6), 1098(ST6), 1099(ST6), 1100(ST6), 1101(ST6), 1102(IR3), 1103
(IR3), 1104(IR3), 1105(IR3), 1106(ST6), 1107(ST6), 1108(ST6), 1109(AT3), 1110(AT3)[c], 1111(IR3)[c],
1112(ST6)[c].

DECEMBER: 1113(HY6), 1114(HY6), 1115(SA6), 1116(SA6), 1117(SU3), 1118(SU3), 1119(WW5),
1120(WW5), 1121(WW5), 1122(WW5), 1123(WW5), 1124(WW5)[c], 1125(BD1)[c], 1126(SA6), 1127
(SA6), 1128(WW5), 1129(SU3)[c], 1130(PO6)[c], 1131(HY6)[c], 1132(PO6), 1133(PO6), 1134(PO6),
1135(BD1).

VOLUME 83 (1957)

JANUARY: 1136(CP1), 1137(CP1), 1138(EM1), 1139(EM1), 1140(EM1), 1141(EM1), 1142(SM1),
1143(SM1), 1144(SM1), 1145(SM1), 1146(ST1), 1147(ST1), 1148(ST1), 1149(ST1), 1150(ST1),
1151(ST1), 1152(CP1)[c], 1153(HW1), 1154(EM1)[c], 1155(SM1)[c], 1156(ST1)[c], 1157(EM1), 1158
(SM1), 1159(SM1), 1160(SM1), 1161(SM1).

FEBRUARY: 1162(HY1), 1163(HY1), 1164(HY1), 1165(HY1), 1166(HY1), 1167(HY1), 1168(SA1),
1169(SA1), 1170(SA1), 1171(SA1), 1172(SA1), 1173(SA1), 1174(SA1), 1175(SA1), 1176(SA1),
1177(HY1)[c], 1178(SA1), 1179(SA1), 1180(SA1), 1181(SA1), 1182(PO1), 1183(PO1), 1184(PO1),
1185(PO1)[c].

MARCH: 1186(ST2), 1187(ST2), 1188(ST2), 1189(ST2), 1190(ST2), 1191(ST2), 1192(ST2)[c], 1193
(PL1), 1194(PL1), 1195(PL1).

APRIL: 1196(EM2), 1197(HY2), 1198(HY2), 1199(HY2), 1200(HY2), 1201(HY2), 1202(HY2), 1203
(SA2), 1204(SM2), 1205(SM2), 1206(SM2), 1207(WW1), 1208(WW1), 1209(WW1), 1210(WW1),
1211(WW1), 1212(EM2), 1213(EM2), 1214(EM2), 1215(PO2), 1216(PO2), 1217(PO2), 1218
(SA2), 1219(SA2), 1220(SA2), 1221(SA2), 1222(SA2), 1223(SA2), 1224(SA2), 1225(PO)[c], 1226
(WW1)[c], 1227(SA2)[c], 1228(SM2)[c], 1229(EM2)[c], 1230(HY2)[c].

c. Discussion of several papers, grouped by Divisions.